The *FUSE* Archival Data Handbook

June 17, 2009 Edition

EDITORS: Paule Sonnentrucker, Derck Massa, Jeffrey Kruk, and William Blair

PRIMARY CONTRIBUTORS:

Thomas Ake, B-G Andersson, Pierre Chayer, Van Dixon, Alex Fullerton, Mary Elizabeth Kaiser, Jeffrey Kruk, Warren Moos, and David Sahnow

WITH ADDITIONAL CONTRIBUTIONS FROM:

Martial Andre, Paul Barrett, James Caplinger, Jean Dupuis, David Ehrenreich, Scott Friedman, Bernard Godard, Helen Hart, Guillaume Hébrard, Sylvestre Lacour, Edward Murphy, William Oegerle, Benjamin Ooghe-Tabanou, Mary Romelfanger, Kathy Roth, Ravi Sankrit, and Kenneth Sembach

Contents

List of Tables

List of Figures

Chapter 1

Introduction

The *Far Ultraviolet Spectroscopic Explorer* (*FUSE*) was a NASA mission designed, built, and operated by the Johns Hopkins University Department of Physics and Astronomy in Baltimore, MD. *FUSE* operated between 24 June 1999 and 18 October 2007. During that time, it acquired spectra over the wavelength range $905 \lesssim \lambda \lesssim 1187$Å, with a spectral resolving power of 15000–20000. *FUSE* routinely obtained high quality spectra of point sources with continuum flux levels between a few $\times 10^{-14}$ and 5×10^{-10}erg cm^{-2}s^{-1}Å^{-1}. The upper limit was set by safety considerations for the detectors. The lower limit is a rough estimate for normal observations and, with effort and attention to detail, usable spectra can be extracted for sources up to ten times fainter.

The primary focus of this handbook is to document the *FUSE* data products. However, in order to understand them and work with them, we have included a brief description of the *FUSE* instrument and the *FUSE* science data processing pipeline system (CalFUSE) used to produce them. More complete descriptions of these can be found in the *Instrument Handbook (2009)*, and in Dixon et al. [2007]: "CalFUSE Version 3: A Data Reduction Pipeline for the Far Ultraviolet Spectroscopic Explorer".

The contents of the remaining chapters of this handbook are:

Chapter 2 provides a basic description of the *FUSE* satellite and science instrumentation.

Chapter 3 gives an overview of the data processing pipeline used to produce the data.

Chapter 4 describes the naming and contents of the science data files and the preview files. It also lists some issues that can affect the fidelity of the different types of data products, and indicates which files are best suited for which applications.

Chapter 5 describes the naming and contents of ancillary data from the satellite that can be used to supplement the primary science data products.

Chapter 6 details the contents of the FITS headers of the science and ancillary data files.

Chapter 7 lists the various features and instrumental effects that can compromise the quality of *FUSE* data as well as methods to check for their occurrence.

Chapter 8 gives an overview of methods to retrieve, read, display and analyze *FUSE* data. It also provides a list of the various stellar and interstellar line atlases that can help

familiarize users with the *FUSE* spectral range. References to atomic and molecular line lists relevant to analyze the *FUSE* spectra are also given.

Chapter 9 lists examples of types of observations that required non-standard analysis techniques. Frequently asked questions are also reported in this chapter.

It is expected that this handbook will be used by investigators with three broad levels of interest, and that not all of the information will be needed by everyone. Consequently, the following roadmap is provided:

Casual users who simply wish to assess whether *FUSE* data are relevant to their goals. Their major need is to quickly examine the data. These users may not be too concerned about the details, accuracy or idiosyncrasies of the data at this stage.

Intermediate users who wish to understand *FUSE* data well enough to publish scientifically meaningful results based upon them. These users should examine the exposure-level calibrated spectrum files in order to verify the integrity of the data. They should also be fully aware of the different systematics that can affect the data. A prior knowledge of the software developed to analyze *FUSE* data and the tools available to determine if the target of interest is in a crowded field would be useful.

Advanced users who have scientific objectives that require data products beyond the archived spectra, and must perform additional processing to achieve their goals. Such users may, for example, wish to extract information from spectra of very faint objects, or use *FUSE* to analyze times series data. These users should be acquainted with most if not all of the material in this handbook. Their major focus will probably be on using the intermediate data files (IDFs). Knowledge of the suite of IDL routines or *FUSE* Tools in C, and in some cases of the CalFUSE pipeline itself, is strongly recommended.

Table 1.1 gives a list of the chapters and appendices that the users need to become familiar with based on the expertise level they seek to acquire prior to using *FUSE* data. This table is aimed at helping the user navigate through this document (and the *FUSE Instrument handbook 2009* to some extent) according to their scientific needs. It is by no means exclusive.

Table 1.1: *FUSE* Data Information According to Expertise Level

Expertise Level	Chapter	Appendix
Casual	1, 4, 7, 8	A
Intermediate	1, 2, 3, 4, 7, 8	A, C, F
Advanced	1, 2, 3, 4, 5, 6, 7, 8, 9	A, B, C, D, E, F

Chapter 2

The Instrument

2.1 Introduction

To understand *FUSE* data, the "Intermediate" and "Advanced" users need to acquire some familiarity with the instrument and data acquisition. Thus, this section gives a brief description of these subjects. More details are given in Moos et al. [2000], Sahnow et al. [2000], and in the *Instrument Handbook (2009)*.

2.2 Optical Design

The *FUSE* instrument (Figure 2.1) was a Rowland circle design consisting of four separate optical paths, or *channels*. A channel consists of a telescope mirror, a Focal Plane Assembly (FPA, which contains the spectrograph apertures), a diffraction grating, and a portion of a detector. The channels must be co-aligned to optimally observe a single target across the full *FUSE* bandpass. At the focal plane of the telescope, ∼90% of the light in the point spread function (PSF) lies within a circle of diameter 1.5″.

Two of the four channels used mirrors and gratings coated with SiC (to maximize sensitivity for $\lambda \lesssim 1000$ Å), and the other two were coated with aluminum and LiF (to maximize sensitivity for $\lambda \gtrsim 1000$ Å). The four channels comprise two nearly identical "sides" of the instrument, where a side consists of one LiF and

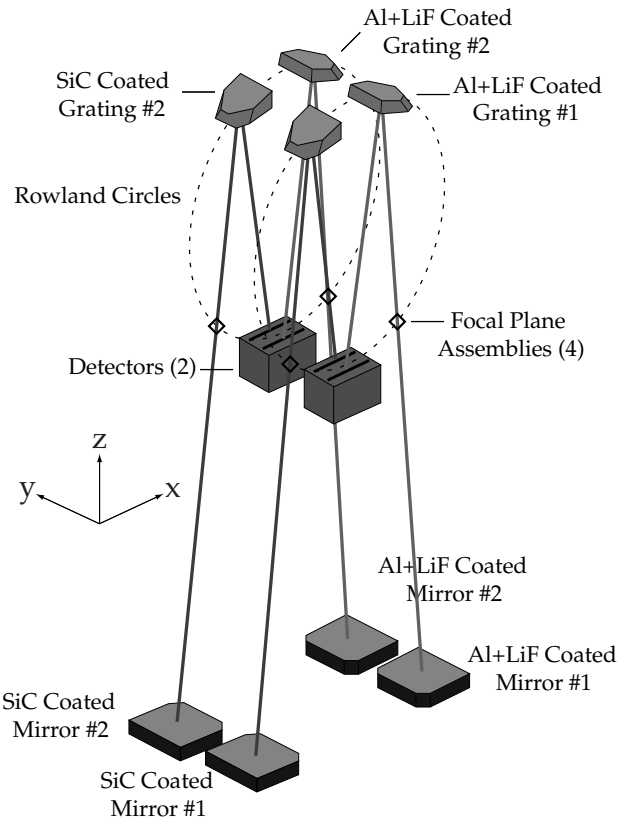

Figure 2.1: *Optical layout of the FUSE instrument showing the 4-channel design.*

one SiC channel, each producing a spectrum which falls onto a single detector. Each channel has a bandpass of about 200 Å. Thus, at least two channels are required to cover the ∼290 Å wavelength range of the instrument.

Figure 2.1 also shows the orientation of the instrument prime coordinate system (X,Y,Z). The two LiF channels are on the $+X$ side of the instrument, which is always kept in the shade (i.e., the $-X$ side was always facing toward the sun). This orientation minimizes the amount of sunlight that can make its way down the baffles surrounding the LiF channels. Minimizing stray light in the LiF channels was crucial to the operation of the Fine Error Sensor (FES) guidance camera, which operated at visible wavelengths (see Chapter 5). The orientation of the satellite was biased by several degrees in roll around the Z axis in order to keep the radiator of the operational FES in the shade.

2.2.1 Focal Plane Assemblies

Each telescope focused on an FPA that served as the entrance aperture for its spectrograph. An FPA was a flat mirror mounted on a two-axis adjustable stage which contained three apertures. The apertures were not shuttered, so whatever light fell on them was dispersed by the gratings and focused onto the detectors.

The orientation of the three apertures is depicted in Fig. 2.2, and their properties are summarized in Table 2.1. The HIRS aperture ensured maximum spectral resolution, minimum sky background and sometimes allowed for spatial discrimination for extended objects or crowded stellar fields. However, it blocked part of the point spread function, and small, thermally induced mirror motions often led to the loss of all light from one or more channels during an observation. The MDRS aperture, with stable mirror alignment, provided maximum throughput and a spectral resolution comparable to the HIRS aperture for a point source with only slightly more airglow contamination than HIRS. However, it too, was susceptible to thermal drifts of the separate channels. The LWRS aperture was the least sensitive to alignment issues, but it allowed the largest sky background contamination. Although image motion could degrade the resolution of LWRS spectra, this was largely corrected by the pipeline processing for TTAG data. The LWRS aperture was also used to observe faint extended objects, producing a filled-aperture resolution of ∼100 km s^{-1}. LWRS was the default aperture throughout most of the mission because of the thermal image motions that occurred on orbit.

In addition, a target could also be placed outside the apertures at the reference point (RFPT), which did not transmit light. When a target was placed at the RFPT, the three apertures sampled the background sky nearby.

Each FPA could be moved independently in two directions. Motion tangential to the Rowland circle, which is roughly in the dispersion direction, and perpendicular to the apertures. These motions allowed co-alignment of the channels and permitted focal plane splits (FP splits, see Chapter 7) for high signal-to-noise ratio observations of bright targets. Motion in Z enabled focusing of the apertures with respect to the mirrors, spectrograph grating, and detector.

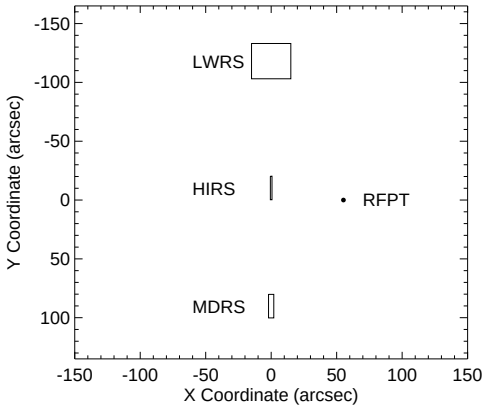

Figure 2.2: *Locations of the FUSE apertures and reference point (RFPT) on the FPA. Note that the RFPT is not an aperture. With north on top and east on the left, this diagram corresponds to an aperture position angle of 0°. Positive aperture position angles correspond to a counter-clockwise rotation of the spacecraft (e.g. this FOV) about the target aperture. Projected onto an FES camera, this diagram only represents a small portion of the full 19′×19′ active area of the FES, whose center would be out of the field to the right from this Figure. The aperture centers shown in this coordinate system are reported in Table 2.1.*

Table 2.1: Apertures

Aperture	Name	Dimensions	Number(a_n)$^+$	Comments	X Position	Y Position
Medium resolution	MDRS	$4.0 \times 20''$	2	–	$0.00''$	$+90.18''$
High resolution	HIRS	$1.25 \times 20''$	3	–	$0.00''$	$10.27''$
Low resolution	LWRS	$30 \times 30''$	4	Nominal Aper.	$0.00''$	$-118.07''$
Reference Point	RFPT	–	4	–	$55.18''$	$0.00''$

$^+$ Aperture naming convention. $a_n = 1$ corresponded to the PINHOLE aperture which was never used.

2.2.2 Spectrograph

FUSE spectra covered $905 \lesssim \lambda \lesssim 1187$Å. The spectra from each of its four channels were imaged onto two microchannel plate detectors. Each detector had one SiC and one LiF spectrum imaged onto it, thereby covering the entire wavelength range. The two channels imaged on each detector were offset perpendicular to the dispersion direction to prevent them from overlapping. The dispersion direction of the SiC and LiF spectra were in the opposite sense (see Figure 2.3). Each detector consisted of two functionally and physically independent segments (A and B) separated by a small gap. To ensure that the same wavelength region did not fall into the gap on both detectors, the detectors were offset slightly with respect to each other in the dispersion direction. Table 2.2 lists the wavelength coverage for each of the eight detector segment and channel combinations. Nearly the entire wavelength range was covered by more than one channel, and the important 1015–1075 Å range was covered by all four, providing the highest effective area and the greatest redundancy.

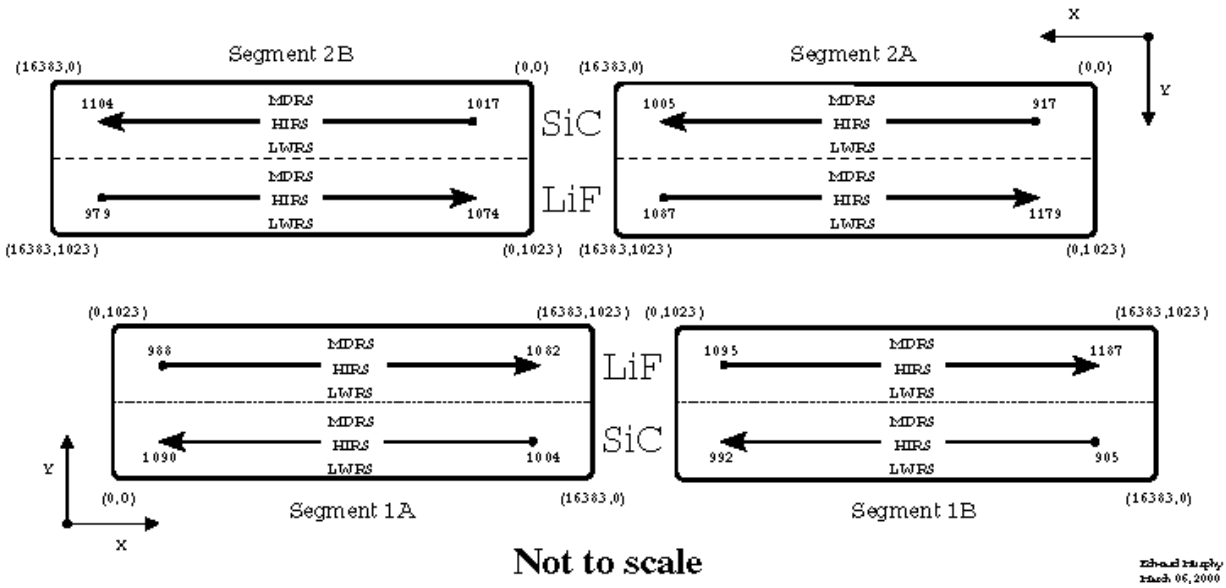

Figure 2.3: *Schematic view of the wavelength coverage, dispersion directions, and image locations for the FUSE detectors. In this figure, the detector pixel coordinates of the corner of each segment are shown. The X, Y axes indicate orientation on the sky. Wavelength ranges shown are approximate (see Table 2.2).*

The SiC channels had an average dispersive plate scale of 1.03 Å/mm while the LiF channels had a scale of 1.12 Å/mm (Moos et al. [2000]). Coupled with the detector pixel size, this resulted in a scale of ∼6.7 mÅ/pixel in the LiF channel and ∼ 6.2 mÅ/pixel in the SiC channel (in the X or dispersion direction).

The optical design of the *FUSE* spectrographs introduced astigmatism. The astigmatic height of *FUSE* spectra perpendicular to the dispersion was significant; the dispersed image of a point source had a vertical extent of 200 – 900 μm, or 14 – 63″, on the detector. An extended source filling the large aperture was as large as 1200 μm, or 100″. This vertical astigmatic height was a function of both wavelength and detector segment. This meant that the spatial imaging capability of *FUSE* was extremely limited. For the spectral region near the minimum astigmatic heights in each spectrum, there was marginal spatial information ($> 10''$), but to recover this requires careful, non-standard processing. The minimum astigmatic points were near 1030 Å on the LiF channels and near 920 Å on the SiC channels.

Moreover, spectral features showed considerable curvature perpendicular to the dispersion, especially near the ends of the detectors where the astigmatism was greatest. This astigmatism is corrected for in the data prior to collapsing it into a 1-D spectrum (see Chapter 7 and the *Instrument Handbook (2009)* for details).

Table 2.2: Wavelength Ranges for Detector Segments[a] (in Å)

Channel	Segment A	Segment B
SiC 1	1003.7 – 1090.9	905.0 – 992.7
LiF 1	987.1 – 1082.3	1094.0 – 1187.7
SiC 2	916.6 – 1005.5	1016.4 – 1103.8
LiF 2	1086.7 – 1181.9	979.2 – 1075.0

[a] Note the redundancy especially in the 1015–1075 Å range.

2.2.3 Detectors

The *FUSE* instrument included two photon-counting microchannel plate (MCP) detectors with delay line anodes. Each detector, which was a single optomechanical unit, consisted of two functionally independent segments. Each segment could be separately controlled since it had its own high voltage control, anode, and digitizing electronics. The two segments in a detector were separated by a several millimeter gap, which was not sensitive to photons. In order to ensure that the same wavelength interval did not fall into the gap on both detectors, the two detectors were offset by several degrees with respect to each other along the Rowland circle. The two detectors were designed to be identical, although variations in MCP properties and electronics adjustment led to a number of minor differences between them.

Each segment included a stack of three MCPs with its own double delay line anode. A photon incident on the front surface of one of the MCPs resulted in a shower of $\sim 10^7$ electrons at the bottom of the stack. This charge cloud was collected by the anode and event locations were determined by measuring the time propagation along the delay line in the spectral dispersion direction and by charge division in cross dispersion. The measured positions were then digitized into $16,384 \times 1024$ pixels. Thus the *FUSE* "pixels" were not physical objects, but rather the digitization of analog measurements.

On all segments, the X (dispersion dimension) pixel size was ~ 6 μm. However, the Y (orthogonal to the dispersion) pixel size was different for the different detector segments in the raw data (in the calibrated data, all segments were adjusted to a common Y scale). For segments 1A and 1B, the Y pixel size was ~ 10 μm, and it was somewhat larger for segments 2A and 2B. However, the detector resolution (i.e., the ability of the electronics to locate an event) was $\sim 20 \times 80$ μm. Hence, the detector resolution was oversampled by a factor of 4 or more.

The two units were designated Detector 1 and Detector 2, and the segments were labeled A and B. Thus, the four segments were denoted as 1A and 1B (on side 1 of the instrument), and 2A and 2B (on side 2) (see Fig. 2.3).

Because X and Y coordinates were calculated from timing and voltage measurements of the charge cloud, the detector coordinate system was subject to distortions caused by temperature changes and other effects. To track changes in this distortion as a function of time, electronic "stim pulses" were injected into the detector electronics at the beginning and end of each exposure. The stim pulses appear near the upper left and upper right corners of each

detector segment, outside of the active spectral region. The stim pulses were well placed for tracking changes in the scale and offset of the X (dispersion) coordinate, but they were not well enough separated in Y (spatial) to track scale changes along that axis. CalFUSE used the stim positions to correct for thermal effects.

Detector Background: Microchannel plates possess an inherent background rate, which is due mainly to beta decay in the MCP glass. On orbit, cosmic rays added to this to give a total rate of ∼0.5 counts cm^{-2} sec^{-1}. Since there was no shutter in the optical system, airglow emission, which constantly changed, also contributed to the overall background.
Stim Lamp: A stimulation, or "stim" lamp was located just below the internal spectrograph baffles on each side of the instrument, and about 1.25 m above each detector. These lamps were used in orbit as an aid in calibration.
Counters: Several types of event counters were calculated by the *FUSE* detectors in parallel with all observations. Two counters that are important for calibration purposes are the Fast Event Counter (FEC), which measures the count rate at the detector anode, and the Active Image Counter (AIC), which yields count rates at the back end of the detector electronics. These count rates were used by CalFUSE to monitor a variety of effects, to screen the data for various anomalies, and to determine dead time corrections.

More details about the detector subsystem and its performance can be found in the *FUSE Instrument Handbook (2009)* and the references provided therein.

2.2.4 Fine Error Sensors

The front surface of the two LiF FPAs had a reflective coating, and light not passing through the apertures was reflected into a CCD camera for each side. Images of the field of view (FOV) around the apertures were used for acquisition and guiding by a camera system called the Fine Error Sensor (FES). The FES cameras imaged a $19' \times 19'$ field around (but not centered on) the apertures. Each FES imaged the FPA onto a quadrant of a 1024×1024 pixel CCD, which was masked to a 512×512 pixel image, with pixels of 24×24 μm and a plate scale of $2.55''$pixel^{-1}. Only one of the two FESs was used at a time. The FWHM of the FES PSF was typically $\sim 5''$. More details can be found in Chapter 5 and in the *Instrument Handbook (2009)*.

2.3 Instrument Alignment and Target Centering

The four-channel design of *FUSE* allowed for redundancy in spectral coverage and improved total instrument throughput. With multiple spectra overlapping different wavelength regions, the user can cross-check spectral measurements from the independent spectrographs and, in theory, improve the signal-to-noise of the data. This has to be done carefully, however, since the spectra have different resolutions, wavelength shifts, and small scale structure due to differing detectors and optical effects. While narrow apertures were available with *FUSE*, most observations used the large LWRS aperture, for which the spectrographs operated in a slitless mode. In this case, wavelength accuracy and resolution were dependent on how well the target was centered in the aperture and how stable the position was maintained during the observation. Because there were four channels, accurate target pointing had to be achieved in four

apertures simultaneously for best results.

Due to several hardware problems in the instrument and spacecraft, target placement was not completely stable during most exposures. Movements of the target and spectra often induced errors in measured fluxes, absolute wavelengths, and resolution. Most of these effects were corrected by processing in the CalFUSE pipeline software especially for Time-Tag mode data (see below). Nonetheless, the user of *FUSE* data should be aware of these problems since the corrections are imperfect (see Chapter 7).

Thermal effects that occurred with the instrument included: mirror misalignment and motion, and motions of the spectrograph gratings. Gradual failure of the spacecraft gyroscopes and reaction wheels over the course of the mission degraded the pointing control at times. These problems are discussed in the next sections.

2.3.1 Mirror Alignment

Coalignment of the *FUSE* channels was difficult to maintain because the telescope mirror benches were thermally coupled to the space environment external to the instrument. Thermal expansion and contraction of the baffles is suspected to have moved the optical bench on which the mirrors were mounted, causing a shift of the sky viewed by each aperture. If the thermal environment of a target was significantly different than the previous one, there could be a secular shift of the mirrors over several hours. On top of this, there would be smaller orbital variations as *FUSE* went in and out of sunlight. The shifts could be large enough to move the target out of the aperture for a channel, especially for HIRS and MDRS observations. The SiC mirrors showed larger shifts than the LiF ones since they were on the sunlit side of the instrument. The channel with the best alignment was always the LiF side used with the guiding FES. For that channel, any shift of the star field would automatically be detected and removed by the spacecraft attitude control system. Prior to 12 July 2005, LiF1 was the guiding channel, and consequently, the LiF1 spectra where well centered in the aperture, resulting in the best wavelength and photometric accuracies. After that, LiF2 was used for guiding (Table 2.3).

Several observing strategies were implemented to help maintain alignment. An empirical model was devised to predict the alignment based on target orientation with respect to the Sun and Earth and prior history of pointing. At the beginning of an observation, the mirrors or FPAs would be adjusted to a predicted setting. If the change in thermal environment was expected to be large, the instrument would be allowed to thermalize until the target was predicted to be within the LWRS aperture. Residual motions associated with the completion of the thermalization process are removed in the pipeline processing. Sky background observations (e.g., S405/S505 programs) were sometimes acquired during long thermalization periods.

Periodically, an alignment procedure would be run, which scanned the instrument across a star to locate the aperture edges (e.g., M112/M212 programs). After assessment on the ground, the mirrors would be adjusted into alignment. Finally, if the MDRS or HIRS apertures were being used, one or more target peakups would be scheduled even multiple times per orbit to recenter the FPAs before starting exposures. This was a time-consuming and operationally complex activity and was only performed when deemed necessary for the science program.

For TTAG observations, CalFUSE applied a model for expected mirror motions during an orbit and performed photon position corrections for the non-guiding channels for point sources. This model was developed empirically from on-orbit measurements of actual thermal

misalignments. The FPA position reading at the beginning of an exposure was used to set the wavelength zero point for a channel. No corrections of fluxes were made for the target being outside the apertures. For HIST data, exposures were kept short enough to minimize any smearing due to thermal motions during a single exposure. Individual exposures could be aligned before co-adding to remove any detected offsets.

2.3.2 Grating Motion

Besides movement of the telescope mirrors within the instrument, the spectrograph gratings also rotated slightly with changes in thermal environment. This caused the spectra to move on the detector. Since airglow emission lines shifted as well, an empirical model could be developed to predict the orbital motions and was used by CalFUSE to remove these shifts.

2.3.3 Pointing Stability

FUSE was built with six gyroscopes and four reaction wheels, and at the beginning of the mission, the Attitude Control System (ACS) could obtain subarcsec pointing stability during an exposure. Pointing errors were much smaller than all the apertures and were an insignificant contributor to wavelength offsets and spectral resolving power. Except for rare circumstances, such as loss of guide stars during an exposure, guidance stability was not an issue when a user worked with the science data.

As the mission progressed, ACS hardware components began to fail and maintaining stable pointing at a target became more difficult. As with the telescope mirror motions, a target could wander around inside the aperture during an exposure, degrading the spectral resolution and wavelength accuracy, or leave the aperture entirely, sometimes to return later in the exposure. But unlike the instrument motions, the location of the target can be estimated from the pointing information, and the data corrected in ground processing. Since the correction is an estimate, though often an accurate one, the user needs to be vigilant with *FUSE* spectra. Details about guiding are found in the jitter file associated with each exposure (Section 5.2). Table 2.3 lists the dates when significant changes were made to *FUSE* pointing control.

2.4 Instrument Data System

The Instrument Data System (IDS) was a computer processor that controlled the *FUSE* instrument. The IDS communicated with all instrument subsystems, and was responsible for controlling all instrument functions, including thermal control, actuators on the mirror assemblies and FPAs, and detector and Fine Error Sensor (FES) operations. It received data from the FUV detectors and FES, and packaged them for transmission to the onboard solid-state recorder. The IDS also collected the housekeeping telemetry (temperatures, voltages, etc.) from these subsystems, packaged them, and sent them to the recorder.

The IDS played a crucial role in the pointing performance of the instrument. After a slew, it processed the FES image of the new field and determined the pointing based on comparison with a star table uplinked from the ground for each observation. This measured pointing was

sent to the spacecraft Attitude Control System (ACS) to update the current pointing and the spacecraft was slewed to the desired target position. Once the FES acquired guide stars, it began sending centroid information for the guide stars to the IDS. The IDS computed the measured pointing vector (quaternion) once every second and sent it to the ACS to maintain pointing stability. Guiding was terminated prior to each occultation of the target by the earth. As long as guide stars had been acquired prior to entry into the South Atlantic Anomaly (SAA), guiding often proceeded through the SAA period even though observations were halted.

2.5 Science Data Collection Modes

Although the *FUSE* detectors were photon-counting devices, memory considerations resulted in the science data being saved in two different ways. For each incident photon the detector measured the X (14 bits) and Y (10 bits) positions, along with the pulse height (5 bits). A 32 bit word containing this information, along with detector and segment bits and one bit marking it as a photon event, was then constructed. An Active Image Mask was then applied. (The purpose of the mask was to allow the exclusion of detector regions which had very high count rates, e.g. due to a hot spot or other effect, that might overwhelm the science data bus. During the mission, however, no data needed to be excluded on any segment using the Active Image Mask.) The IDS collected the photon data from the detector and then stored it in memory as a photon list for lower count rates (time-tag or TTAG mode), or created a two-dimensional histogram of the data for higher count rates (histogram or HIST mode). For more details on detector data processing and masks, see the *FUSE Instrument Handbook (2009)*.

2.5.1 TTAG (Photon Address) mode

When using photon address or time-tag (TTAG) mode, the position of each photon coming from the detector, along with its pulse height, was saved in IDS memory. Time markers were inserted into this data stream at a regular rate (typically once per second) by the IDS. Later, when the `*fraw.fit` files (see Section 4.2.1.1) were created by OPUS, the time taken from the preceding time marker was assigned to each photon event, so that raw TTAG data files include a floating point time, X (0 – 16383), Y (0 – 1023), and pulse height (0 – 31) for each photon. The data files include photon events from all apertures, along with background detector regions. One aperture in each channel contained the spectrum of the target, while the others only contained spectra of the sky plus airglow and detector background. Occasionally, in crowded fields, stars nearby the target object could enter a non-prime aperture and thus be recorded.

2.5.2 HIST (Spectral Image) mode

Data obtained in TTAG for very bright targets could not be transferred fast enough resulting in partial data loss. Consequently, when the UV flux of a target was expected to produce count rates larger than 2500 cps from all detector segments combined, the IDS was commanded to store the data in spectral image, or histogram (HIST) mode. In this case, the photons were binned in X and Y and the arrival times and pulse heights of the photons were lost. The size and positions of these bins were determined by the Spectral Image Allocation (SIA) table, which

was uploaded to the IDS before each HIST observation. The SIA table was a buffer made up of 512 rectangles. The size of each rectangle was 2048 pixels in X and 16 pixels in Y. Thus, the 512 elements of the SIA table constitute an 8×64 image which spans the 16384×1024 elements of the detectors. The SIA table specifies which of these rectangles should be saved (mask bit set "on"), i.e., if the IDS received a photon event from the detector whose (X, Y) coordinates map to a location in an active rectangle, then that photon event is stored by incrementing a counter in a histogram bin at the specified binning. The default histogram binning size was 1×8 (X, Y) detector pixels. The default SIA table specified storage of a region around the aperture containing the target, and required ∼20 MB of storage for an orbit's worth of exposures. Note that in HIST mode, only data taken through the science aperture were recorded. Because Doppler compensation was not performed on-board, HIST exposures times were kept short to avoid losing spectral resolution and minimize smearing from thermal motions. Typical HIST exposure times were ∼ 400 s. More information can be obtained in the *Instrument Handbook (2009*.

2.6 *FUSE* Mission Short Biography

A series of events impaired optimal use of the *FUSE* spacecraft and impacted the data acquisition and processing during those times. A list of the most significant events affecting *FUSE* data quality is given in Table 2.3 where Column (1) lists the chronology of these events since the *FUSE* launch; Column (2) gives a brief description of the events that took place; and Column (3) points to Notes to the table. A complete listing of such events can be found in the *Instrument Handbook (2009)*.

Table 2.3: Significant Events

Date	Event	Notes
24 June 1999	Launched	...
12 December 1999	LiF1 Focus Finalized	(1); (3)
16 March 2000	LiF2, SiC1,2 Focus Finalized	(1); (3)
25 November 2001	Yaw RWA failed	(2)
10 December 2001	Pitch RWA failed	(2); Science operations suspended
February 2002	Two-wheel mode begins	Observations resumed
03 February 2003	Segment 2A HV confined	(4)
31 July 2003	Yaw IRU-B failed	(2); Gyroless control mode used
27 December 2004	Roll RWA failed	(2); Science operations suspended
March 2005	One-wheel mode begins	Observations resumed
12 July 2005	LiF2 made default guiding channel	(3)
12 July 2007	Skew RWA failed	End of *FUSE* pointed observations
18 October 2007	Decommissioning	End of *FUSE* mission

NOTES to table:

(1) Data taken prior to completion of the telescope focus should be used with care. See the *Instrument Handbook (2009)* for details of the focus process.

(2) Each reaction wheel (RWA) and gyroscope (IRU) failure resulted in a degradation of the *FUSE* target acquisition and pointing (see Section 2.3). The target shifts could be large enough to move the source in and out of one or more channels leading to potential errors in the measurement of the flux, the wavelength scale and resolving power. While CalFUSE compensates for the time-dependent wavelength scale changes, flux measurement errors and resolving power variations are more difficult to correct (see Chapters 4 and 7). Users should examine the jitter file (Section 5.2) and count-rate plots associated with each exposure (Section 4.2.1.4) before performing scientific measurements.

(3) Misalignment of the mirrors could occur for the non-guiding channels causing the target to miss the apertures. With very few exceptions, LiF1 was the default guide channel until 12 July 2005, and LiF2 thereafter. Since the guiding channel always offers the best photometric and wavelength accuracies, users are encouraged to check the observation dates when analyzing the data.

(4) Segment 2A high-voltage stopped being raised in 2003 (see Table 7.4). Charge depletion in the LWRS aperture region of the detector could not be compensated for thereafter. Users are encouraged to use LiF2A and SiC2A measurements with care and verify them against measurements obtained in other channels when possible. See Section 7.3.4 and the *Instrument Handbook (2009)* for additional information.

Chapter 3

Pipeline Processing

3.1 Introduction

The science data processing pipeline for *FUSE* data is called CalFUSE. This chapter gives a brief overview of CalFUSE. While the "Intermediate" user might only be interested in getting acquainted with the *FUSE* data analysis software provided on the CalFUSE homepage, the "Advanced" user needs to be fully familiar with the pipeline functionalities and tools provided along with it. Because CalFUSE was run in tandem with the Operations Pipeline Unified System (OPUS), a brief description of its function is included as well.

3.2 OPUS

FUSE science data were dumped from the spacecraft solid state recorder 6–8 times a day when the satellite passed over the ground station at the University of Puerto Rico at Mayaguez. After the data were transferred to the Satellite Control Center at JHU and checked for completeness, corresponding data about the instrument and spacecraft were extracted from the engineering telemetry archive. The science and engineering data files were sent to a *FUSE*specific version of the automated processing system, OPUS (Rose et al. [1998]). OPUS ingested the data downlinked by the spacecraft and produced the data files that served as input to the CalFUSE pipeline. OPUS generated six data files for each exposure; the four raw data files (one for each detector segment, see Section 4.2.1); and two time-resolved engineering files (the housekeeping and jitter files, see Section 5.2). It then managed the execution of CalFUSE as well as the files produced by CalFUSE and called the additional routines that combine spectra from each channel and exposure into a set of observation-level spectral files. OPUS read the *FUSE* Mission Planning Database (which contained target information from the individual observing proposals and instrument configuration and scheduling information from the mission timeline) to populate raw file header keywords and to verify that all of the data expected from an observation were obtained.

3.3 Overview of CalFUSE

The CalFUSE pipeline was designed with three principles mind. The first was that CalFUSE would follow the path of a photon backwards through the instrument, correcting for the instrumental effects introduced in each step, if possible. The interested reader is referred to Dixon et al. [2007] for details regarding each of the steps that data go through when running CalFUSE.

The second principle was to make the pipeline as transportable and modular as possible. CalFUSE is written in C and runs on the Solaris, Linux, and Mac OS X (versions 10.2 and higher) operating systems. The pipeline consists of a series of modules called by a shell script. Individual modules may be executed from the command line. Each performs a set of related corrections (screen data, remove motions, etc.) by calling a series of subroutines.

The third principle was to maintain the data as a photon list in an Intermediate Data File (IDF) until the final module of the pipeline. Input arrays are read from the IDF at the beginning of each module, and output arrays are written at the end. Bad photons are flagged but not discarded, so the user can examine, filter, and combine processed data files without re-running the pipeline. **This makes the IDF files important for those who wish to perform customized operations on *FUSE* data.** The contents of the IDFs are discussed in Section 4.2.1 and on the CalFUSE Page at MAST (see below).

Investigators who wish to re-process their data (mostly "Advanced"users) may retrieve the CalFUSE C source code and all associated calibration files from the CalFUSE Page: http://archive.stsci.edu/fuse/calfuse.html. Detailed instructions for running the pipeline and descriptions of the calibration files are provided there as well.

Chapter 4

The Science Data Files

This chapter describes the science data files available from the *FUSE* archive. Ancillary data files, which provide additional information about the state of the instrument and spacecraft, are described in Chapter 5.

The "Casual" user mostly needs to examine *FUSE* preview files and understand their limitations while the "Intermediate" and "Advanced" users need to be knowledgeable about some or all of the *FUSE* data files for an observation. Table 4.1 in the next section lists all *FUSE* data file extensions available for download from the MAST archive. This table is aimed at helping all users determine which files are essential to their project and to find the relevant information throughout this document. It is, therefore, strongly recommended that potential *FUSE* users read the Overview Section (below) and familiarize themselves with the contents of these tables before retrieving any data files.

4.1 Introduction to the Science Data Files

4.1.1 Overview

A *FUSE observation* is a set of contiguous *exposures* of a particular target through a specific aperture. Each exposure generated four raw science data files, one for each detector segment (1A, 1B, 2A and 2B). There are two pairs of spectra (one LiF and one SiC) for the target on each detector segment. When all of the data are extracted, 8 calibrated spectra result from a single exposure. Figures 4.1 and 4.2 show geometrically corrected images of spectra on Side 1 and Side 2 detectors for a single exposure. Observations may consist of any number of exposures between 1 and (in principle) 999.

Spectra are extracted by CalFUSE only for the target aperture and are binned in wavelength. The default binning is 0.013 Å, which corresponds to about two detector pixels, or one fourth of a point source resolution element. After processing, a series of combined observation-level spectral files are generated along with a variety of preview files. These files will be discussed in detail in the next sections.

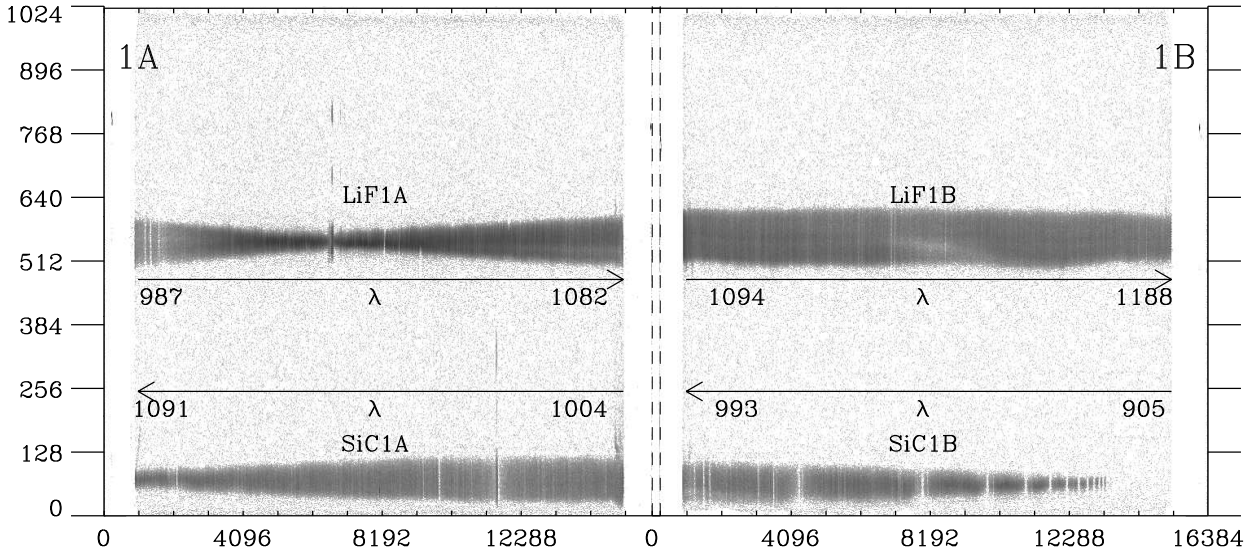

Figure 4.1: *A geometrically corrected image of spectra on the Side 1 detector for a single exposure, shown with a log display function. For each exposure, four spectra are produced for each side. The variable vertical height of the spectra is the result of astigmatism introduced by the FUSE spectrographs. Note the minimum astigmatic points, as mentioned in the text. The vertical emission line near the narrowest part of the LiF1A spectrum is due to Lyβ airglow (the airglow from the HIRS and MDRS apertures can be seen faintly above it). The horizontal stripes visible in the LiF1A and LiF1B spectra are termed "worms" (see Chapter 7). The small dots near $Y \sim 800$ are due to STIM pulses injected into the electronics (see Section 2.2.3). Slight misalignments between the detector segments are due to varying pixel scales.*

FUSE spectra are susceptible to a variety of systematic effects that are described in detail in Chapter 7. These systematics can affect a portion or all of a spectrum from one or more channel and detector combinations. **Hence, it is important to compare channels with overlapping wavelength ranges for consistency** (see Table 2.2). A discrepancy between the spectra from overlapping channels may indicate the presence of one or more of these effects. Such systematic errors may be considerably larger than the statistical errors provided in the extracted spectra.

All *FUSE* data are stored as FITS files containing one or more Header + Data Units (HDUs). The first is called the primary HDU (or HDU1); it consists of a header and an optional N-dimensional image array. The primary HDU may be followed by any number of additional HDUs, called "extensions". Each extension has its own header and data unit. *FUSE* employs two types of extensions, image extensions (2-dimensional array) and binary table extensions (rows and columns of data in binary representation). FITS files can be read by a number of general and astronomical software packages (see Chapter 8).

Table 4.1 lists all the files types available for retrieval from the MAST archive interface. In the table the following are listed: Column (1), file types; Column (2), detector side; Column (3),

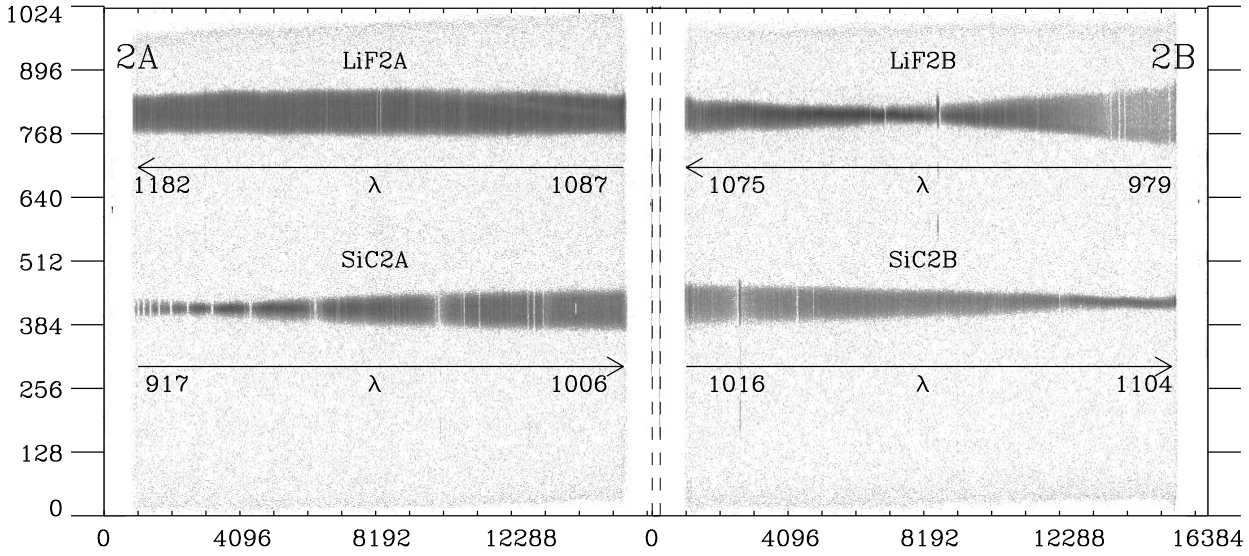

Figure 4.2: *Same as Fig. 4.1, but for the Side 2 detector. Again a log display function has been used to show the faintest emission features.*

detector segment; Column (4), channels; Column (5), aperture used for observation; Column (6), observing mode; Column (7), data type; Column (8), section where each file is discussed; and Column (9), "Expertise Level" corresponding to the readers' motivation for using *FUSE* data: Casual (Cas), Intermediate (Int), or Advanced (Adv; see Chapter 1). Hence, inspection of this table will provide the user with instant information about 1) which files are required for his/her purposes, and 2) in which sections those files are discussed in detail throughout this document.

Table 4.1: *FUSE* Data File Types

File Types	Side	Segment	Channel	Aperture	Mode	Type	Section	Expertise
Raw Files								
∗fraw.fit	1, 2	a, b	···	···	ttag, hist	photon list, image	4.2.1.1	Adv
∗fes∗raw.fit	a, b	···	···	···	···	raw FES	5.1	Adv
∗snapf.fit	···	···	···	···	···	engineering snapshot file	5.3	Adv
∗snp∗f.fit	a, b	···	···	···	···	FES associated snapshot	5.3	Adv
∗hskpf.fit	···	···	···	···	···	housekeeping table	5.2	Adv
∗jitrf.fit	···	···	···	···	···	jitter table	5.2	Adv
Calibrated Files								
∗fcal.fit	1, 2	a, b	SiC, LiF	2, 3, 4	ttag, hist	spectrum	4.2.1.2	Int, Adv
∗00all∗fcal.fit	···	···	···	2, 3, 4	ttag, hist	header	4.2.2.1	Int, Adv
∗00000all∗fcal.fit	···	···	···	2, 3, 4	ttag, hist	spectrum	4.2.2.1	Cas, Int, Adv
∗00000ano∗fcal.fit	···	···	···	2, 3, 4	ttag, hist	spectrum	4.2.2.1	Int, Adv
∗fidf.fit	1, 2	a, b	···	···	ttag, hist	photon list (IDF)	4.2.1.3	Adv
∗f.trl	1, 2	a, b	···	···	ttag, hist	processing trailer	4.2.1.5	Int, Adv
∗asnf.fit	···	···	···	···	···	association table	5.4	Int, Adv
∗fes∗fcal.fit	a, b	···	···	···	···	calibrated FES image	5.1	Adv
∗hskpf.fit	···	···	···	···	···	housekeeping table	5.2	Adv
∗jitrf.fit	···	···	···	···	···	jitter table	5.2	Adv
Preview Files								
∗fext.gif	1, 2	a, b	···	···	ttag, hist	extraction window plot	4.2.1.4	Int, Adv
∗frat.gif	1, 2	a, b	···	···	ttag, hist	count-rate plot	4.2.1.4	Int, Adv
∗00000∗f.gif	1, 2	···	SiC, LiF	···	ttag, hist	plot	4.2.2.2	Cas, Int, Adv
∗00000∗spec∗f.gif	···	···	···	···	ttag, hist	plot	4.2.2.2	Cas, Int, Adv
∗00000∗nvo∗fcal.fit	···	···	···	···	ttag, hist	spectrum	4.2.2.2	Cas, Int, Adv

4.1.2 File Name Conventions and Useful Program IDs

All *FUSE* file names are composed of several identifying elements, but not all files contain each one of these elements. However, all exposure-level file names have the form {*pppp*}{*tt*}{*oo*}{*eee*} and begin with the following four elements:

1. A four-digit *program ID* searchable in MAST (*pppp*: a letter plus a three-digit number; see Tables 4.2, 4.3 & 4.4).
2. A target number (1–99), which identifies the target within the program (*tt*).
3. An observation number (1–99) which specifies an observing sequence on the target (*oo*). Note that a target might have multiple observation numbers if multiple visits at different times and under different observing conditions were required.
4. An exposure number (1–999) within the given observation (*eee*).

An example of an exposure-level file name is D0640301004. Note that observation-level files have $eee = 000$.

FUSE program ID codes convey general information about the category of the program, be it primarily for science or calibration. As indicated in Tables 4.2, 4.3 and 4.4, the dividing line is not hard. Sometimes useful science data can be extracted from data that were obtained for calibration purposes (for example, the flux calibration programs). Other times, the requirements of the calibration activity itself may seriously compromise the use of any spectral data for science. For some 'I' programs (in-orbit checkout), the data may be useful for science but only with great caution since the instrument may not have reached its final science configuration and focus yet. Many targets observed during in-orbit checkout were re-observed later in the mission, and the user should be wary of the IOC observation. However, these data are archived at MAST, so the user should be cognizant. Information on the sequence of instrument focus activities during in-orbit checkout can be found in the *Instrument Handbook (2009)*; this may assist the user in evaluating the utility of the IOC observations.

Table 4.2: Science Programs

Code	Category
Annn	Cycle 1 Guest Investigator (GI) programs
Bnnn	Cycle 2 GI programs
...	...
Hnnn	Cycle 8 GI programs
Pnnn	PI Science team guaranteed time (US)
Qnnn	PI Science team guaranteed time (France)
Sn05	[n=4-9] Sky Background Observations
Unnn	Non-proprietary re-observations of science targets
Xnnn	Early Release Observations (EROs)
Z0nn	Project Scientist Discretionary Programs
Z9nn	Observatory Programs[a]

[a] Observatory programs were non-peer-reviewed science programs executed at the discretion of the NASA Project Scientist. These programs were designed to fill a gap in science target availability after the initial reaction wheel problems in late 2001.

Table 4.3: Instrument Programs Possibly Useful for Science[a]

Code	Category
I8nn	Spectrograph Focus and Alignment
I904	Random Science fillers
M10n[b]	Calibration/Maintenance Programs
S601-701	Science Verification (SV) programs

[a] These data might reveal interesting science. For example, McCandliss (2003) used wavelength-calibration data from program M107.

[b] See Table 4.4 for exceptions.

Table 4.4: Instrument Programs NOT Appropriate for Science[a]

Code	Category
Innn[b]	Instrument In-Orbit Check-out (IOC) programs
Mn12-n14	Periodic Alignment Programs, [n=1,2]
M717-727	Channel Alignment
M9nn[b]	Detector Characterization Programs
Snnn[b]	Science Verification (SV) programs

[a] These data should NOT be used for science purposes because they were typically obtained with settings far from nominal. The spectra, if they exist for these programs, suffer from unusual systematic effects.

[b] See Tables 4.2 and4.3 for exceptions.

NOTE 1: Two types of **airglow** observations were obtained during the course of the mission: i) dedicated bright-earth observations (see Chapter 9); and ii) airglow exposures obtained as part of a science program execution. Observations (i) are archived under program codes M106 and S100. Airglow exposures (ii) are archived with their respective science program codes. They are assigned exposure numbers > 900 to distinguish them from the regular science exposures. For further details, see the **NOTES** in Sections 4.2.1.2, 4.2.1.3, and 4.2.2.1. A separate interface to retrieve airglow data is available at the MAST archive.
NOTE 2: Separate from airglow observations are **sky background** observations, found in programs S405, S505, S605, S705, S805, and S905. The *FUSE* sky backgrounds program started in an attempt to get potentially scientifically useful data during thermalization periods prior to channel alignment activities (when normal science observing could not be done). For programs S405 and S505 targets, the alignment target was placed at the RFPT and thus the "sky" position was a randomly-accessed region roughly an arcminute away (exact position dependent on the roll angle, hence the day of observation). Multiple observations of the same target in these programs thus do not correspond exactly to the same piece of sky, but for diffuse emission it was not expected to matter very much.

Beginning in 2005, after the reaction wheel problems, it became useful to define sky positions in stable regions of the sky, to provide targets for stable pointing when no regular science target was available. Again, the intent was to obtain science data from periods that would otherwise have gone to no good purpose. These include programs S605, S705, S805, and S905. These were all pointed observations, so the given coordinates correspond to the LWRS aperture for these observations. Hence, multiple observations in these programs correspond to the same piece of sky, albeit with a different aperture position angle (which should be negligible).

It is gratifying that these observations have resulted in interesting diffuse background measurements. The reader is referred to Dixon et al. [2006] and references therein.

The alignment scan observations involved stepping a star across the LWRS aperture in each channel. Correlation of photon events with pointing position and reconstruction of a spectrum may be possible. However, in most instances the effective exposure time will be short and the results will not warrant the labor involved.

4.1.3 Notation Convention

Because up to eight spectral files can be produced by a single *FUSE* exposure, and since a single observation can be composed of multiple exposures, we introduce a compressed notation to summarize the different sets of files. In the following, we depict file names as a group of italic and typewriter type faces, as indicated in Table 4.5.

Table 4.5: Notation

Typeface	Group property
italic	variable which depends on a specific file
`typewriter`	always present
`typewriter array {}`	each combination is always present.

Two variables that often appear in the file names are the aperture number $a_n = \{2, 3, 4\}$ (see Table 2.1), and the data collection $mode = \{ttag, hist\}$ (see Section 2.1.7). A target can

also be placed at the reference point (RFPT). In that case, data from the LWRS aperture are extracted and archived by CalFUSE by default, and the files are labeled with the LWRS code, a_n =4.
NOTE: The string "cal" appearing in FITS file names stands for "calibrated" and indicates that the data have been completely processed through CalFUSE; see (Dixon et al. [2007]).

4.2 Contents of the Science Data Files

This section describes the names and contents of the *FUSE* data files. Details of the FITS header keywords are given in Chapter 6.

4.2.1 Exposure-level Files (`*fraw.fit`,`*fcal.fit`,`*fidf.fit`, `*ext.gif`,`*rat.gif`)

CalFUSE creates several data (FITS) and preview (GIF) files for each exposure. We begin with the unprocessed raw data files (`*fraw.fit`) and continue through the various levels of processing. In this case, there are two levels of processing: the extracted spectral files (`*fcal.fit`) and the intermediate data files (`*fidf.fit`).

4.2.1.1 Raw Data Files (`*raw.fit`)

RAW data files contain the unprocessed science data. There is one RAW file for each detector segment. The RAW file names have the following format:

$$\{pppp\}\{tt\}\{oo\}\{eee\}\left\{\begin{array}{c}1\\2\end{array}\right\}\left\{\begin{array}{c}\texttt{a}\\\texttt{b}\end{array}\right\}\left\{\begin{array}{c}\texttt{ttag}\\or\\\texttt{hist}\end{array}\right\}\texttt{fraw.fit}$$

The contents of the RAW TTAG and HIST data files are different. RAW TTAG data are saved as event lists. In the TTAG FITS file, HDU1 is empty, containing only a header, HDU2 contains a list of *time*, X, Y and pulse height amplitude (PHA) for all of the photon events, and HDU3 contains the start and stop times of the Good Time Intervals (GTIs). The time resolution is ordinarily 1 second, but in a few instances the resolution was set to 8ms for diagnostic purposes. Note that in the latter case, the IDS-inserted timestamps don't provide an exact representation of 8ms: the effective LSB is closer to 1/128 second instead of 1/125 second. The result is an apparent periodic irregularity in the count rate. For TTAG, the initial GTI values are copied over from raw data files. By convention, the start value of each GTI corresponds to the arrival time of the first photon in that interval. The stop value is the arrival time of the last photon in that interval plus one second. The length of the GTI is thus STOP − START. For HIST data, a single GTI is generated with start = 0 and stop = the exposure time. These are summarized in Table 4.6.

Table 4.6: Format of Raw Time-Tag Files[a]

FITS Extension	Format	Description
HDU 1: Empty (Header only)		
HDU 2: Photon Event List (binary extension)		
TIME	FLOAT	Photon arrival time (seconds)
X	SHORT	Raw X position (0–16383)
Y	SHORT	Raw Y position (0–1023)
PHA	BYTE	Pulse height (0–31)
HDU 3: Good-Time Intervals (binary extension)		
START	DOUBLE	GTI start time (seconds)
STOP	DOUBLE	GTI stop time (seconds)

[a] Times are relative to the exposure start time, stored in the header keyword EXPSTART.

RAW HIST observations are transmitted from the satellite as images of the portions of the detector selected in the SIA table. Typically, there are two binned images corresponding to the parts of the detector where the specified SiC and LiF apertures fall. The binning is normally 8 in Y, and unbinned in X (with the exception of observations M999 which are binned 2×2 and cover the full detector) and, depending upon the channel, the images are usually 16384 in X, and between 12–20 binned pixels in Y. In addition to these data, the RAW HIST file also contain two 2048×2 images of the regions containing the stim pulses. These are used to determine the amount of drift in the image (see Chapter 2). Table 4.7 summarizes the contents of the RAW HIST data files.

Table 4.7: Format of Raw Histogram Files

FITS Extension	Description	Format
HDU	Contents	Image Size[a] (binned pixels)
1[b]	SIA Table[c]	8×64 – BYTE
2	SiC Spectral Image	$16384 \times (12–20)$ – INT
3	LiF Spectral Image	$16384 \times (12–20)$ – INT
4	Left Stim Pulse	2048×2 – INT
5	Right Stim Pulse	2048×2 – INT

[a] Quoted image sizes assume the standard histogram binning: unbinned in X, by 8 pixels in Y. Actual binning factors are given in the primary file header and keywords SPECBINX, SPECBINY.

[b] Header keywords of HDU 1 contain exposure-specific information.

[c] The SIA table indicates which regions of the detector are included in the file (see Section 2.5.2).

4.2.1.2 Extracted Spectral Files (`*fcal.fit`)

These data are fully calibrated, extracted spectra for each channel and segment. The spectra are extracted only for the science aperture and specified in the keyword APERTURE (see Chapter 6). Note that for TTAG data the other apertures may contain useful information, but one must use the IDF files (see below) to extract them. For HIST data, spectra are only available for the science aperture specified by the observer since the data from the other apertures were not recorded.

Exposure times for TTAG observations can be anything up to the duration of one orbit for objects observed in the Continuous Viewing Zone (CVZ) because spacecraft motions and other time-dependent effects can be corrected in the TTAG photon event list. On the other hand, HIST observations are typically quite short (about 400 s) in order to minimize Doppler smearing by the motion of the spacecraft.

For a single exposure, CalFUSE produces 8 extracted spectra, named as follows:

$$\{pppp\}\{tt\}\{oo\}\{eee\}\left\{\begin{array}{c}1\\2\end{array}\right\}\left\{\begin{array}{c}\texttt{a}\\\texttt{b}\end{array}\right\}\left\{\begin{array}{c}\texttt{lif}\\\texttt{sic}\end{array}\right\}\{a_n\}\left\{\begin{array}{c}\texttt{ttag}\\or\\\texttt{hist}\end{array}\right\}\texttt{fcal.fit}$$

Extracted spectral files have 2 HDUs. HDU1 contains only the header, while HDU2 is a binary extension containing 7 arrays, as described in Table 4.8.

Table 4.8: Format of Extracted Spectral Files

FITS Extension	Format	Description
HDU 1: Empty (Header only)		
HDU 2: Extracted Spectrum (binary extension)		
WAVE	FLOAT	Wavelength (Å)
FLUX	FLOAT	Flux (erg cm^{-2} s^{-1} Å^{-1})
ERROR	FLOAT	Gaussian error (erg cm^{-2} s^{-1} Å^{-1})
COUNTS	INT	Raw counts in extraction window
WEIGHTS	FLOAT	Raw counts corrected for dead time
BKGD	FLOAT	Estimated background in extraction window (counts)
QUALITY	SHORT	Percentage of window used for extraction (0–100)

NOTE: Occasionally, exposures containing airglow emission alone were obtained while executing a science program. To differentiate these data from the science data, the airglow observations were assigned exposure numbers `eee`>900 in the spectral file names. The SRC_TYPE keyword is set to EE, and the following warning is written to the file header: "Airglow exposure. Not an astrophysical target."

4.2.1.3 Intermediate Data Files (`*fidf.fit`)

As processing proceeds, CalFUSE keeps the TTAG data in the form of a photon event list until spectral extraction. HIST data are converted into a pseudo event list in which all photons are

tagged with the same time value for a given exposure. These event lists are stored in IDF files. The IDF file is a FITS file with four HDUs comprised of a header and three FITS binary table extensions (see Table 4.9). A brief description of each HDUs' content is given below. For more details, the user is referred to Appendix B of this document and Dixon et al. [2007].

The first header data unit (HDU1) consists of the header originally copied from the `raw` data file. This header is modified as the IDF goes through the different pipeline steps. This header contains basic information about the proposal, the exposure, the observation, and the calibration as well as engineering and housekeeping data.

HDU2 is a time-tagged list of photon events with their raw X, Y coordinates, weights, and pulse height. Other parameters are set to dummy values at the creation of the IDF file and later modified as the IDF file runs through the pipeline modules.

HDU3 is the list of good time intervals (see Section 4.2.1.1).

HDU4 lists, for each second of an exposure, various engineering parameters from the housekeeping file if present. When the housekeeping file is not present, the time-line event list is filled with best guesses from engineering keywords of the main header (see Chapter 5).

Since the events listed in the IDF files are flagged as "good" or "bad" but never discarded, users can change the event selection criteria without re-running the pipeline. For example, IDF files can be combined to create a higher S/N image for more robust spectral extraction of very faint targets. They can be used to examine the flux and extract spectra in apertures other than the target aperture, or they can be divided into temporal segments to examine the time-dependence of an object. Brief descriptions of how to perform such tasks can be found on the MAST webpage in the document *"FUSE Tools in C"*.

Table 4.9: Format of Intermediate Data Files[a]

FITS Extension	Format	Description
HDU 1: HIST files	BYTE	SIA Table
HDU 1: TTAG files	Empty	Header only
HDU 2: Photon-Event List (binary extension)		
TIME	FLOAT	Photon arrival time (seconds)
XRAW	SHORT	Raw X position (0–16383)
YRAW	SHORT	Raw Y position (0–1023)
PHA	BYTE	Pulse height (0–31)
WEIGHT	FLOAT	Photons per binned pixel for HIST data; initially 1.0 for TTAG data
XFARF	FLOAT	X coordinate in geometrically-corrected frame
YFARF	FLOAT	Y coordinate in geometrically-corrected frame
X	FLOAT	X coordinate after motion corrections
Y	FLOAT	Y coordinate after motion corrections
CHANNEL	BYTE	Aperture+channel ID for the photon (Table 4.10)
TIMEFLGS	BYTE	Time flags (Table 4.11)
LOC_FLGS	BYTE	Location flags (Table 4.12)
LAMBDA	FLOAT	Wavelength of photon (Å)
ERGCM2	FLOAT	Energy density of photon (erg cm^{-2})
HDU 3: Good-Time Intervals (binary extension)		
START	DOUBLE	GTI start time (seconds)
STOP	DOUBLE	GTI stop time (seconds)
HDU 4: Time-Line Table (binary extension)		
TIME	FLOAT	Seconds from exposure start time
STATUS_FLAGS	BYTE	Status flags
TIME_SUNRISE	SHORT	Seconds since sunrise
TIME_SUNSET	SHORT	Seconds since sunset
LIMB_ANGLE	FLOAT	Limb angle (degrees)
LONGITUDE	FLOAT	Spacecraft longitude (degrees)
LATITUDE	FLOAT	Spacecraft latitude (degrees)
ORBITAL_VEL	FLOAT	Component of spacecraft velocity in direction of target (km/s)
HIGH_VOLTAGE	SHORT	Detector high voltage (digital units)
LIF_CNT_RATE	SHORT	LiF count rate (counts/s)
SIC_CNT_RATE	SHORT	SiC count rate (counts/s)
FEC_CNT_RATE	FLOAT	FEC count rate (counts/s)
AIC_CNT_RATE	FLOAT	AIC count rate (counts/s)
BKGD_CNT_RATE	SHORT	Background count rate (counts/s)
YCENT_LIF	FLOAT	Y centroid of LiF target spectrum (pixels)
YCENT_SIC	FLOAT	Y centroid of SiC target spectrum (pixels)

[a] Times are relative to the exposure start time, stored in the header keyword EXPSTART. To conserve memory, floating-point values are stored as shorts (using the FITS TZERO and TSCALE keywords) except for TIME, WEIGHT, LAMBDA and ERGCM2, which remain floats.

4.2.1.3.1 Corrupted Data

Occasionally, photon arrival times in raw TTAG data files are corrupted. When this happens, some fraction of the photon events have identical, usually large TIME values, and the good-time intervals (GTI) contain an entry with START and STOP set to the same large value. The longest valid exposure spans 55 ks. If an entry in the GTI table exceeds this value, the corresponding entry in the timeline table is flagged as bad using the "photon arrival time unknown" flag; (see Dixon et al. [2007]). Bad TIME values less than 55 ks will not be detected by the pipeline.

Raw HIST files may also be corrupted. OPUS fills missing pixels in a HIST image with the value 21865. The pipeline sets the WEIGHT of such pixels to zero and flags them as bad. This is done by setting the photon's "fill-data bit" (see Dixon et al. [2007]). Single bit-flips are corrected on-board, but occasionally a cosmic ray will flip two adjacent bits. Such double bit-flips are not detected by the correction circuitry, producing (for high-order bits) a "hot pixel" in the image. The pipeline searches for pixels with values greater than 8 times the average of their neighbors, and masks out the higher-order bits.

One or more image extensions may be missing from a raw HIST file. If no extensions are present, the keyword EXP_STAT in the IDF header is set to -1. Exposures with non-zero values of EXP_STAT are processed normally by the pipeline, but are not included in the observation-level spectral files ultimately delivered to MAST. Though the file contains no data, the header keyword EXPTIME is not set to zero.

4.2.1.3.2 Airglow Observations

When creating the IDF files for bright-earth observations (programs M106 and S100) or 900-level airglow exposures, CalFUSE sets the header keyword EXP_STAT = 2. For 900-level exposures, the SRC_TYPE is set to EE, and the following warning is written to the file header: "Airglow exposure. Not an astrophysical target." The pipeline then processes the file as usual. In particular, the limb-angle flag is set in the timeline table (extension 3 of the IDF), and the "Time with low limb angle" is written to the file header. However, the following things change:

- no jitter correction is performed;
- when the time-dependent flags are copied from the timeline table to the individual photons, the limb-angle flag is masked out; and
- when the good-time intervals and exposure time are calculated, the limb-angle flag is ignored.

The extracted spectra include photons obtained at low limb angles. The detector-image plots (`*spec.gif`) do, too. But the count-rate plots (`*ext.gif; *rat.gif`) still indicate times when the line of sight passed below the nominal limb-angle limit.

Table 4.10: IDF Channel Array Aperture Codes

Aperture	LiF	SiC
HIRS	1	5
MDRS	2	6
LWRS	3	7
Not in an aperture		0

Table 4.11: Bit Codes for IDF Time Flags[a]

Bit	Value
8	User-defined bad-time interval
7	Jitter (target out of aperture)
6	Not in an OPUS-defined GTI *or* photon arrival time unknown
5	Burst
4	High voltage reduced
3	SAA
2	Limb angle
1	Day/Night flag (N = 0, D = 1)

[a] Flags are listed in order from most- to least-significant bit.

Table 4.12: Bit Codes for Location Flags[a]

Bit	Value
8	Not used
7	Fill data (histogram mode only)
6	Photon in bad-pixel region
5	Photon pulse height out of range
4	Right stim pulse
3	Left stim pulse
2	Airglow feature
1	Not in detector active area

[a] Flags are listed in order from most- to least-significant bit.

4.2.1.4 Preview Files (`*rat.gif, *ext.gif`)

Two types of exposure-level diagnostic preview files are available, and both serve as useful tools to verify the integrity of spectra derived from the exposure.

`*rat.gif`: These files display the count rate throughout the exposure (see Fig. 4.3). For TTAG data, this is the actual count rate for events occurring within the region of the detector corresponding to the target aperture (excluding airglow features) evaluated every second. For HIST data, these are the dead time corrected counter data from the time engineering files (housekeeping file, see Section 5.2), which are sampled once every 16 seconds (see Table 4.9). For non-variable objects, these are useful diagnostics, since they enable the user to determine whether the target remained within the aperture throughout the exposure.

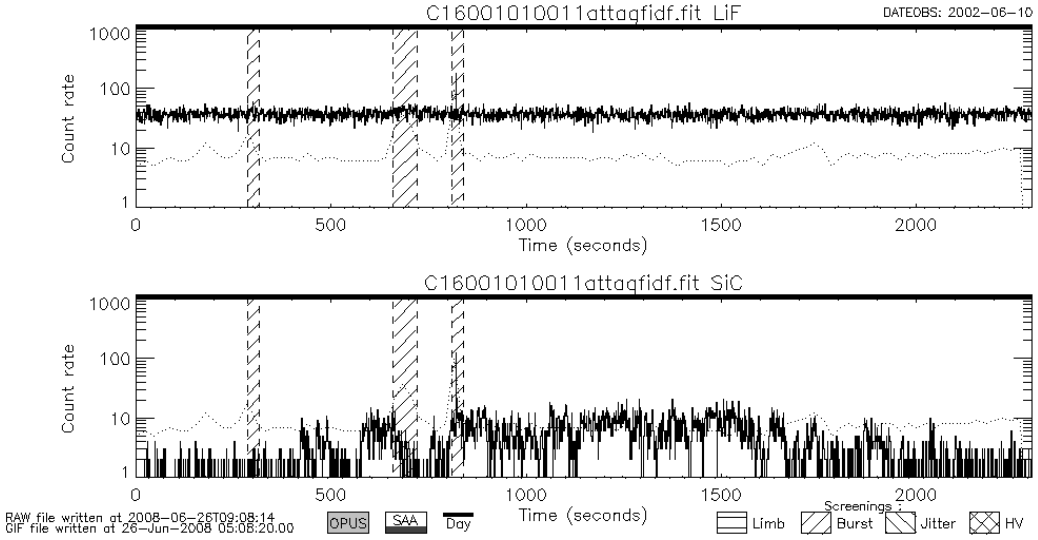

Figure 4.3: *Example of a count rate plot (`*rat.gif`) for detector segment 1A of exposure 001 for the TTAG observation C1600101. These plots show the count rates within the science apertures. The various reasons for flagging bad data are shown below the figure. The dashed curve is the count rate from the sections of the detector used for burst detection. In this case, the plot shows that the observation was obtained during the day, and that several bursts were detected and eliminated from the final spectrum. It also shows that the SiC1A count rate varied significantly during the observation. Because the same plot for LiF1A is stable, we conclude that the target was wandering in and out of the SiC1 aperture (see Chapter 7). As a result, the flux level of the SiC1A spectrum will be less than other channels covering similar wavelengths (see Fig. 4.7). CalFUSE cannot check for this effect since different segments are processed independently and cannot be compared. However, users can use the FUSE tools to exclude these regions (see Chapters 3 and 8).*

*ext.gif: These files show a calibrated image of the detector, corrected for geometric thermal distortions and spacecraft and instrumental motions. The appearance of these images depends on whether the exposure was TTAG or HIST observation (see Figs. 4.4 and 4.5). These plots only display the data from the "good time" intervals. *Warning*: if all of the data are flagged as bad, then, instead of producing an empty plot, all of the data are plotted. Therefore, users are recommended to systematicaly check the count rate plots first.

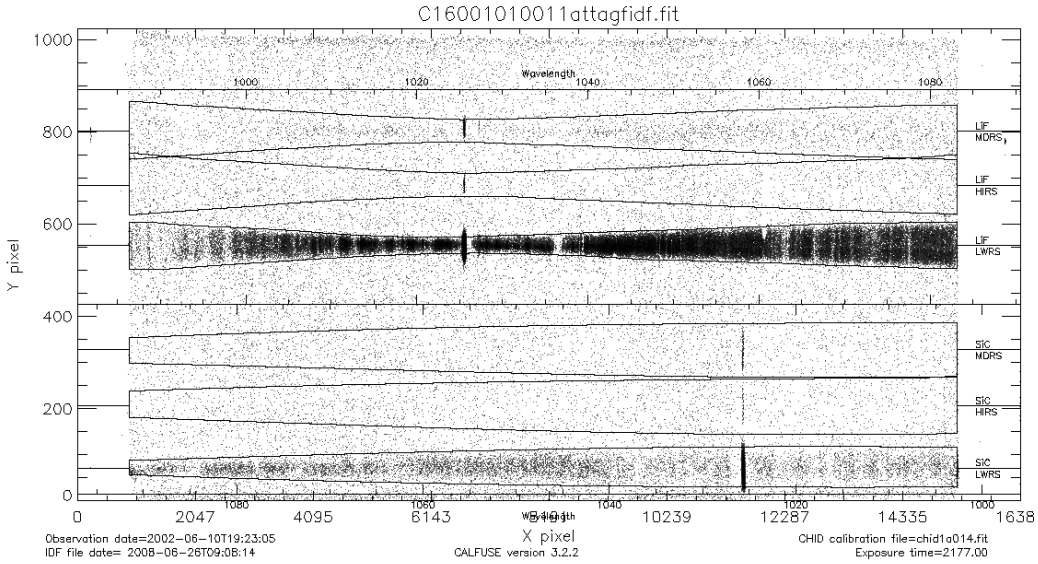

Figure 4.4: *Example of a detector image (*`*ext.gif`*) for the same segment as shown in Figure 4.3 for a target in the LWRS aperture. This image is made from the IDF file and has been geometrically corrected for instrumental effects. It is not to scale since the actual detector has a 16:1 aspect ratio. Both pixel and wavelength scales are shown, as are the locations of the spectra from the different apertures on the segment. In the TTAG data, the effect of the different aperture sizes on airglow line intensity is clearly apparent. The vertical lines appearing at Lyman β in both spectra are due to airglow emission. Some of the airglow emission falls outside of the extraction window because it is an extended emission. Note that the colors are reversed so that absorption features appear as bright stripes and emission features appear as dark stripes.*

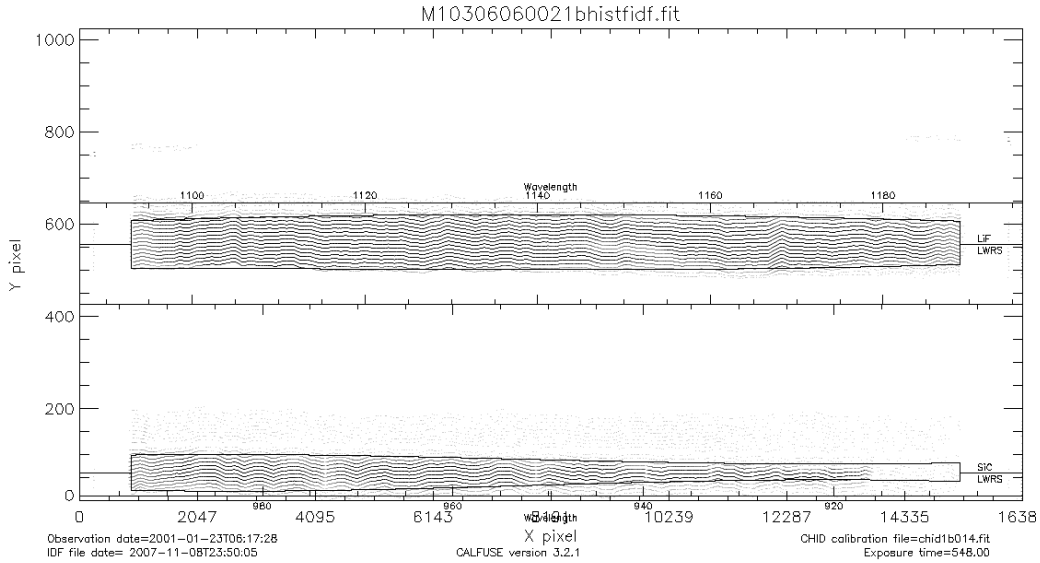

Figure 4.5: *Similar to Fig. 4.4, except for the 1B segment of the HIST observation M1030606002. In this case, the data have a striped appearance. This is because the raw HIST image is binned in Y, and the pipeline simply maps all of events registered by a binned pixel onto the mean value of the bin. This results in rows of filled pixels, separated by several rows of vacant pixels. The rows in this image are curved because they have been corrected for geometric distortions. The top part of the plot is an image of the LiF1B segment. The elongated white stripe in LiF1 near 1150 Å in this segment is due to the "worm" (see Section 7.5). For HIST, data are only collected from the region around the science aperture, LWRS in this case. So no data are seen on most of the segment. Note that the colors are reversed so that absorption features appear as bright stripes and emission features appear as dark stripes.*

4.2.1.5 Trailer Files (`*.trl`)

The trailer files contain run-time information for all pipeline modules. They also list any warnings that these modules may have generated. The "Intermediate" and "Advanced" users will want to look at the trailer files before using any data. A trailer file is produced for each detector segment that is processed and its name has the following form:

$$\{pppp\}\{tt\}\{oo\}\{eee\}\left\{\begin{array}{c}1\\2\end{array}\right\}\left\{\begin{array}{c}\texttt{a}\\\texttt{b}\end{array}\right\}\left\{\begin{array}{c}\texttt{ttag}\\\texttt{hist}\end{array}\right\}\texttt{f.trl}$$

If all modules of the CalFUSE pipeline are executed without anomaly then the trailer file for each detector segment will look like the example given below in file D06403010011bttagf.trl.

2007 Aug 21 03:47:30 calfuse.csh-1.15: Begin TTAG file D06403010011bttagfraw.fit
cf_ttag_init-1.41: This is CalFUSE v3.2.1
cf_timeline-1.41: Housekeeping file exists: using it to fill timeline.

2007 Aug 21 03:47:35 cf_ttag_init-1.41: Finished processing

2007 Aug 21 03:47:37 cf_convert_to_farf-1.21: Finished processing

2007 Aug 21 03:47:39 cf_screen_photons-1.28: Finished processing

2007 Aug 21 03:47:40 cf_remove_motions-1.41: Finished processing

IDL Version 6.1.1, Solaris (sunos sparc m32). (c) 2004, Research Systems, Inc.

Compiled module: CF_PLOT_RATE3.

IDL Version 6.1.1, Solaris (sunos sparc m32). (c) 2004, Research Systems, Inc.

Compiled module: CF_PLOT_EXTRACT3.

2007 Aug 21 03:47:47 cf_assign_wavelength-1.15: Finished processing

2007 Aug 21 03:47:47 cf_flux_calibrate-1.12: Finished processing

2007 Aug 21 03:47:48 cf_bad_pixels-1.38: Finished processing
cf_standard_or_optimal_extraction-1.7: Attempting optimal extraction.
cf_scale_bkgd-1.25: Background count too small for a detailed fit.
cf_scale_bkgd-1.25: Assuming an intrinsic count rate of 3.3 cts/s

2007 Aug 21 03:48:06 cf_extract_spectra-1.32: Finished processing

2007 Aug 21 03:48:06 calfuse.csh-1.15: End TTAG file D06403010011bttagfraw.fit

---

When rerunning CalFUSE, the content of the trailer file can be extended simply by changing the "verbose" level in the CalFUSE parameter file. By default, the verbose level is set to 1. Table 4.13 gives a short description of the verbose levels available to the users who wish to rerun CalFUSE ("Advanced" level) along with corresponding examples of CalFUSE messages.

Table 4.13: Trailer File Verbosity

Verbose Level:	0
Type	Minimal trailer file
Messages	Lists only warning and error messages; Provides full time/program/version information
Example	2003 Mar 21 10:01:01 cf_ttag_init-1.12: WARNING - Detector voltage is high
Verbose Level:	1 (Default)
Type	Standard trailer file
Messages	Lists all decisions made by the pipeline; Output from cf_timestamp when printing "Finished Execution"; Provides program/version information for other modules
Example	cf_timeline-1.1: Housekeeping file exists - use it to fill timeline. 2003 Mar 21 14:44:37 cf_timeline-1.1: Finished execution
Verbose Level:	2
Type	Verbose trailer file
Messages	Lists calls to cf_timestamp when printing "Begin execution" and "Finished execution" for all routines. Lists values calculated by the pipeline. Output from cf_timestamp has the Level 0 format; other entries are simply indented.
Example	2003 Mar 21 14:44:37 cf_timeline-1.1: Begin execution State vector at MJD= 52577.192924 days x= 6712.928955 y= 106.584626 z= -2409.340612 km vx= 0.557736 vy= 7.210211 vz= 1.901099 km/s Number of samples in the HK file = 329 2003 Mar 21 14:44:37 cf_timeline-1.1: Finished execution
Verbose Level:	3
Type	Debugging mode
Messages	Lists milestones in each subroutine. Lists calibration files (especially when recorded elsewhere).
Example	Correcting y centroid Reading background calibration files Housekeeping file = M1070312001hskpf.fit Background calibration file = bkgd1a009.fit

Note that verbose level N includes all information from level N−1 in addition to what is listed in the Table. If a user chooses to rerun CalFUSE, occasional error and warning messages might appear in the trailer files if a pipeline module fails to run successfully. Appendix C lists the warning messages along with a short description of the problems likely to cause them. The error messages are self-explanatory.

4.2.2 Observation-level Data Files (`*all*.fit, *ano*.fit, *nvo*.fit`)

Observation-level files combine all of the individual exposures for each specific set of channel (LiF1, LiF2, SiC1 or SiC2) and segment (A, B). The result is 8 independently obtained combined spectra with considerable wavelength overlap. These overlapping regions provide redundancy in spectral coverage in order to assess the consistency of the data and look for anomalies (see Chapter 7).

4.2.2.1 ALL and ANO Files

The two observation-level combined files are the ALL files, which contain all of the data for a particular observation, and the ANO (All Night Only) files, which contain only data obtained during orbital night. The former give the highest signal-to-noise for instances where airglow is not an issue, and the latter provide the best possible signal-to-noise with minimum airglow contamination (see Chapter 7).

For each combination of detector segment and channel (LiF1A, SiC1A, etc.), the pipeline combines data from all exposures constituting one observation into separate extensions in a single ALL file. The combination results from cross-correlating and shifting the individual exposures over the 1000-1100 Å overlap range. While the ALL files are well-suited for basic feature searches, **they are not optimized for science purposes**. The "Intermediate" and "Advanced" users are strongly advised to perform the spectral combinations carefully and as most appropriate to their science goals.

Each ALL file extension has 3 arrays: WAVE, FLUX and ERROR (see Table 4.14). For instance, the first extention of the ALL file contains the combined LiF1A data for a given observation. For each channel, the shift calculated for the detector segment spanning 1000–1100 Å is applied to the other segment as well. If the individual spectra are too faint for cross correlation, the individual Intermediate Data Files (IDF) images are combined and a single spectrum is extracted from the combined IDFs (see Section 4.2.1.3).

The ANO files are identical to the ALL files, except that the spectra are constructed using data obtained during the night-time portion of each exposure only. They are generated only for TTAG data, and only if part of the exposure occurs during orbital night. The shifts calculated for the ALL files are applied to the ANO data and not recomputed. These data are essential to identify airglow emission and to minimize their effect on overlapping stellar and/or interstellar

features (see Chapter 7).

The ALL and ANO file names have the following structure:

$$\{pppp\}\{tt\}\{oo\}\{\texttt{00000}\}\left\{\begin{array}{c}\texttt{all}\\ \texttt{ano}\end{array}\right\}\{a_n\}\left\{\begin{array}{c}\texttt{ttag}\\ or\\ \texttt{hist}\end{array}\right\}\texttt{fcal.fit}$$

Examples are:

`D064030100000all4ttagfcal.fit, E511220100000ano2ttagfcal.fit`

The first is the ALL file for LWRS ($a_n = 4$), TTAG ($mode =$ `ttag`) data with for program $pppp$ = D064, target number $tt = 03$, observation ID $oo = 01$. The second is an ANO file for MDRS aperture ($a_n = 2$), TTAG ($mode =$ `ttag`) with program $pppp$ = E511, target number $tt = 22$, observation ID $oo = 01$.

NOTE: For dedicated airglow observations in programs M106 and S100, all of the data are included in the observation-level ALL, ANO, and NVO files (see below). For all other programs, 900-level airglow exposures are *excluded* from the sum. A single preview plot showing the summed spectrum from all of the 900-level exposures in the observation is produced with a name like M112580100000airgttagf.gif.

NOTE: The cataloging software used by MAST requires the presence of an ALL file for each exposure, in addition to the *observation*-level ALL file. Therefore, *exposure*-level ALL files are also generated, but they contain no data, only a FITS file header. The *observation*-level ALL files are distinguished by the string "00000all" in their names.

Table 4.14: Format of observation-level ALL *and* ANO Spectral Files

FITS Extension	Format	Description
HDU 1: Empty (Header only)		
HDU 2: Mean LiF1A Extracted Spectrum (binary extension)		
WAVE	FLOAT	Wavelength (Å)
FLUX	FLOAT	Flux (erg cm^{-2} s^{-1} Å^{-1})
ERROR	FLOAT	Gaussian error (erg cm^{-2} s^{-1} Å^{-1})
HDU 3: Same as **HDU2** for mean LiF1B Spectrum		
HDU 4: Same as **HDU2** for mean LiF2B Spectrum		
HDU 5: Same as **HDU2** for mean LiF2A Spectrum		
HDU 6: Same as **HDU2** for mean SiC1A Spectrum		
HDU 7: Same as **HDU2** for mean SiC1B Spectrum		
HDU 8: Same as **HDU2** for mean SiC2B Spectrum		
HDU 9: Same as **HDU2** for mean SiC2A Spectrum		

4.2.2.2 Preview Files (`*00000*.gif, *spec*.gif, *nvo*.fit`)

Coadded Detector Spectra (`*00000*.gif`)

The ALL files are used to generate a set of flux plots for the 4 channels of each observation. These files have names of the type D0640301000000lif1ttagf.gif or D0640301000000lif2ttagf.gif, etc.

Figures 4.6 and 4.7 show preview plots for the SiC1 (*left*) and LiF1 (*right*) channels of observations D0640301 and C1600101, respectively. Notice that even though the wavelength coverage of SiC1A and LiF1A have considerable overlap, they may have significantly different flux levels, as is the case for observation C1600101. Discrepancies of this type are common in *FUSE* data and usually indicate that the source was either partly or completely out of the aperture of one channel during part of the observation. Hence, the data obtained for the guiding channel are always the most reliable. With very few exceptions, LiF1 was the guiding channel before 12 July 2005, and LiF2 thereafter (see Table 2.3). These figures demonstrate the value of the diagnostic files for identifying systematic effects (see also Fig. 4.3 and Section 4.2.1.4).

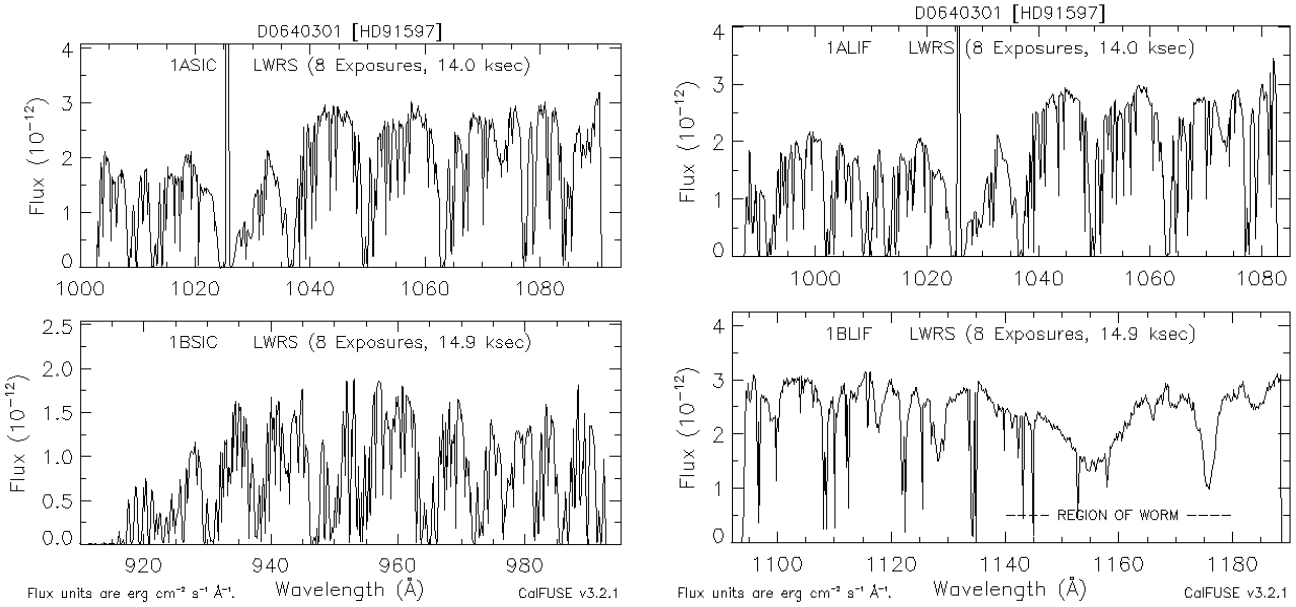

Figure 4.6: *Examples of coadded detector spectra for two channels of observation D0640301. These plots are for both segments of the SiC1 (left) and LiF1 (right) channels. Note that total exposure times for each segment can be different, since CalFUSE may eliminate different portions of the data for each segment from the final spectra due to its detection of various anomalies (see Chapter 7).*

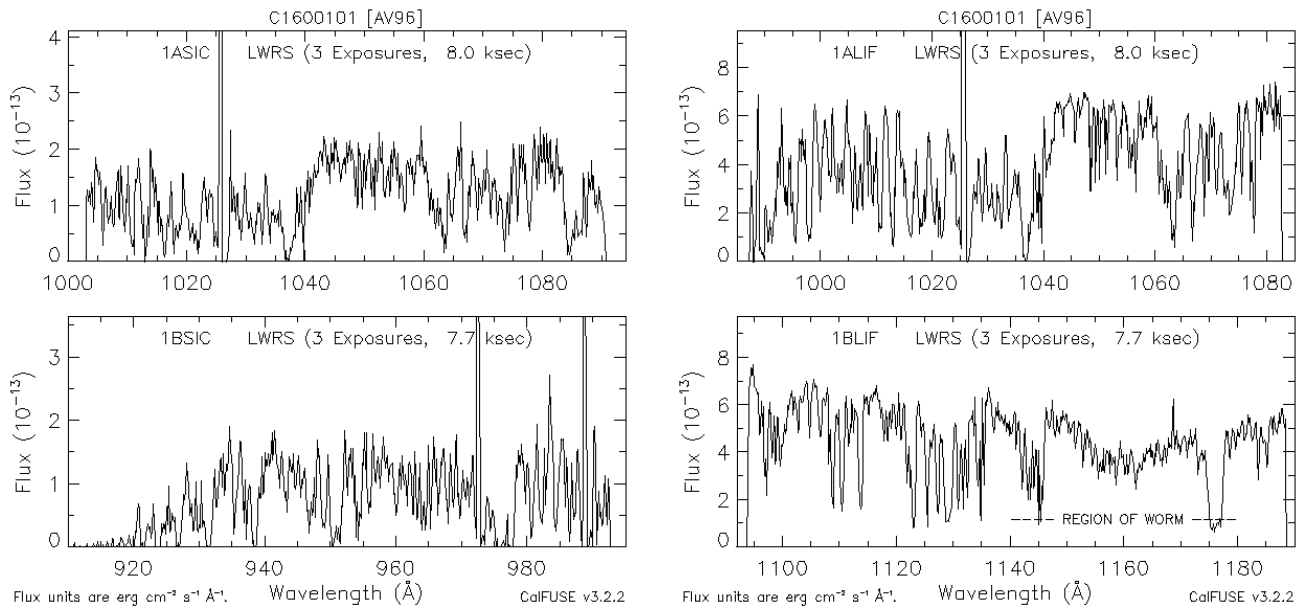

Figure 4.7: *Examples of coadded detector spectra for two channels of observation C1600101. These plots are for both segments of the SiC1 (left) and LiF1 (right) channels. Note the difference in flux level over the wavelength range common to both channels. Such discrepancies usually indicate that the target was either partly or completely out of the aperture of one channel during part of the observation.*

Preview Spectra (`*spec*.gif`)

These spectral plots are generated from the ALL files for the channels exhibiting the highest S/N in the 900–1000, 1000–1100 and 1100–1200 Å regions and thus offer a quick look at the entire *FUSE* wavelength range for a given observation. These are the preview files presented by MAST when *FUSE* data are queried. Figure 4.8 displays the preview file D064030100000specttagf.gif for observation D0640301.

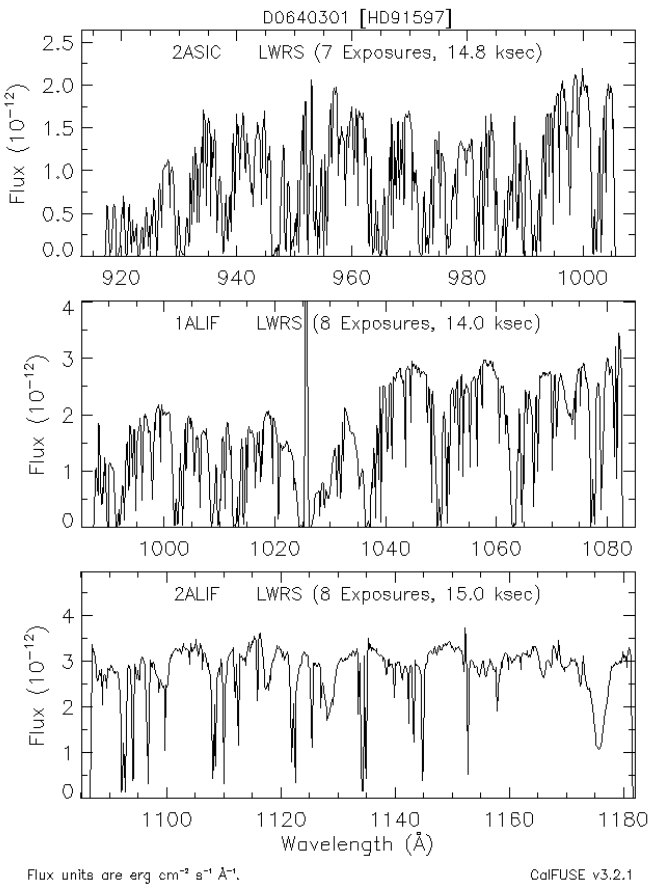

Figure 4.8: *Example of a combined, observation-level preview file for observation D0640301. The image presents spectra from three segments that span the FUSE wavelength range. It also contains the number of exposures that were combined and the total observation time of the combined exposures. Note that the total exposure time as well as the number of exposures can be different for each segment since CalFUSE processing may eliminate portions of the data affected by various effects or anomalies (see Chapter 7).*

Summed Exposures (`*nvo*.fit`)

One National Virtual Observatory (NVO) file is generated for each observation. This file contains one single spectrum spanning the entire *FUSE* wavelength range ($905 \leq \lambda \leq 1187$Å). The spectrum is assembled by cutting and pasting segments from the ALL file using the channel with the highest signal-to-noise (S/N) ratio at each wavelength. Segments are shifted to match the guide channel (either LiF1 or LiF2) between 1045 and 1070Å.

Warning: While these NVO spectra form a convenient overview of each data set, their direct use for scientific analysis is not encouraged without detailed checking. Because of possible channel drifts, the target may have been outside of one or more apertures for some fraction of the observation. Not only might the resulting spectrum be non-photometric, but the photometric error may be wavelength-dependent, because of the way that the NVO files

are constructed. It is thus recommended that users examine the count-rate plots (see Section 4.2.1.4) for the individual exposures before accepting the NVO file at face value.

Additionally, cross-correlation may fail, even for the spectra of bright objects, if they lack strong, narrow spectral features. Examples are nearby white dwarfs with weak interstellar absorption lines. If cross-correlation fails for a given exposure, that exposure is excluded from the sum. Thus, the exposure time for a particular segment in an NVO file may be less than the total exposure time actually available for a given observation.

NVO data files contain columns with WAVE, FLUX, and ERROR stored in a single binary table extension (see Table 4.15). Figure 4.9 shows the NVO spectrum of observation D0640301 for target HD91597, with corresponding filename: D064030100000nvo4ttagfcal.fit.

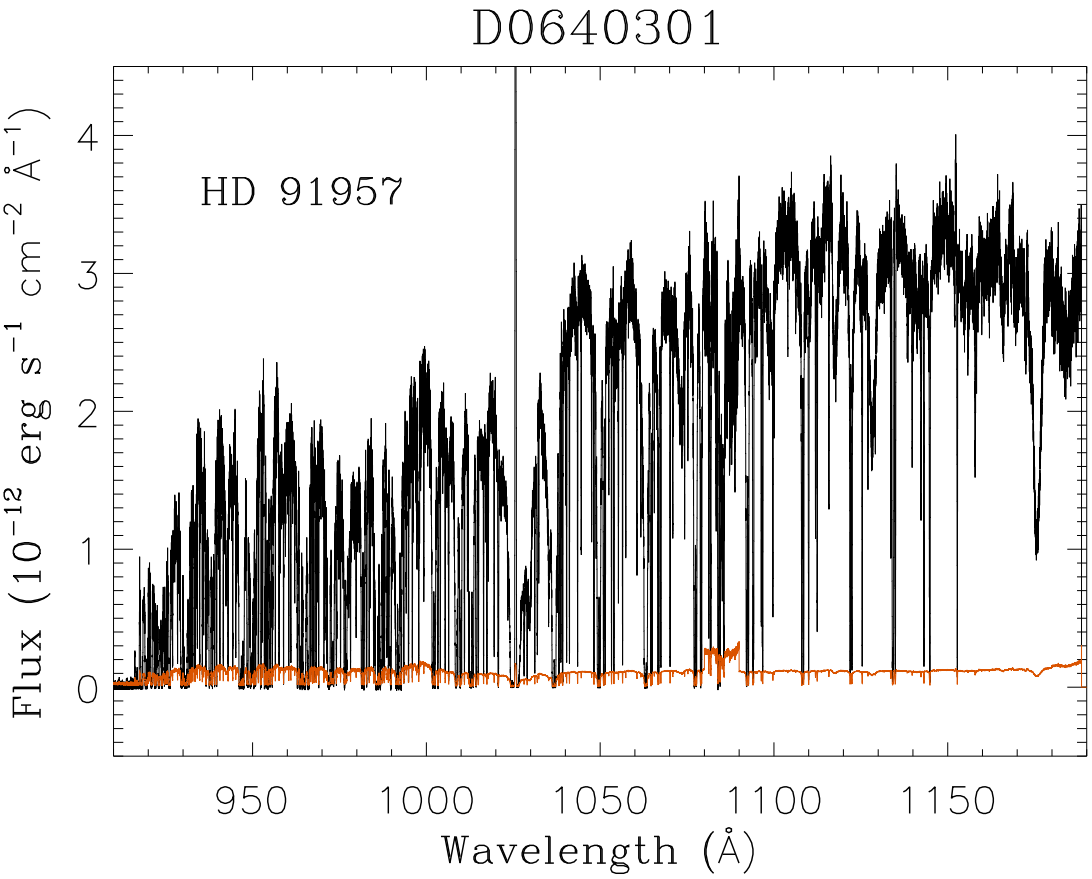

Figure 4.9: *Plot of an exposure-summed spectrum (black trace) and its associated error array (red trace) for observation D0640301 (*`*nvo.fit`*). The error array contains sharp discontinuities due to the fact that the data from different segments have been spliced together to form this overview spectrum.*

Table 4.15: Format of NVO Spectral Files

FITS Extension	Format	Description
HDU 1: Empty (Header only)		
HDU 2: Extracted Spectrum (binary extension)		
WAVE	FLOAT	Wavelength (Å)
FLUX	FLOAT	Flux (erg cm^{-2} s^{-1} $Å^{-1}$)
ERROR	FLOAT	Gaussian error (erg cm^{-2} s^{-1} $Å^{-1}$)

Chapter 5

Ancillary Files

This section describes additional data files available from the *FUSE* archive that can be used to support the analysis and understanding of *FUSE* data. Some of these data files were used by CalFUSE to produce the calibrated data products, and others contain information which can be used to verify the pointing, performance, or status of the satellite or instrument during data acquisition.

This chapter contains information potentially useful to the "Advanced" and "Intermediate" users. However its contents are not of immediate relevance to the "Casual" user. The file naming convention used throughout this chapter has been described in Section 4.1.2.

5.1 FES Image Files (`*fesfraw.fit, *fesfcal.fit`)

Two nearly identical Fine Error Sensor (FES) cameras were available on *FUSE*. FES A was prime for most of the mission, and observed the LiF1A FPA. FES B became prime on 12 July 2005 and was used for the remainder of the mission. It observed the LiF2A FPA. Because the two cameras are on opposite sides of the instrument, the astronomical orientation in the images will appear flipped with respect to each other. Referring to the guide star plots for a given observation will provide confirmation of the expected astronomical orientation and star field expected for a given target (see Section 5.6 below).

An image from the active FES camera was routinely acquired at the end of an observation to allow verification of the pointing of the spacecraft. Depending on the phase 2 observing proposal instructions provided by the user, this FES image would be obtained either with the target in the observing aperture or at the reference point (55.18″ from the HIRS aperture, displaced towards the center of the FES field of view; see Fig. 2.2). By convention, this exposure always has exposure ID 701, which is used to distinguish this image from acquisition images.

Other FES images were obtained throughout each observation during the initial guide star acquisition and subsequent reacquisitions (usually after the target had been occulted). These images are also stored and are available to the observer, although the target may be offset or even absent in these images (e.g. if the target had drifted during occultation, etc.). These

images have observation IDs and exposure IDs identical to the those used for the associated (usually directly following) FUV exposure. After the gyroless target acquisition software was loaded, it was routine to obtain multiple images during each acquisition, and also during reacquisitions resulting from loss of pointing stability. Each of the resulting images is stored in a separate extension in the FITS file. For most users, the final "end-of-observation" FES image (exposure 701) will be the only image of interest.

The active image area of the FES CCD images was 512×512 pixels, with pixel size of $2.55''$. An unbinned image has 8 rows and 8 columns of overscan, resulting in a 520×520 raw image. These are the sizes for the FES images obtained at the end of each exposure. Binned images also have binned overscan, so a 2×2 binned image will have size 260×260 pixels. After the gyroless target acquisition software was loaded, 4×4 binned images were routinely obtained during acquisitions in addition to 2×2 binned images, resulting in a size of 130×130 pixels.

The raw data (*fesfraw.fit files) are stored as unsigned integers in FITS extensions. The calibrated FES images (*fesfcal.fit images) are processed by stripping the overscan areas, and subtracting the bias level. Distortion maps of each FES camera were made and used onboard by the guidance system, but distortion corrections were *not* part of the calibration pipeline process, and so the calibrated images have not had this correction applied. Distortions are generally small, however. The calibrated data values are 4-byte floating-point numbers.

Figure 5.1 shows an example of a 512×512 FES A image. Note that the apertures are near the top of the image along the line defined by $Y_{FES} = 399$ (see Table 5.2. Once again, users will find the guide star plots (see Section 5.6) useful for verifying the astronomical orientation expected for a given observation.

The contents of an FES file are listed in Table 5.1 and the locations of the apertures in pixels coordinates are listed in Table 5.2 for both FES A and B at the nominal LiF FPA positions. Details of the distortion corrections and the conversion of FES pixel coordinates to sky coordinates are provided in Section 8 of the *FUSE Instrument Handbook (2009)*.

Table 5.1: Formats of Raw and Calibrated FES Image Files[a]

FITS Extension	Format	Description
HDU 1: Empty (Header only)		
HDU 2: FES Image[a]		
IMAGE	SHORT	COUNTS

[a] Image size can be either 520×520, 260×260 or 130×130.

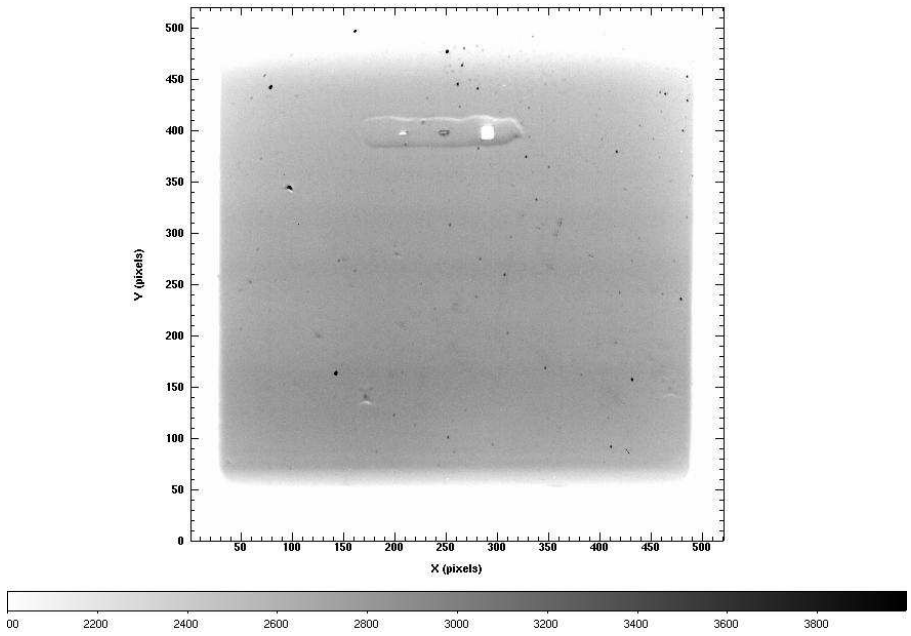

Figure 5.1: *A calibrated FES A image for exposure P1171901701. In this case, there is significant scattered light on the FPA, so that the apertures are visible (see Table 5.2), along with a few stars. (The distorted region around the apertures is an artifact of the manufacturing process.) Note that the colors are reversed in this image so that bright objects appear as black points.*

Table 5.2: Aperture Centers (1× 1 binning)

	FES A		FES B	
Slit	X	Y	X	Y
MDRS	207	399	292	426
HIRS	247	399	252	425
LWRS	289	399	209	425

5.2 Time-Resolved Engineering Files (`*jitrf.fit`, `hskpf.fit`)

Jitter Files (`*jitrf.fit`): At launch, the pointing stability of *FUSE* was approximately 0.3″ in the science X and Y axes. Since this is considerably smaller than the instrumental PSF, guiding performance was not an issue for observing. However, as the mission progressed, problems with the Attitude Control System (see Table 2.3) required magnetic torquer bars and magnetometers be used to help control the pointing. The ability of the torquer bars to stabilize the spacecraft depended on their orientation relative to the direction of the instantaneous

Earth's magnetic field, which was a function of orbital position. As a result, large, rapid pointing deviations caused by temporary loss of pointing control could cause the target to move about in the aperture or leave it completely for part of an exposure. Figures 5.2 and 5.3 show examples of pointing performance and its effects on the *FUSE* count rates.

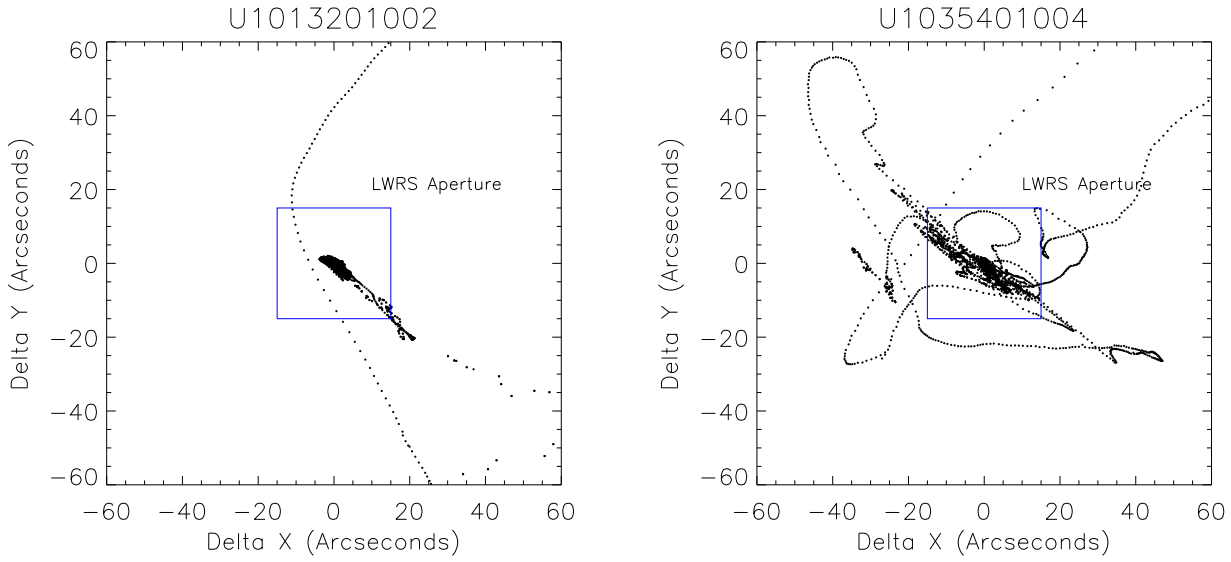

Figure 5.2: *FUSE pointing in 1 second intervals for an exposure scheduled with stable pointing (left) and one with unstable pointing (right). For the former case, loops outside of the LWRS aperture occur while settling during the target acquisition. The target remains well-centered for the exposure. For the case with unstable pointing, excursions can take the target out of the aperture, but the target returns when pointing control is regained.*

The orientation of the telescope is described by a four-element quaternion. The spacecraft produced two sets of pointing estimates. The first was derived from the measured positions of two to six guide stars; these are referred to as the FPD (for Fine Pointing Data) quaternions. The second combines guide-star data with data from the gyroscopes and magnetometers. Since they are generated by the onboard ACS (Attitude Control System) computer, they are referred to as the ACS quaternions, although the former are not always available. The guide stars are generally more accurate than the gyroscopes and magnetometers, so the FPD quaternions are generally more accurate than the ACS estimates. The commanded quaternions for the target can be found from the telemetry stream or computed from the RA and DEC in the FITS file header (see the *Instrument Handbook 2009*, for more details).

The jitter data files contain time-resolved data of the spacecraft pointing relative to the commanded pointing and are used by CalFUSE to correct for these effects. These data are derived from the housekeeping files. This file is a binary table (see Table 5.3) with 1 s time resolution, and contains the following four variables:

TIME is the time in seconds since the science exposure start time (DATEOBS and TIMEOBS keywords in the jitter header).

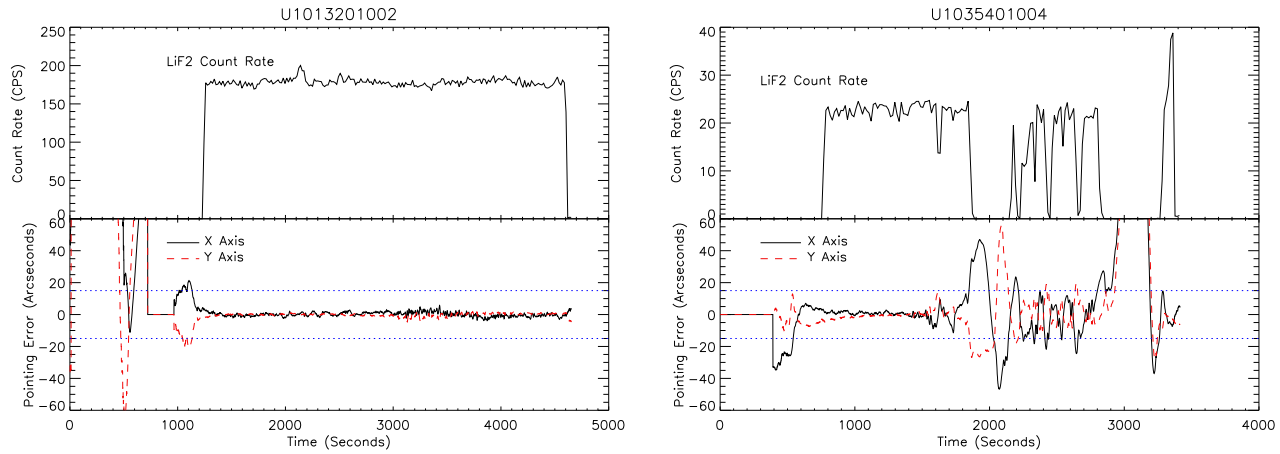

Figure 5.3: *The time series of LiF2 count rates and pointing errors for the exposures shown in Fig. 5.2. For the one with stable pointing (left), the target remains well within the aperture and the count rate is constant during the exposure. For the other, when control becomes unstable, photons are lost when the target is out of the aperture (right).*

DX,DY represent the difference in position between the telescope and the target in arcseconds along the science instrument X and Y axes.

TRKFLG is the tracking-quality flag. Its value ranges from 5 to -1, representing decreasing levels of fidelity for DX and DY: 5 means they were calculated from the FPD quaternions and the commanded quaternions extracted from the telemetry stream; 4 indicates they were calculated from the ACS quaternions and the commanded quaternions; 3 indicates they were calculated from a less-reliable state of the ACS and the commanded quaternions; 2 indicates they were calculated from the FPD quaternions and the target coordinates from the FITS header; 1 indicates they were calculated from the ACS quaternions and the target coordinates from the FITS header; 0 indicates that tracking information is unavailable; -1 indicates that the spacecraft never achieved known tracking, so the pointing is assumed to be bad.

Table 5.3: Format of Jitter Files[a]

FITS Extension	Format	Description
HDU 1: Empty (Header only)		
HDU 2: Pointing Data (binary extension)		
TIME	FLOAT	(seconds)
DX	FLOAT	ΔX position (arcsec)
DY	FLOAT	ΔY position (arcsec)
TRKFLG	SHORT	Quality Flag

[a] Sampled once per second, and dimension set length of the exposure.

Housekeeping Files (`*hskpf.fit`): In addition to providing inputs for the calculation of jitter parameters and the evaluation of pointing quality, the housekeeping files contain time-resolved

engineering data used by CalFUSE to correct science data for instrument or pointing problems during exposures.

The housekeeping files are produced by the *FUSE* OPUS HSKP process from files of telemetry extracted from the *FUSE* telemetry database for each science exposure (TTAG or HIST). The time period included in the telemetry files begins 0.5–1.0 minutes before the science exposure and ends 1.0 minute after the science exposure ends, to ensure that all the necessary information is included.

A brief description of the contents of housekeeping file is given in Appendix D. The data are stored in a binary table. Array names are derived from the telemetry parameter in the engineering telemetry database. Telemetry values are placed in time bins according to the time at which the parameter is reported by the spacecraft (in units of MJD days). The update rates are given in Table 5.4. Due to lack of precision, the bins are not precisely integer seconds in length. Nominal update rates range from once per second to once every 16 s depending on the telemetry item, but different telemetry modes sometimes changed the rates. The time duration (in seconds) of the telemetry included in the file can be obtained from the value of NAXIS2 in the HDU2 header. Any parameter not reported in a given second is given the value of "−1" in the housekeeping file. Occasionally, parameters are reported twice in a second, in which case only the final value reported during that second is placed into the housekeeping file. Each type of parameter is checked for telemetry gaps based on its nominal update period. Gaps are reported in the trailer file for each exposure.

Table 5.4: Housekeeping Nominal Sample Periods

Parameter(s)	Period (sec)
AATTMODE	5
ATTQECI2BDY	2 (rarely, 0.2 s)
I_FPD	1[a]
CENTROID	1[a]
any I_ not already covered	16
AQECI2BDYCMD	3 (rarely, 1 s)

[a] Only updated when using guide stars. The integration time for faint guide stars is 1.4 s.

5.3 Engineering Snapshot Files (`*snapf.fit`, `*snpaf.fit`, `*snpbf.fit`)

The engineering snapshot data described in this section are somewhat of an anachronism, and are included primarily for completeness. The contents of all of these files are similar (see Appendix E), and provide a sampling of the satellite and detector telemetry at the time they were

recorded.

Engineering telemetry and science data for *FUSE* were stored and downlinked in different data streams. Certain engineering parameters from the instrument, such as detector temperatures and voltages, were identified before launch as potentially being necessary for processing and calibrating the science data. To capture that information, engineering snapshots were taken at the beginning of an exposure and every 5 minutes thereafter, with a final one taken at the end. These data were transmitted in the science telemetry stream. The time of the first and last snapshot were used by OPUS to define the exposure start and stop time for the science data. Other snapshot data were used by OPUS to populate parameters in the FITS header for the exposure files. A subset of these data for the detector are available in the engineering snapshot files.

As the mission progressed, it was discovered that more engineering telemetry at higher sampling rates were needed for CalFUSE to properly process the science data. As a result, the housekeeping files, described in previous sections, were created from direct extractions from the engineering archive, and they were used to provide the necessary supplemental data.

Engineering snapshot data filenames have syntax as shown below, where `*snapf*` is used for standard engineering snapshot files, `*snpaf*` is used for engineering snapshots associated with FES A, and `*snpbf*` is used for engineering snapshots associated with FES B. Example file names are D0640301001snapf.fit and D0640301001snpaf.fit.

$$\{pppp\}\{tt\}\{oo\}\{eee\} \left\{ \begin{array}{l} \texttt{snapf} \\ \texttt{snpaf} \\ \texttt{snpbf} \end{array} \right\} \texttt{.fit}$$

5.4 Association Tables (`*asnf.fit`)

One Association Table is generated and used by OPUS (see Section 3.2) for each observation. The file is formed of two HDUs as shown in Table 5.5. HDU1 is a header containing basic information about the proposal, the observation and the target. HDU2 is a list of which files were associated with a given observation, their type and whether the files were found. An example is D0640301000asnf.fit with a generic naming as follows.

$$\{pppp\}\{tt\}\{oo\}\texttt{000asnf.fit}$$

Table 5.5: Format of the Association Table.

FITS Extension	Format	Description
HDU 1: Empty (Header only)		
HDU 2: Exposure association information		
MEMNAME	STRING	Exposure names
MEMTYPE	STRING	EXPOSURE
MEMPRSNT	STRING	T/F

5.5 Mission Planning Schedule (MPS) Files (`mps*.pdf`)

This section describes the graphical timeline plots of the Mission Planning Schedules (MPS). These plots provide an overview of activities and orbital events throughout the mission and may be useful for placing observations and exposures into context. These plots indicate the PLANNED sequence of activities, and do not reflect any anomalies that might have occurred during actual execution of the observations. (For that see the daily count rate plots discussed in Section 5.7.) The MPS plots were generated for use by the Science Operations staff, and some of the items shown are specific to their needs. However, many of the parameters may be of interest to those who want to use the data as well. Hence, MPS plots have been added to the available FUSE products at MAST as part of the FUSE mission close-out activities.

The files are named according to the starting date of the MPS and *FUSE* orbit number (since launch). For instance: mps_2002_318_17869.001.pdf corresponds to an MPS which begins on year 2002, day 318 (e.g., November 14) and *FUSE* orbit number 17,869.

Figure 5.4 provides an example of a one day MPS timeline plot. The plots are PDF files, usually with a day per page, and Day/Universal Time as the abscissa. Each calendar day is broken into two panels, each covering 12 hours. During nominal operations, MPSs typically covered a one-week period, although actual times could be longer or shorter, depending on conditions at the time of planning. Later MPSs were usually multi-day schedules (up to 2 weeks in length) unless a re-delivery or re-plan had taken place.

MPS plots relevant to each observation can be accessed from the MAST preview pages. The link connects to the PDF file of the MPS containing the observation, but the user will need to page through the MPS file to find the specific observation of interest. Inspection of these plots allows the user to assess many aspects of the observation, including (for example) whether SAA passages impacted the scheduling, whether low or grazing earth limb angles may have caused unusual airglow in the observation, and which observations were scheduled before or after the observation of interest.

A variety of parameters are shown in sub-panels along the ordinate of these plots. The parameters plotted on these plots changed during the course of the mission, reflecting changing operational constraints and the evolution of mission planning tools. The following is a complete list of all possible parameters (and explanations) that appear in various MPS timeline plots.

RAM: The instantaneous angle of the telescope boresight to the direction of spacecraft motion.

LIMB: The angle of the boresight from the earth limb (lower dashed line indicates 10 degree limb angle; upper dashed line indicates 30 degree limb angle).

OBS: A bar showing the active observation, labeled with ProgramID:targetID:observationID, coordinates in degrees, target name, expected count rate and (late in the mission) the skew wheel bias. The bias values are:

- LN - Low Negative
- LP - Low Positive
- HN - High Negative

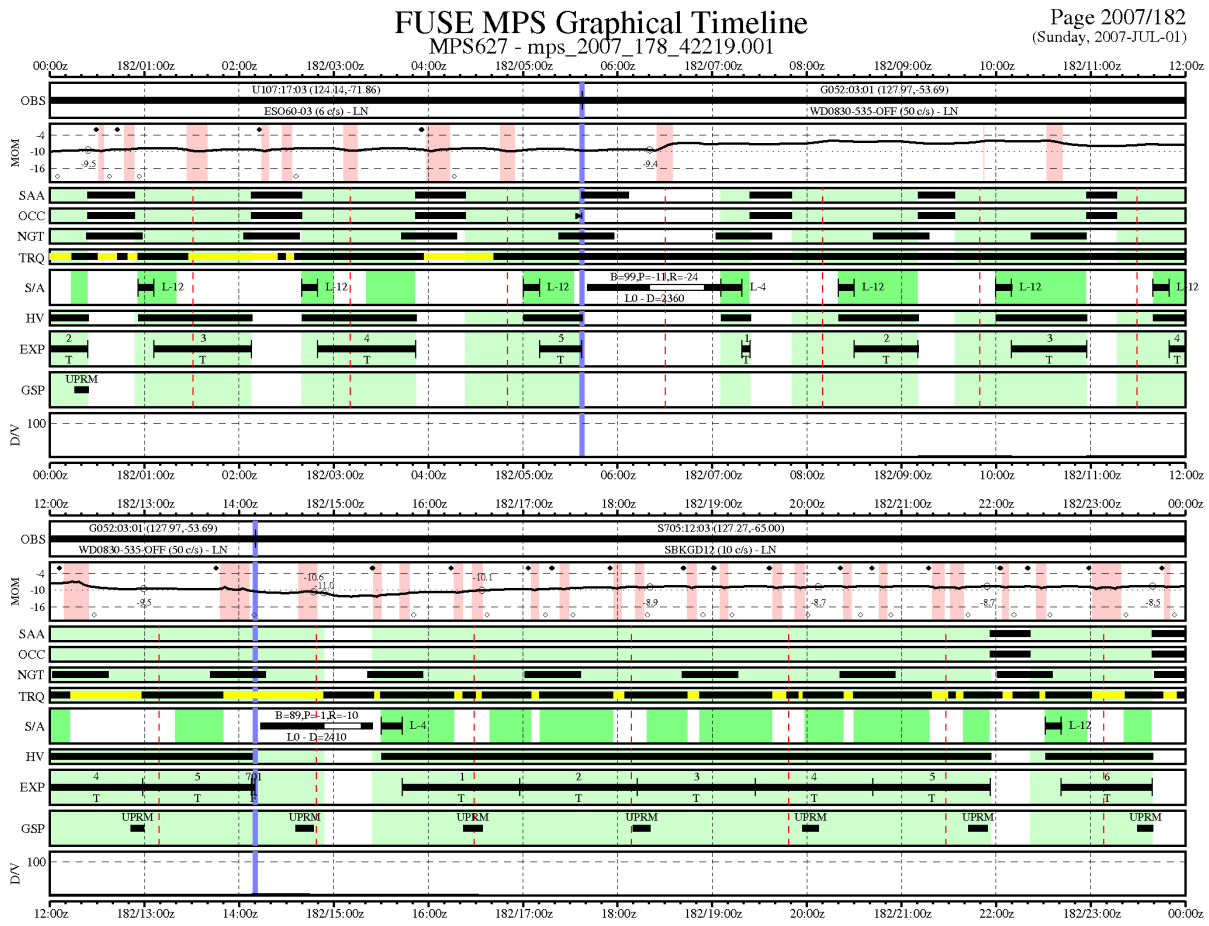

Figure 5.4: *Example of an MPS timeline chart for a 24h period, demonstrating several of the features described in the text.*

- HP - High Positive

SLEW, SLW, S/A, or ACQ: Spacecraft slews, labeled with the beta angle (B), pole angle (P), roll offset (R), and hemisphere of the attitude at the end of the slew (+ or - roll offset angle: + north, - south), speed of the slew (LO or HI), and the delay in seconds (D) from the beginning of the observation to the start of the slew. A bar is shown for any commanded slew, with the first black section indicating the length of the slew start delay, the white section showing the slew duration, and the next black section indicating the slew settle time. The black bar between the short vertical lines indicates an acquisition or a small slew for, e.g. an offset acquisition.

Small slews and acquisitions. Acquisitions are labeled with the aperture (L - low, M - medium, H - high, R - reference point) and the acq_case. The acq_cases are:

0 - No Acq (acquisition) performed

1 - FUV (Far UltraViolet) Peak-up

2 - FES (Fine Error Sensor) Target Acq and FUV Peak-up

3 - FES Target Acq

4 - FES Guide Star Acq

11 - Unknown Star Acq

12 - GS (Guide Star) Re-Acq

15 - Offset Acq

16 - Offset Re-acq

18 - FES target correction only

EXP: Exposures, labeled with the exposure ID above the block and the exposure type below the block (T - Time Tag, H - Histogram, F - FES exposure, S - FPA adjustment for an FP-split, P - Peakup, A/C - Alignment scans, G - GNRA (Generic/Null Activity).

SAA: Bars on this line show the calculated periods where the spacecraft is passing through the SAA (South Atlantic Anomaly). FUV observations cease during these periods. An indicator of the SAA model in use is sometimes also shown.

OCC: Bars on this line indicate periods when the active target is occulted (behind the earth or below the earth limb threshold used for planning). If nothing is present on this line, the target was in the CVZ (Continuous Viewing Zone).

TMX, NGT: This stands for "Terminator Crossing". Bars effectively indicate when the target is being viewed during orbital night. Blank regions are orbital day.

GSP: Bars on this line indicate the positions of any ground station passes that were planned during the observation period. The passes are labeled with the ground station involved:

UPRM: University of Puerto Rico at Mayaguez

TDRS: Tracking and Data Relay Satellite System

Hawaii: A commercial station in Hawaii used early in the mission

TRQ: Predicted positive torque authority (i.e. stable pointing) intervals. A solid black line indicates that the target should be in the slit (i.e., no or very few losses of torque authority). A yellow interval denotes expected pointing errors whose magnitude is up to 5 degrees. Larger errors correspond to red intervals (up to 10 degrees) and red crossed intervals, more than 10 degrees.

HV: Bars on this line indicate periods when the detector high voltage is planned to be at full voltage (normal science data acquisition mode).

DV: Data Volume stripchart, showing how much memory usage was expected on the science data recorders. The nominal limit of 100MB is indicated by the horizontal dashed line.

MOM: Predicted skew wheel momentum stripchart. The nominal operating range in effect for the particular MPS is shown by the dashed horizontal lines. Discrete numerical momentum values are plotted and referenced by the open circles on the stripchart line.

Also shown on some of the plots are colored regions, and vertical lines. These indicate:

Light Green: Visibility intervals (unocculted, SAA free times) during which FUV exposures can occur.

Dark Green: Acquisition intervals, indicates times when the acquisitions and re-acquisitions were allowed.

Pink: Periods when the "skew wheel axis to magnetic field" angle is suitable for skew wheel momentum unloading. A filled circle to the upper left of the pink region and an unfilled circle to the lower right of the pink region indicate times when the unloading is switched ON and OFF, respectively.

Red dashed line: (Vertical). Indicates orbital noon.

Blue line: (Vertical). Boundary between defined observations.

Table 5.6 lists the time ranges when different combinations of parameters were plotted on MPS plots.

Table 5.6: Dates for MPS Parameter Usage

Dates[a]	MPS Nos.	Parameters
1999-203 – 2000-309	001-222	RAM, LIMB, OBS, SLEW, ACQ, EXP, SAA, OCC, TMX, GSP
2000-313 – 2001-179	223-282	OBS, LIMB, SAA, OCC, NGT, SLW, ACQ, EXP, GSP, DV
2001-181 – 2002-115	283-344	OBS, LIMB, SAA, OCC, NGT, S/A, HV, EXP, GSP, DV
2002-120 – 2005-250	345-533	OBS, LIMB, SAA, OCC, NGT, TRQ, S/A, HV, EXP, GSP, DV
2005-264 – 2007-262	534-633	OBS, MOM, SAA, OCC, NGT, TRQ, S/A, HV, EXP, GSP, DV

[a] The format is: YYYY-DDD – YYYY:DDD

5.6 Mission Planning Guide Star Plots

Guide star plots (see Fig. 5.5) were used by the mission planners to identify potential field stars to use for tracking during each observation. Early in the mission, these manually selected stars were actually the ones passed to the ACS and used for tracking, but starting in 2005 the onboard software could find and use autonomously selected stars near each object. Hence, planners simply made a sanity check for available guide stars. The guide star plots show objects from the HST Guide Star Catalog superposed over the expected FES field of view, and show

the positions of the apertures. These plots can be useful for interpreting *FUSE* pointings in crowded fields, especially when used in conjunction with the FES images (remembering that the target may be in the aperture, and thus not visible to the FES). The indicator of North and East on the guide star plots is also useful for interpreting the actual FES images obtained for an observation.

As with other FUSE products, guide star plots evolved in format over the mission, but most of the information given on the plots is straightforward to interpret. The location of the requested aperture is indicated as a box with cross-hairs, and the acq_case codes shown are the same ones used on the MPS plots (see section directly above). The FLDT numbers used to identify certain stars, and listed at the bottom of the plots, refer to an internal numbering system used by the mission planners. Guide star plots for each observation are accessible from the MAST preview pages.

5.7 Daily Count Rate Plots

These plots show the actual on-orbit sequence of *FUSE* activities, all orbital events, and any anomalies that occurred, with each plot covering a 24-hour period. To the "Intermediate" and "Advanced" user, these plots will be useful for placing observations into context since they provide a quick visual assessment of the actual execution of a given observation and indicate various times associated with each observation (i.e., high-voltage status, SAA passage, etc...) Figure 5.6 displays an example of such a plot. (For more details on the content of these plots and their generation, the user is referred to the *Instrument Handbook (2009)*). Each file contains 4 sets of plots with the count rates for SiC, LiF, FEC, and ACS counters. A brief description of the SiC plot is provided below. From top to bottom, one can read the following:

Subplots 1-4 show for segments 1A, 1B, 2A, 2B the:
count rate (black); high voltage (red if nominal, blue if not); SAA times (blue horizontal shading); science data taken (green shading). The OBSID, target, TTAG/HIST flag, and aperture are also shown if the data are available; low limb angle times (orange shading); and low ram angle times (purple shading).

Subplot 5 shows the: Pole angle; Beta angle; Ram angle; Roll; RA; and OBSID (this will be marked at the time when the observation script began, which is normally well before the actual observation start time).

Subplot 6 shows the:
latitude; longitude; limb angle; Dec; and Day/Night Flag (shaded yellow if Day)

Subplot 7 shows the:
FPA positions; QMEAS flag (scaled); and AT_CMD_ATT flag (scaled).

5.8 Science Data Assessment Forms

Science data assessment forms, or SDAFs, were used internally by the operations team to provide a quick look assessment of science data quality for each observation. The assessment process was an important part of identifying problems, and if need be, placing revised observations back into the scheduling pool for timely re-execution. The SDAFs are available through the MAST Preview pages for each observation and provide some insight into how a given observation actually executed on-orbit in comparison to how it was planned.

Automated checking routines populated the majority of each SDAF. The software used information from the file headers, some of which was supplied by the user, and compared it to the actual data from each exposure to produce an overview of the success of the observation. This automated process was geared toward the typical *FUSE* target, which is to say, a moderately bright continuum source. The checks looked for the target in the expected aperture for all four channels and compared the exposure levels to provide an assessment of channel alignment. Hence, very faint sources and emission-line objects could look problematic to the automated process when in reality they might be just fine. Also, the software assumed that LiF1 was the guiding channel, and made comparisons of the other channels to LiF1. After July 12, 2005, when the guiding channel changed to LiF2 (i.e. to FES B), the software was not updated. Hence, some comparisons shown in the SDAF need to be taken in the context of the larger picture of *FUSE* operations. They are a useful, but imperfect, record of initial data quality assessment.

A brief description of each section of an SDAF is given below. An example SDAF is shown for reference in Fig. 5.7.

Summary Information: A table at the top of each SDAF provides summary information about the target and the observation, populated automatically from the file headers. Included are the actual achieved time for the observation as compared with the planned time in the timeline. If problems occurred, or if the processing deleted some data sections as bad, these numbers will be different.

Exposure checklist: This tabular section contains one line for each exposure in the observation. At left are the UT start time of each exposure and the integration achieved in that exposure (from the LiF1A segment). In the middle are the Raw Data Check blocks that use various symbols to indicate the presence (or absence) of data in the various channels and apertures. This raw data check scans all apertures for TTAG data or the primary aperture for HIST data. The key for this section includes:

An "X" indicates data is present at a level of at least twice the background level.

A "W" indicates data is present at 1.8-2.0 times the background level.

A "-" indicates data is not present.

A "D" indicates that the detector high voltage was off or significantly reduced, likely due to an anomaly.

Total exposure times are listed at the bottom of each raw data check for each channel. The full exposure time of each exposure is included in the total if the primary aperture is marked "X".

The example in Fig. 5.7 shows the source present in all exposures and in all LWRS (prime) apertures. Also, since the exposure times are the same for all four apertures, there was apparently no drifting of the target in and out of the various apertures. This is also confirmed by the Extracted Data Check blocks to the right, which show a consistent signal in LiF1 in all channels, and ratios near unity compared to the LiF1 for the other channels throughout the exposures. In crowded fields and for TTAG exposures, sources could sometimes be present in the non-prime apertures. If this was true, one would also see "X" or "W" in other apertures where flux was present. Finally, if telemetry indicated that the high voltage was down for a particular channel, the indicator would show "D" and no data would be present in that channel for that exposure.

Continuum Flux Check: Part of the exposure checklist also includes a check on the CalFUSE pipeline extracted output. This section of the SDAF provides a sanity check against expectations. For each *FUSE* target, the observer was asked to provide continuum fluxes at 950, 1050, and 1150 Å (if appropriate for their target type). The Continuum Flux Check box just makes a simple comparison of actuals against these expectations, and performs some comparisons between channels. The LiF1 fluxes are used as a benchmark. If the flux in another overlapping segment is significantly lower or higher, then a comment is added later in the form (see below). Also, if flux is detected in the extracted spectrum at a level greater than the LiF1 level and the raw data indicates that no data should be present, a warning is issued in the comments. In some cases, observers had only rough estimates of the expected fluxes, so it is not uncommon to see significant differences from unity. Also, lower values could indicate channel drifts are affecting the observation, especially for MDRS and HIRS observations. (Note again that data taken after 12 July 2005 did not use the LiF1 channel for guiding, but the SDAF software was never updated for this.)

Comments Section: This section contains a number of comments, exposure by exposure, generated by the CalFUSE processing sotfware as it processed the data. The example shows comments related to the presence of bursts and time removed because of them. Sometimes a general alert will be present in red, indicating a flux much lower than expected or similar criterion that can be measured automatically. Usually such problems would already be obvious from inspection of information at the top of the SDAF, but the red comment flags the probable causes of problems specifically. Warnings are more serious than alerts, and when initially issued, would prevent archiving of the data until an assessment was made by *FUSE* personnel. (Few if any warnings remain in the final SDAF forms generated in the reprocessing performed at the end of the mission, however.)

For observations made in the MDRS or HIRS apertures, the standard procedure involved performing a peak-up acquisition (sometimes multiple times per orbit) to align the channels at the beginning of the observation. When this is the case, one will find an ascii peak-up table appended to the end of the SDAF for that observation. This information is provided for completeness, but it is not expected that most users will need it for analyzing their data.

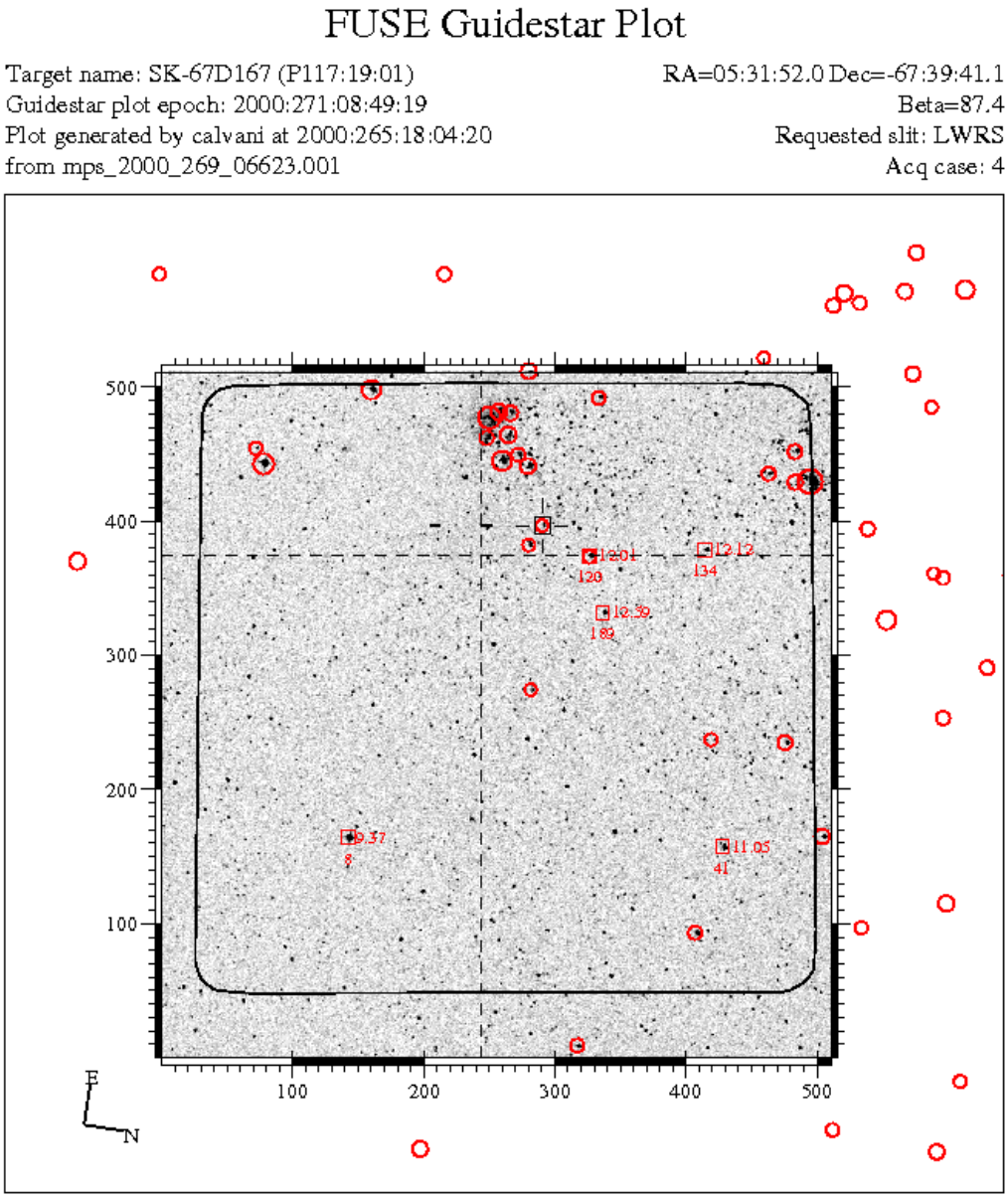

Figure 5.5: *Example of a mission planning guide star plot. The apertures are located at ∼Y=400. The crosshairs show which aperture is being used, LWRS in this case.*

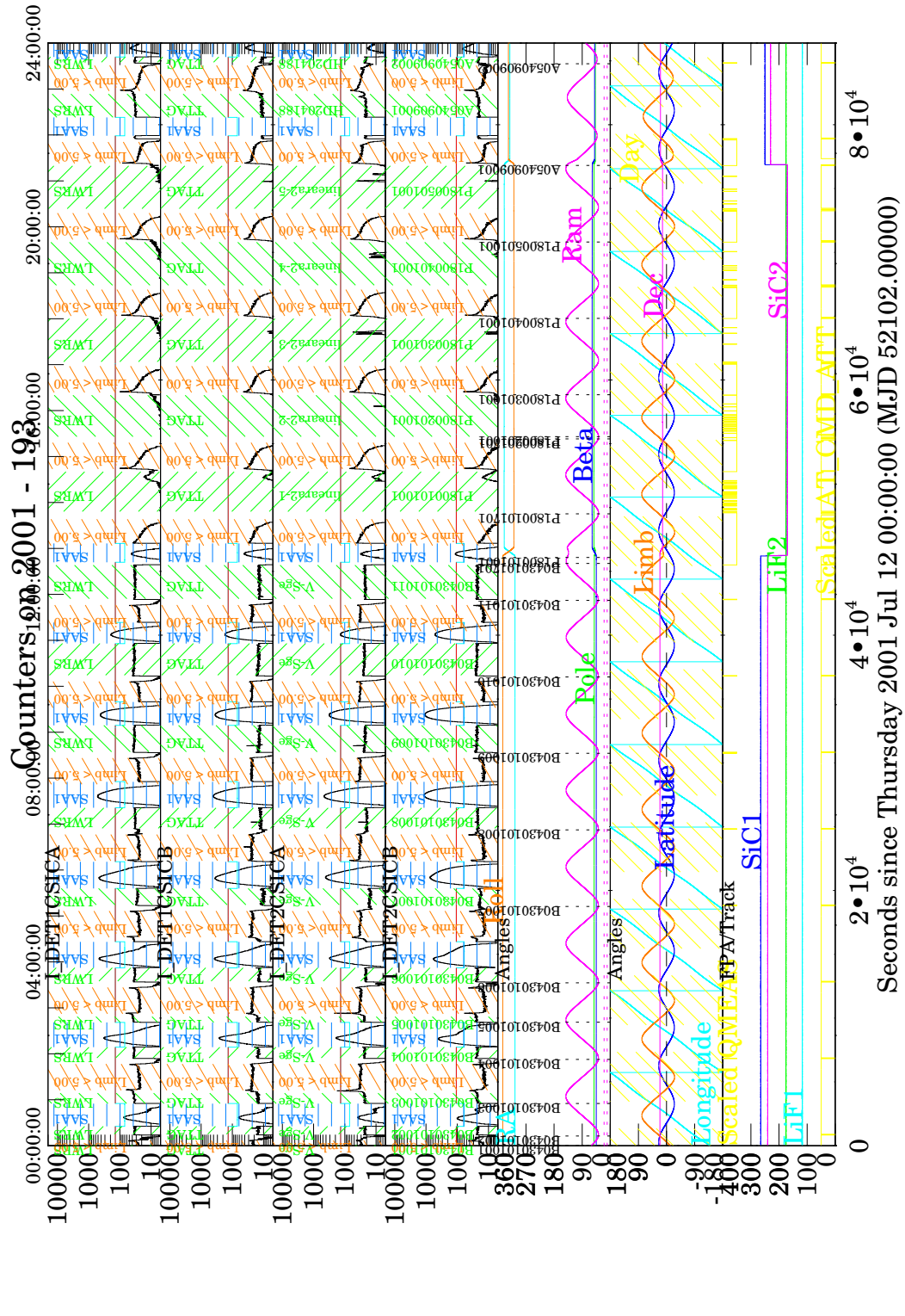

Figure 5.6: *Example of a daily count rate plot. See text for details.*

Science Data Assessment Form

P2041101

Summary for observation: P2041101 Form Information

Object: WD0004+330	Sp. Type: DA	Aper: LWRS	Mode: TTAG
Object ID: P204-11	Source Type: PC	Aper. PA: 175.52	PI: Moos
RA (J2000): 00 07 32.30	Vmag: 13.80	Exp. Time: 9999	CALFUSE Vers: 3.2.1
Dec (J2000): +33 17 28.00	E(B-V): 0.00	Plan Time: 10264	Obs. Date: 2000-11-24

Exposure Checklist			Raw Data Check										LWRS Extracted Data Check			
Exp	UT Start	Exptime (sec)	LiF1A			SiC1A			LiF2B			SiC2B			Flux Ratios (1040-1070)			
			L	M	H	L	M	H	L	M	H	L	M	H	F(LiF1)	S1/L1	L2/L1	S2/L1
001	13:30:19	2421	X	-	-	X	-	-	X	-	-	X	-	-	3.01E-12	0.99	0.99	1.03
002	15:11:05	2132	X	-	-	X	-	-	X	-	-	X	-	-	3.02E-12	1.00	0.99	1.03
003	16:56:24	2153	X	-	-	X	-	-	X	-	-	X	-	-	3.01E-12	1.00	0.99	1.02
004	18:41:03	462	X	-	-	X	-	-	X	-	-	X	-	-	3.03E-12	0.98	0.98	1.00
005	18:49:58	1337	X	-	-	X	-	-	X	-	-	X	-	-	3.00E-12	1.00	0.99	1.00
006	20:25:37	1494	X	-	-	X	-	-	X	-	-	X	-	-	3.01E-12	1.01	0.99	1.02
Exptime Totals		9999	9999			9999			9999			9999						

"X" = Present "W" = Present, weak "D" = Detector off "-" = Not present

Continuum Flux Check (Exposure 001)	950 A SiC1B / SiC2A	1050 A LiF1A	1150 A LiF1B / LiF2A
Expected Continuum Fluxes	1.28E-12	3.33E-12	2.61E-12
Observed Continuum Fluxes (10 A averages)	1.34E-12 / 1.38E-12	3.00E-12	1.42E-12 / 2.40E-12

Comments

Exposure 001: Possible burst activity on segment 2A.
Exposure 001: Possible burst activity on segment 2B.
Exposure 001: Exposure time lost to screening = 170 sec.
Exposure 002: Possible burst activity on segment 1A.
Exposure 002: Possible burst activity on segment 2A.
Exposure 002: Possible burst activity on segment 2B.
Exposure 002: Exposure time lost to screening = 408 sec.
Exposure 003: Possible burst activity on segment 2B.
Exposure 003: Exposure time lost to screening = 63 sec.
Exposure 004: Possible burst activity on segment 2B.
Exposure 005: Possible burst activity on segment 2B.
Exposure 005: Exposure time lost to screening = 61 sec.
Exposure 006: Possible burst activity on segment 2B.

Overall Assessment

Observation should be archived

This data assessment form was generated automatically by the SDOG on 23-Oct-2007 02:35:56.

Figure 5.7: *Example of a Science Data Assessment Form.*

Chapter 6

FITS File Headers

6.1 Science Data File Headers

The main header, or HDU1, typically contains most of the information about the file, while the headers for the extensions usually give additional information about the data in each extension. The main headers are parsed into sections, and all science data files (RAW, CAL, IDF, ALL, ANO, and NVO) contain the same sections. However, for the RAW images, not all of the fields are populated. Several of the ancillary files contain similar information. The following sections describe these standard header sections.

This chapter contains general information useful to the "Advanced" and "Intermediate" user. Its contents are not, however, of immediate relevance to the "Casual" user.

DATA DESCRIPTION KEYWORDS: This set of keywords is fairly self-explanatory. For exposure level files, OBS_STAT is replaced with EXP_STAT.

```
              DATA DESCRIPTION KEYWORDS

TELESCOP= 'FUSE              ' / Telescope used to acquire data
INSTRUME= 'FUV               ' / Instrument in use (one of FUV, FESA, or FESB)
ROOTNAME= 'A1330147002       ' / Rootname of the observation set (pppptttooeee)
FILENAME= 'A13301470021bsic4ttagfcal.fit' / Name of file
FILETYPE= 'CALIBRATED EXTRACTED SPECTRUM' / Type of data found in data file
EXP_STAT=                    0 / Science data processing status (0=good)
```

PROPOSAL INFORMATION: This section is populated from the Mission Planning Database (MPDB).

```
              PROPOSAL INFORMATION

PRGRM_ID= 'A133              ' / Program ID from data header
TARG_ID = '01                ' / Target ID from data header
SCOBS_ID= '47                ' / Observation ID from data header
EXP_ID  = '002               ' / Exposure ID from data header
```

```
OBS_ID  = '47                ' / Observation ID from proposal database
PR_INV_L= 'Fullerton         ' / Last name of principal investigator
PR_INV_F= 'Alex              ' / First name of principal investigator
```

TARGET INFORMATION: These keywords are also populated from the MPDB and are not measured quantities. The expected fluxes and count rates come from the Phase 2 Proposal form submitted by the observer. A key to the numerical Object Classes are given in Section 8.4.5.

```
              TARGET INFORMATION

TARGNAME= 'SK-67D166         ' / Target name on proposal
RA_TARG =            82.934625 / [deg] Right ascension of the target (J2000)
DEC_TARG=             -67.6335 / [deg] Declination of the target (J2000)
APER_PA =            23.518158 / [deg] Position angle of Y axis (E of N)
EQUINOX =               2000.0 / Equinox of celestial coordinate system
ELAT    =  -8.705045834317E+01 / [deg] Ecliptic latitude
ELONG   =   3.354528613035E+02 / [deg] Ecliptic longitude
GLAT    =  -3.248583704098E+01 / [deg] Galactic latitude
GLONG   =   2.778388799536E+02 / [deg] Galactic longitude
OBJCLASS=                   13 / Object class (modified IUE classification)
SP_TYPE = 'O4If+             ' / MK spectral type and luminosity class (or other
SRC_TYPE= 'PC                ' / [P]oint or [E]xtended, [C]ontinuum, [E]mission
VMAG    =                12.27 / Target V magnitude
EBV     =                  0.1 / Color excess E(B-V)
Z       =                  0.0 / Redshift
EFLX_950=              1.9E-12 / Expected flux at 950 A
EFLX1050=              2.7E-12 / Expected flux at 1050 A
EFLX1150=              2.6E-12 / Expected flux at 1150 A
HIGH_PM = 'F                 ' / High proper motion target (T or F)
MOV_TARG= 'F                 ' / [F]ixed or [M]oving target
PCNTRATE=               1592.9 / Expected count rate (sum of all channels)
```

SUMMARY EXPOSURE INFORMATION: This section contains the date and time of the observation, including the exposure start and end time, and the computed exposure time. Exposure start and end times are expressed in Modified Julian Date (MJD = JD–2400000.5). The EXPENDC keyword indicates the reason for the termination of the exposure – entry into South Atlantic Anomaly (SAA), occultation (OCC), end of night (NGHT), or the natural end of exposure (ENDE) or end of observation (ENDO). The Sun and Moon angles, and the minimum pointing angle above the Earth limb are computed by the calibration software, and are therefore 0 in the raw data files. For TTAG data, the calibration software also screens photon address data, and ignores bad data taken in, for instance, the SAA. There are a number of keywords reporting the actions taken by this screening step, and are shown below. The meanings of these codes are summarized in Tables 4.10, 4.11, and 4.12 of Section 4.2.1.3. If data are screened out, then EXPTIME will be smaller than RAWTIME in the IDF and the calibrated files.

```
              SUMMARY EXPOSURE INFORMATION

DATEOBS = '2000-10-12'         / UT date of start of exposure (yyyy-mm-dd)
TIMEOBS = '14:38:30'           / UT start time of exposure (hh:mm:ss)
EXPSTART=   5.182961006944E+04 / Exposure start time (Modified Julian Date)
EXPEND  =   5.182962262750E+04 / Exposure end time (Modified Julian Date)
EXPTIME =                1085. / [s] Total time after screening
EXPENDC = 'ENDO              ' / End condition (ENDO; SAA; OCC; NGHT; ENDE)
NEVENTS =               421399 / Number of events in raw data file
RAWTIME =   1.085015625000E+03 / [s] Exposure duration of raw data file
PLANTIME=                 1020 / [s] Planned exposure time
SUNANGLE=     92.1169468703347 / [deg] Angle between sun and Z axis
MOONANGL=     83.0809764100487 / [deg] Angle between moon and Z axis
POLEANGL=     160.545069830942 / [deg] Angle between orbit pole and Z axis
GEO_LONG=     164.355774107397 / [deg] Geocentric longitude
GEO_LAT =     24.3003425210518 / [deg] Geocentric latitude
MAG_LAT =     30.5899872994262 / [deg] Geomagnetic latitude
MIN_LIMB=     11.9518247749345 / [deg] Minimum angle above Earth limb

NBADEVNT=               10910 / Number of events deleted in screening
NBADPHA =                 919 / Number of events deleted in PHA screening
EXP_BAD =                   0 / [s] Time lost to screening
EXP_BRST=                   0 / [s] Time lost to event bursts
EXP_HV  =                   0 / [s] Time lost to low voltage/FIFO overflow
EXP_JITR=                   0 / [s] Time lost to jitter
EXP_LIM =                   0 / [s] Time with low limb angle
EXP_SAA =                   0 / [s] Time while in SAA
EXPNIGHT=                1085 / [s] Night time after screening
V_GEOCEN=     2.38573645263126 / [km/s] Observed to geocentric velocity
V_HELIO =    -1.08708418297615 / [km/s] Geocentric to heliocentric velocity
V_LSRDYN=    -12.7521820068359 / [km/s] Heliocentric to dynamical LSR
V_LSRSTD=     -15.775110244751 / [km/s] Heliocentric to standard solar LSR
             Geocentric and helocentric conversions are applied by the
             CALFUSE calibration pipeline.  LSR conversion is not.
```

SCIENCE INSTRUMENT CONFIGURATION: These keywords contain planned as well as telemetered values for the instrument configuration. Most of the keywords shown below are self-explanatory. For the detector mask, DET_MASK, AIC1 is an open mask, i.e., none of the photon events are masked out. The focal plane assembly (FPA) X and Z positions from the telemetry are recorded in the header keywords. Note that the FES_FILT keyword is always set to CLR. The mirror focus MIR*FOC keywords are populated only for bright object defocus test exposures.

```
              SCIENCE INSTRUMENT CONFIGURATION
```

```
INSTMODE= 'TTAG              ' / Instrument mode (TTAG or HIST)
DETECTOR= '1B                ' / Detector for data in this file (1A, 1B, 2A, 2B)
APERTURE= 'LWRS              ' / Planned target aperture: HIRS, MDRS, LWRS, RFPT
BRIT_OBJ= 'NO                ' / Special configuration for bright-object obs
APER_ACT= 'LWRS_SIC'           / Extracted aperture in this file
DET_MASK= 'AIC1              ' / Detector mask used
NUM_APS =                    1 / Number of apertures in use in the observation
INITBINX=                    1 / Initial binning in X coordinate
INITBINY=                    1 / Initial binning in Y coordinate
SPECBINX=                    1 / Current binning in X coordinate
SPECBINY=                    1 / Current binning in Y coordinate
SIA_TBL = '                  ' / SIA Table name
NUM_HIST=                    0 / Number of histograms in the observation
INT_CAL = '                  ' / Internal Calibration (STIM, NONE)
FPSPLIT =                    0 / Number of FP Split positions
FPASXPOS=              140.145 / [microns] FPA SiC X position
FPALXPOS=              116.107 / [microns] FPA LiF X position
FPASZPOS=             -98.9776 / [microns] FPA SiC Z position
FPALZPOS=             -34.4119 / [microns] FPA LiF Z position
MIRL1FOC=             0.000000 / [microns] LiF 1 mirror position
MIRL2FOC=             0.000000 / [microns] LiF 2 mirror position
MIRS1FOC=             0.000000 / [microns] SiC 1 mirror position
MIRS2FOC=             0.000000 / [microns] SiC 2 mirror position
TTPERIOD=                  1.0 / [s] Time marker insertion period
ENGSNAPT=                  300 / [s] Engineering snapshot period
TACQSEQ = 'ACQ-T-NOPKUP      ' / Target acquisition sequence
ROLLOFF =                  0.0 / [Deg] Roll offset
FES_BIN =                    1 / FES binning factor (1;2;4;8)
FES_FILT= 'CLR               ' / FES filter wheel position: CLR=Clear, COL=Color
FES_TPOS= 'OUT               ' / FES target position: IN or OUT
```

DETECTOR HV BIAS RANGES: These keywords list the minimum and maximum high voltage level for all segments during the exposure. The minimum and maximum for a given segment should normally be the same. The nominal high voltage levels were adjusted periodically during the mission; see Table 7.4.

```
              DETECTOR HV BIAS RANGES

DET1HVAL=                  128 / Det1 MCP A HV bias minimum setting
DET1HVAH=                  128 / Det1 MCP A HV bias maximum setting
DET1HVBL=                  128 / Det1 MCP B HV bias minimum setting
DET1HVBH=                  128 / Det1 MCP B HV bias maximum setting
DET2HVAL=                  128 / Det2 MCP A HV bias minimum setting
DET2HVAH=                  128 / Det2 MCP A HV bias maximum setting
```

```
DET2HVBL=                  101 / Det2 MCP B HV bias minimum setting
DET2HVBH=                  101 / Det2 MCP B HV bias maximum setting
HV_FLAG =                    4 / Detector voltage full throughout exposure
```

ORBITAL EPHEMERIS: These keywords contain the Keplerian elements for the *FUSE* orbital ephemeris. Together with the time of observation, these values can be used to calculate where the satellite was in its orbit (although much of this information is already in the timeline table in the IDF files). The calibration software, for instance, uses these values to compute the Doppler correction to apply as it produces the calibrated data.

```
              ORBITAL EPHEMERIS

EPCHTIMD=               51829. / Epoch time of parameters whole day (MJD)
EPCHTIMF=    0.943173899999238 / Epoch time of parameters fraction of day (MJD)
INCLINAT=              24.9842 / [deg] Inclination
ECCENTRY=            0.0011377 / Eccentricity
MEANANOM=             238.2636 / [deg] Mean anomaly
ARGPERIG=             121.8967 / [deg] Argument of perigee
RASCASCN=              301.572 / [deg] RA of ascending node
SEMIMAJR=     7137.84084370588 / [km] Semi-major axis
MEANMOTN=          14.39635355 / [revs/day] Mean motion
FDM2COEF=             9.37E-06 / First time derivative of mean motion / 2
SDM6COEF=                   0. / Second time derivative of mean motion / 6
DRAGCOEF=            0.00023849 / B star drag coefficient
PROPMODL= 'SGP4    '           / Propagation model
```

SCIENCE DATA PROCESSING STEPS: These keywords indicate which steps of the calibration pipeline have been applied to the data. All processing steps are set to a value of INITIAL in the raw data files. The first pipeline module sets them to either PERFORM or OMIT, depending on whether the corresponding calibration step is to be performed or not. Once a step is completed, its keyword is changed to a value of COMPLETE. If a pipeline module decides not to perform a step labeled PERFORM, it changes the keyword to SKIPPED. Thus, COMPLETE, OMIT, and SKIPPED are all valid keywords in extracted spectral files (see Dixon et al. [2007]).

```
              SCIENCE DATA PROCESSING STEPS

INIT_COR= 'COMPLETE'           / Initialize processing
DIGI_COR= 'COMPLETE'           / Check digitizer values
ELEC_COR= 'COMPLETE'           / Detector dead-time correction
IDS__COR= 'COMPLETE'           / IDS dead-time correction
FIFO_COR= 'COMPLETE'           / FIFO overflow correction
DEAD_COR= 'COMPLETE'           / Apply all dead-time corrections
THRM_COR= 'COMPLETE'           / Thermal distortion correction
RATE_COR= 'COMPLETE'           / Count-rate Y distortion
TMXY_COR= 'COMPLETE'           / Temporal X and Y corrections
```

```
GEOM_COR= 'COMPLETE'           / Geometric distortion
PHAH_COR= 'OMIT    '           / Assign pulse heights to HIST data
PHAX_COR= 'COMPLETE'           / Low pulse-height X distortion (walk)
ACTV_COR= 'COMPLETE'           / Define detector active region
LIMB_COR= 'COMPLETE'           / Limb-angle screening
SAA__COR= 'COMPLETE'           / SAA screening
VOLT_COR= 'COMPLETE'           / Confirm detector voltage
BRST_COR= 'COMPLETE'           / Screen for bursts
APER_COR= 'COMPLETE'           / Screen for target out of aperture
UGTI_COR= 'COMPLETE'           / Set user good-time intervals
FLAG_COR= 'COMPLETE'           / Set individual photon flags
GTI__COR= 'COMPLETE'           / Determine good-time intervals
TIME_COR= 'OMIT    '           / Modify photon arrival times (HIST only)
AIRG_COR= 'COMPLETE'           / Flag events in airglow regions
BPIX_COR= 'COMPLETE'           / Flag events in bad-pixel regions
PHA__COR= 'COMPLETE'           / Pulse-height screening
FIND_COR= 'COMPLETE'           / Find spectra on detector
YMOT_COR= 'COMPLETE'           / Track motion of Y centroid
GRAT_COR= 'COMPLETE'           / Grating motion correction
FPA__COR= 'COMPLETE'           / FPA offset correction
MIRR_COR= 'COMPLETE'           / Mirror motion correction
JITR_COR= 'COMPLETE'           / Satellite jitter correction
YCNT_COR= 'COMPLETE'           / Y centroid of corrected data
CHID_COR= 'COMPLETE'           / Final channel assignment
TCRT_COR= 'COMPLETE'           / Calculate target count rate
ASTG_COR= 'COMPLETE'           / Astigmatism correction
WAVE_COR= 'COMPLETE'           / Assign wavelength to photons
DOPP_COR= 'COMPLETE'           / Heliocentric reference frame
FLAT_COR= 'OMIT    '           / Flat-field correction
FLUX_COR= 'COMPLETE'           / Flux-calibrate each photon
COMB_COR= 'PERFORM '           / Generate observation-level spectrum
```

SCIENCE DATA PROCESSING CALIBRATION FILES: These keywords indicate the names of the SDP calibration files and the ancillary files used by the calibration software. Knowing these filenames is important if one is considering reprocessing the data. Since no flat field or worm corrections were applied to the data these fields always remain empty.

```
              SCIENCE DATA PROCESSING CALIBRATION FILES

AEFF1CAL= 'aeff1b103.fit     ' / Effective-area curve #1
AEFF2CAL= 'aeff1b104.fit     ' / Effective-area curve #2
AIRG_CAL= 'airg1b004.fit     ' / Geocoronal line locations
ASTG_CAL= 'astg1b011.fit     ' / Astigmatism correction
BCHR_CAL= 'bchr1b003.fit     ' / Background characteristics
BKGD_CAL= 'bkgd1b011.fit     ' / Background/scattered-light model
BPM_CAL = 'A13301470021bttagfbpm.fit' / Bad-pixel map for this exposure
```

```
CHID_CAL= 'chid1b014.fit     ' / Windows for spectral extraction
DIGI_CAL= 'digi001.fit       ' / Reference file for digitizer values
ELEC_CAL= 'elec005.fit       ' / Detector parameters
FLAT1CAL= '        '           / Flat-field correction #1
FLAT2CAL= '        '           / Flat-field correction #2
GEOM_CAL= 'geom1b016.fit     ' / X and Y geometric corrections
GRAT_CAL= 'grat005.fit       ' / Grating motions
HSKP_CAL= 'A1330147002hskpf.fit' / Housekeeping data
JITR_CAL= 'A1330147002jitrf.fit' / Spacecraft jitter data
MIRR_CAL= 'mirr002.fit       ' / Mirror motions
PARM_CAL= 'parm1b015.fit     ' / Master parameter file
PHAH_CAL= 'phah1b001.fit     ' / Pulse height map for HIST data
PHAX_CAL= 'phax1b005.fit     ' / Low-pulse-height X distortion
QUAL_CAL= 'qual1b020.fit     ' / Quality flag (bad pixel) map
RATE_CAL= 'rate1b002.fit     ' / Y stretch with count rate
SAAC_CAL= 'saac004.fit       ' / SAA contours for data screening
SCRN_CAL= 'scrn1b015.fit     ' / Parameters for data screening
SPEC_CAL= 'spec002.fit       ' / Spectrograph parameters
STIM_CAL= 'stim1b001.fit     ' / Default thermal drift parameters
TMXY_CAL= 'tmxy1b002.fit     ' / Temporal X and Y corrections
VOLT_CAL= 'volt1b009.fit     ' / Detector bias voltages and dates
WAVE_CAL= 'wave1b023.fit     ' / Wavelength calibration
WGTS_CAL= 'wgts1b011.fit     ' / Pixel weights for extraction
WORM1CAL= '        '           / Worm correction #1
WORM2CAL= '        '           / Worm correction #2
```

SCIENCE DATA PROCESSING KEYWORDS: This section collects other data which are relevant to the calibration. These keywords are populated by OPUS and/or by CalFUSE. Some of these keywords (e.g., limb angle; pulse height) reflect screening limits used when CalFUSE was executed (see *The CalFUSE Page*).

```
              SCIENCE DATA PROCESSING KEYWORDS

OPUSVERS= '2.7               ' / FUSE OPUS version number
CF_VERS = '3.2.1   '           / CALFUSE pipeline version number
HKEXISTS= 'yes     '           / Housekeeping data file exists
DAYNIGHT= 'BOTH    '           / Use only DAY, NIGHT, or BOTH
BRITLIMB=                  15. / [deg] Bright limb avoidance angle
DARKLIMB=                  10. / [deg] Dark limb avoidance angle
ORBPERID=                5998. / [s] Estimate of orbital period
PHALOW  =                    2 / Pulse height screening low limit
PHAHIGH =                   24 / Pulse height screening high limit
OPT_EXTR=                   10 / Number of optimal extraction iterations
STIM_L_X=              256.5767 / X centroid of left stim pulse
STIM_L_Y=              749.4218 / Y centroid of left stim pulse
STIM_R_X=              16144.58 / X centroid of right stim pulse
```

```
STIM_R_Y=             772.1562 / Y centroid of right stim pulse
FPADXLIF=           -0.1579872 / [pixels] Correction for FPA position (LIF)
FPADXSIC=            -5.317671 / [pixels] Correction for FPA position (SIC)
WPC     =                0.013 / [A] Wavelength increment per pixel
W0      =                 900. / [A] Wavelength of first pixel
DET_DEAD=             1.005887 / Mean detector deadtime correction factor
IDS_DEAD=                   1. / Mean IDS deadtime correction factor
TOT_DEAD=             1.005887 / TOTAL deadtime correction factor
```

MEASURED SPECTRAL CENTROIDS: This section gives the position of the centroids of the spectra determined by CalFUSE. The quality keyword is set to HIGH if the centroid is measured from the target spectrum, MEDIUM if it is measured from airglow features, and LOW if it is taken from a reference file (see Dixon et al. [2007] for more details).

```
              MEASURED SPECTRAL CENTROIDS

YCENT1  =             688.1578 / [pixels] Y centroid of LIF HIRS spectrum
YCENT2  =             809.5578 / [pixels] Y centroid of LIF MDRS spectrum
YCENT3  =             558.6619 / [pixels] Y centroid of LIF LWRS spectrum
YCENT5  =             193.9905 / [pixels] Y centroid of SIC HIRS spectrum
YCENT6  =             321.1906 / [pixels] Y centroid of SIC MDRS spectrum
YCENT7  =              60.5411 / [pixels] Y centroid of SIC LWRS spectrum
YQUAL1  = 'MEDIUM  '           / Quality of Y centroid value (LIF HIRS)
YQUAL2  = 'MEDIUM  '           / Quality of Y centroid value (LIF MDRS)
YQUAL3  = 'HIGH    '           / Quality of Y centroid value (LIF LWRS)
YQUAL5  = 'MEDIUM  '           / Quality of Y centroid value (SIC HIRS)
YQUAL6  = 'MEDIUM  '           / Quality of Y centroid value (SIC MDRS)
YQUAL7  = 'HIGH    '           / Quality of Y centroid value (SIC LWRS)
```

BACKGROUND SAMPLE REGIONS: This section provides the details of the regions on the detectors used to determine the backgrounds used by CalFUSE (see Chapter 7).

```
              BACKGROUND SAMPLE REGIONS

BKGD_NUM=                   3 / Number of background regions specified
BKG_MIN0=                 160 / [pixels] bkgd sample region 0 - lower limit
BKG_MIN1=                 665 / [pixels] bkgd sample region 1 - lower limit
BKG_MIN2=                 891 / [pixels] bkgd sample region 2 - lower limit
BKG_MIN3=                   0 / [pixels] bkgd sample region 3 - lower limit
BKG_MIN4=                   0 / [pixels] bkgd sample region 4 - lower limit
BKG_MIN5=                   0 / [pixels] bkgd sample region 5 - lower limit
BKG_MIN6=                   0 / [pixels] bkgd sample region 6 - lower limit
BKG_MIN7=                   0 / [pixels] bkgd sample region 7 - lower limit
BKG_MAX0=                 450 / [pixels] bkgd sample region 0 - upper limit
BKG_MAX1=                 890 / [pixels] bkgd sample region 1 - upper limit
BKG_MAX2=                 930 / [pixels] bkgd sample region 2 - upper limit
```

```
BKG_MAX3=                    0 / [pixels] bkgd sample region 3 - upper limit
BKG_MAX4=                    0 / [pixels] bkgd sample region 4 - upper limit
BKG_MAX5=                    0 / [pixels] bkgd sample region 5 - upper limit
BKG_MAX6=                    0 / [pixels] bkgd sample region 6 - upper limit
BKG_MAX7=                    0 / [pixels] bkgd sample region 7 - upper limit
```

ENGINEERING KEYWORDS: A fair amount of the detector engineering snapshot data (engineering telemetry) is included in the FITS headers. The values included are shown below. Except for the Active Image Counters, only those values from the relevant detector segment are inserted into the header. The example keywords below are for segment 1B. For a description of the counters and masks, see the *Instrument Handbook (2009)*. The counter information is used by CalFUSE (see Dixon et al. [2007]).

```
              ENGINEERING KEYWORDS

THERMCON= 'ON                ' / Thermal control flag
FESSRC  = 'FES A             ' / Source of FES dump data
FESCENT = 'FES A             ' / Source of FES centroid data
GMODE   = 'IDENTIFIED_TRACKING ' / Guidance mode
TRACKON = 'OFF               ' / Moving target tracking on
ATCMDATT= 'AT COMMANDED ATTITUD    ' / At commanded attitude

              Segment 1B Counters

C1BSIC_B=             14101192 / SIC counter at beginning of integration
C1BSIC_E=             14175036 / SIC counter at end of integration
C1BLIF_B=             11704586 / LIF counter at beginning of integration
C1BLIF_E=             12032091 / LIF counter at end of integration
C1BDE_B =             13969564 / Digitized events counter at beginning of integr
C1BDE_E =             14391379 / Digitized events counter at end of integration
C1BAS_B =             15180958 / Autonomous shutdown (SAA) counter at beginning
C1BAS_E =             15182787 / Autonomous shutdown (SAA) counter at end of int
C1BFE_B =              3527277 / Fast event counter at beginning of integration
C1BFE_E =              3954788 / Fast event counter at end of integration
C1BFE_CR=           394.019348 / Count rate from fast event counter

              Active Image Counters

CTIME_B =   5.182961006944E+04 / [MJD] Time of first engineering snapshot
CTIME_E =   5.182962262731E+04 / [MJD] Time of last engineering snapshot
C1AAI_B =             10760595 / Seg 1A at beginning
C1AAI_E =             11259319 / Seg 1A at end of integration
C1BAI_B =             13894835 / Seg 1B at beginning
C1BAI_E =             14316651 / Seg 1B at end of integration
C2AAI_B =              1067178 / Seg 2A at beginning
C2AAI_E =              1679155 / Seg 2A at end of integration
```

```
C2BAI_B =              2067772 / Seg 2B at beginning
C2BAI_E =              2341339 / Seg 2B at end of integration

              Detector 1 parameters

DET1ETMP=              25.9103 / DET1 electronics temperature
DET1PTMP=              18.1937 / DET1 Baseplate temperature
DET1ASCL=                 17.0 / DET1 segment A  Time (X) image scale factor
DET1BSCL=                 91.0 / DET1 segment B  Time (X) image scale factor
DET1AXOF=                183.0 / DET1 segment A  Time (X) image position offset
DET1BXOF=                107.0 / DET1 segment B  Time (X) image position offset
DET1TEMP=              18.4255 / DET1 Detector temperature
DET1HVMT=              24.5318 / DET1 High Voltage Module temperature
DET1HVFT=              20.9761 / DET1 High Voltage Filter temperature
DET1AMAT=              26.3947 / DET1 segment A Amplifier temperature
DET1AMBT=              26.3947 / DET1 segment B Amplifier temperature
DET1TDAT=            21.386000 / DET1 TDC A  temperature
DET1TDBT=               21.792 / DET1 TDC B  temperature
DET1HVA =                 57.0 / DET1 MCP A Bias Current
DET1HVB =                 48.0 / DET1 MCP B Bias Current
DET1AUCT=                227.0 / DET1 TDC-A Upper Charge Threshold setting
DET1BUCT=                228.0 / DET1 TDC-B Upper Charge Threshold setting
DET1ABWK=                165.0 / DET1 TDC-A Begin CFD Walk setting
DET1BBWK=                139.0 / DET1 TDC-B Begin CFD Walk setting
DET1AEWK=                165.0 / DET1 TDC-A End CFD Walk setting
DET1BEWK=                125.0 / DET1 TDC-B End CFD Walk setting
DET1ABSL=                227.0 / DET1 TDC-A charge Baseline threshold setting
DET1BBSL=                228.0 / DET1 TDC-B charge Baseline threshold setting
DET1ALCT=                  7.0 / DET1 TDC-A Lower Charge Threshold setting
DET1BLCT=                  6.0 / DET1 TDC-B Lower Charge Threshold setting
DET1ALTT=                169.0 / DET1 TDC-A Lower Time Threshold setting
DET1BLTT=                143.0 / DET1 TDC-B Lower Time Threshold setting
DET1HVGR=                  1.0 / DET1 Grid High Voltage Status
DET1HVPW=                  1.0 / DET1 Bias High Voltage Status
DET1STIM= 'OFF               ' / DET1 Stimulation Lamp Status
```

ARCHIVE SEARCH KEYWORDS: Finally, keywords used by the archive, and those necessary to associate the exposures that make up an observation are included.

```
              ARCHIVE SEARCH KEYWORDS

BANDWID =             99.99597 / [Angstroms] Bandwidth of the data
CENTRWV =              949.998 / [Angstroms] Central wavelength of the data
WAVEMIN =                 900. / [Angstroms] Minimum wavelength of the data
WAVEMAX =              999.996 / [Angstroms] Maximum wavelength of the data
PLATESC =                1.163 / [arcsec/pixel] Plate scale
```

```
              ASSOCIATION KEYWORDS

ASN_ID  = 'A1330147000       ' / Unique identifier assigned to association
ASN_TAB = 'A1330147000asn.fit  ' / Name of the association table
ASN_MTYP= 'EXPOSURE          ' / Role of the exposure in the association
```

6.2 Engineering Data File Headers

Subsets of the DATA DESCRIPTION keywords, PROPOSAL INFORMATION keywords, and TARGET INFORMATION keywords are also included in the housekeeping and jitter file headers. In addition, their headers contain unique keywords which are described in this section.

Housekeeping Keywords: The HDU1 header for the housekeeping files contains some of the keywords defined above plus a set of engineering housekeeping time keywords (shown below). These specify the start time of the engineering telemetry contained in the file, and are measured quantities. The TIME_ENG keyword value is normally about one-half to one minute before the actual start time of the science exposure.

```
              ENGINEERING HOUSEKEEPING TIME

HSKPVERS= '3.2               ' / Housekeeping version number
DATE_ENG= '2000-09-27        ' / start date (yyyy-mm-dd)
TIME_ENG= '11:03:16          ' / start time (hh:mm:ss)
```

The HDU2 headers of the housekeeping files simply contain definitions of the housekeeping variables listed in Appendix D, so they are not repeated here.

Jitter Keywords: The HDU1 headers for the jitter files contain the engineering housekeeping time keywords described above, as well as a unique set of jitter keywords. The jitter data are computed from the housekeeping data. Most of the jitter keywords reflect the results of that analysis, and are intended as indicators of the overall quality of the pointing during the science exposure.

```
              JITTER KEYWORDS

JIT_STAT=                    0 / Status of jitter data is good
JIT_VERS= '3.5     '           / cf_jitter version number
QREF_SRC= 'TELEMETRY'          / Source of reference quaternion
QREF_0  =  -0.0168658437405577 / Reference quaternion
QREF_1  =    0.318041029256893
QREF_2  =    0.908345046651746
QREF_3  =    0.271062212872567
EXP_DUR =                668. / [s] duration of jitter data
KNOWNTRK=                  1. / fraction of exp in known track
ACSTRK  =                  0. / fraction of exp in ACS track
```

```
NOGDEINF=                    0. / fraction of exp with no guiding info
NGS_USED=                     6 / number of guide stars used
GS1_USED=                    1. / fraction of exp using known guide star 1
GS2_USED=                    1. / fraction of exp using known guide star 2
GS3_USED=                    1. / fraction of exp using known guide star 3
GS4_USED=                    1. / fraction of exp using known guide star 4
GS5_USED=                    1. / fraction of exp using known guide star 5
GS6_USED=                    1. / fraction of exp using known guide star 6
KTRKFINE=                    1. / exp fraction, err < 15 arcsec, known stars
ATRKFINE=                    0. / exp fraction, err < 15 arcsec, ACS
TOTLFINE=                    1. / exp fraction, err < 15 arcsec, total
GS_INUSE=                    1. / fraction of exp tracking on guide stars
SLEWFLG =                   -1 / Slew commanded during obs (if > 0)
SLEWTIME=                    0 / time spent slewing (sec)
POSAVG_X=           0.02662656 / [arcsec] mean DX during known track
POSAVG_Y=          -0.01711245 / [arcsec] mean DY during known track
X_JITTER=             0.326723 / [arcsec] sigma of DX during known track
Y_JITTER=             0.136007 / [arcsec] sigma of DY during known track
XJIT_15 =             0.326723 / [arcsec] sigma of DX for err < 15 arcsec
YJIT_15 =             0.136007 / [arcsec] sigma of DY for err < 15 arcsec
X_JITLRG=           0.03892216 / frac of DX more than 2-sigma from POSAVE_X
Y_JITLRG=           0.05239521 / frac of DY more than 2-sigma from POSAVE_Y
```

JIT_STAT is set to 0 for good jitter data, 1 if there were problems with the jitter data, 2 if the AT_CMD_ATT flag was not set, 3 if the commanded ACS quaternions were not available, 4 if there was no field information, and 5 if there were problems with the tabulated starting time of the exposure.

JIT_VERS is the CalFUSE jitter routine version number used to generate the jitter file. Values less than 3.1 will produce an error in CalFUSE.

QREF_SRC gives the source of the reference quaternion.

QREF_* are the values of the reference quaternions (see *Instrument Handbook (2009)*.

EXP_DUR is the duration of telemetry in the jitter file. The telemetry in the housekeeping data is specified to start 0.5–1.0 minute before the start of the associated science exposure, and to end 1 minute after the end of the associated science exposure. Thus, the jitter EXP_DUR should be 90–120 s longer than the science exposure time EXPTIME.

KNOWNTRK is the fraction of EXP_DUR when the IDS was using known guide stars to compute a guiding solution. In known tracking, the pointing position is the aperture.

ACSTRK is the fraction of EXP_DUR when the IDS was using unknown stars to compute a guiding solution. In unknown tracking, stars are used to control the pointing of the spacecraft, but the identity of these stars is not known. The target may or may not be at the desired place in the aperture, depending on preceding events.

NOGDEINF is the fraction of EXP_DUR for which there was no ACS guidance mode information available.

NGS_USED gives the number of guide stars used to track.

GSn_USED is the fraction of EXP_DUR when guide star n was contributing to the guiding solution computed by the IDS. Normally, 3 to 6 guide stars are used for an observation. Rarely as few as 1 or 2 are scheduled. Values of 0 are assigned to any star not scheduled to be used. Any star with a severe problem preventing use may have a value of 0 for this keyword. In general, these keywords indicate a problem if: (1) the keyword value differs significantly for the guide stars in use during a single exposure; (2) a lower-numbered guide star is 0 while a higher-numbered guide star is non-zero, or; (3) the number of guide stars in use changes among the jitter files in the same observation.

KTRKFINE is the fraction of the exposure using known guide stars when the errors were $< 15''$.

ATRKFINE is the fraction of the exposure using the ACS when the errors were $< 15''$.

TOTLFINE is the fraction of the total exposure when the errors were $< 15''$.

GS_INUSE is the fraction of EXP_DUR when the IDS was using stars for guiding, whether Known or Unknown.

SLEWFLG is the fraction of EXP_DUR when the spacecraft was executing a commanded slew. A non-zero value may indicate a guiding problem during the exposure, except in certain cases. A non-zero value is not a problem for science exposures for which scans were purposely executed, including M112's, M114's, and certain other calibration observations. There are two other cases where a non-zero value may not be a problem. Because the jitter "exposure" starts 30–60 s before the science exposure, a slew that completed prior to the science exposure may be included in the housekeeping data. Certain science exposures are more likely to be affected by this mis-match: the first exposure following the guide star acquisition; and the first exposure following a peakup.

SLEWTIME is the time spent slewing (sec).

POSAVG_X[Y] is the average of DX[Y] during the exposure, where DX[Y] are defined in § 5.2.

X[Y]_JITTER is the standard deviation of DX[Y] in the telemetry file. This value gives some indication of the orbital variation.

X[Y]_JIT_15M , if present, is the standard deviation of DX[Y] during the observation time when the pointing was within $15''$ of nominal. Hence, this value measures the stability while the target was within the LWRS aperture.

X[Y]_JITLRG is fraction of EXP_DUR for which DX[Y] is more than 2σ from the average.

Chapter 7

Factors Affecting *FUSE* Data Quality

Instrumental and observational factors have affected the *FUSE* data quality throughout the mission. The analysis of *FUSE* spectra is complicated by the presence of extra emission (airglow features and scattered light) and strong interstellar absorption (mainly H_2 and H I lines) as well as various artifacts and distortions inherent in the *FUSE* instrument itself. (A complete list of detector artifacts is presented in the *Instrument Handbook (2009)*.)

To fully appreciate the nuances of *FUSE* spectra and to extract the maximum information from them, a familiarity with these issues is essential *regardless of the users expertise level ("Casual", "Intermediate" or "Advanced")*. In this chapter, we discuss these effects, and how to recognize and deal with them.

7.1 Emission Lines Contributing to the Background

7.1.1 Airglow

Airglow is always present to some degree since there was no instrument shutter. Since airglow is a diffuse source, it is strongest in the LWRS and weakest in the HIRS (Figure 4.4). Because airglow is caused by solar excitation of the Earth's upper atmosphere, it is far stronger during orbital day than night. The actual degree of airglow contamination in any particular spectrum will depend on a variety of factors, including the fraction of the observation obtained during orbital day, the orientation of the satellite (which determines the path length through the Earth's atmosphere), and the phase of the solar cycle (which influences the degree of excitation of airglow lines and the extent of the atmosphere). The strongest airglow lines in the *FUSE* range are listed in Table 7.1, and a full discussion of the *FUSE* airglow spectrum can be found in Feldman et al. [2001].

Figure 7.1 shows a comparison of all the data (black trace) versus data obtained during the night-only portion of the observation (red trace) in observation A1330121. The upper panel displays the range where damped H I *Lyβ* absorption occurs (∼1025 Å) in the LiF1A segment. The emission arising at the center of the line is due to airglow contamination by the same atomic species. The bottom panel displays absorption caused by the N I triplet (∼1134 Å) using all the data (black trace) and the night-only data (red trace).

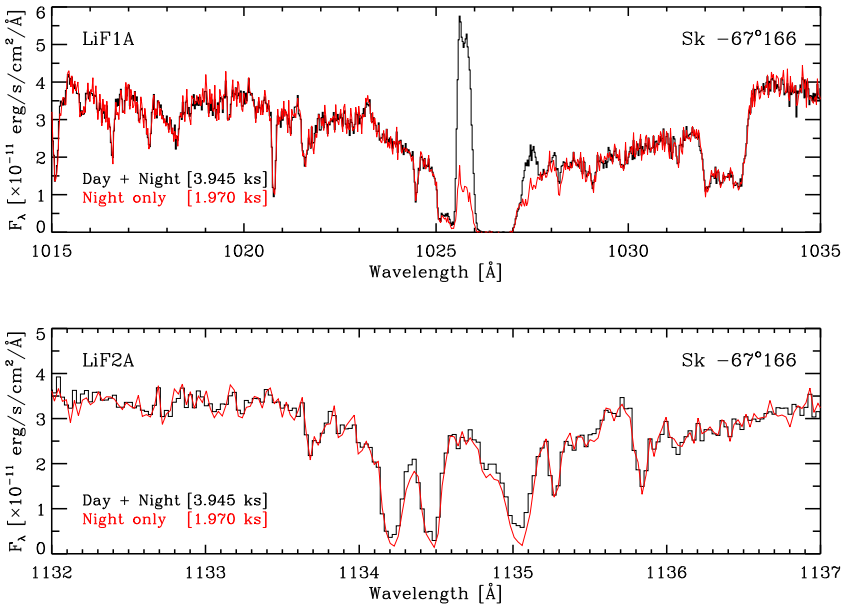

Figure 7.1: *The difference in the degree of airglow contamination between "day + night" spectra and "night-only" spectra of an O4 supergiant in the LMC. This observation (A1330121) was obtained through the LWRS aperture in* `TTAG` *mode. The integration time was divided approximately equally between orbital "day" and "night." Top: Note the greatly decreased airglow contamination from Ly β and the O I λλ1025.76, 1027.43, 1028.16 Å triplet in the "night-only" spectrum. Bottom: Airglow emission partially fills in the interstellar lines of the N I λλ1134.17, 1134.42, 1134.98 Å triplet. If not recognized, this contamination would lead to erroneous inferences concerning N I along this line of sight using these lines alone. Note also that because the airglow emission is extended, the astigmatism correction applied is inaccurate.*

Table 7.1: Prominent Airglow lines

Atom/Ion	Wavelength(s) (Å)
H I Ly δ	949.74
H I Ly γ	972.54
O I	988.77
O I	990.20
H I Ly β	1025.72
O I	1025.76, 1027.43, 1028.16[a]
O I	1039.23, 1040.94, 1041.69[a]
N II	1083.99, 1084.58, 1085.70
N I	1134.17, 1134.42, 1134.98

[a] Very weak

7.1.2 Second Order Solar light

This effect is always present to some extent. The only EUV solar emission lines strong enough to appear in second order arise from neutral helium. These lines are, in order of decreasing strength: He I 584.33, 537.03 and 522.21 Å, which would appear faintly at twice their actual wavelength.

7.1.3 Scattered Solar Light in SiC Channels

In addition to airglow lines, scattered solar emission lines appear in the SiC channels when the observations are taken at high β angles (*i.e.* angle from anti-sun direction) during the sunlit portion of the orbit. The strength of these features also depended on the spacecraft roll angle. When FES A was used, SiC2 was rotated towards the Sun, so scattered light was stronger in these data. Emission from solar-scattered C III (977.0), O VI (1031.9 and 1037.6 Å), and Lyman β (1025.7 Å) has been positively identified. Emission from N III (991.6 Å) and N II (1085.7 Å) may also be present. It is believed that the solar light is scattered off reflective, silver coated Teflon blankets above the SiC baffles. At low β angles, the solar emission disappears because the blankets are in the shade of the SiC baffles and open baffle doors and the radiation strikes the blankets at a high angle of incidence. It is unknown at which β angle, if any, the solar emission completely disappears. The LiF channels are permanently located on the shadowed side of the spacecraft and therefore the solar emission lines will not be present in LiF data. Consequently, C III and O VI emission lines observed in SiC during orbital day should always be compared to emission in the LiF channel or to observations taken during orbital night to diagnose this effect.

From the failure of the third reaction wheel on 27 December 2004 until the end of the mission, *FUSE* mission controllers used non-standard roll angles to improve spacecraft stability. These angles could greatly increase the scattered sunlight in one or both SiC channels. When present, the scattered light, mostly Lyman continuum emission, appears as an increase in the background at $\lambda \lesssim 920$Å, and as strong, resolved Lyman lines at longer wavelengths.

7.1.4 Identifying Airglow and Solar Emission

If one is concerned about the origin of an emission line in a *FUSE* spectrum, there are several precautions that can be taken to determine whether it is from the target or a diffuse source. First, be familiar with the normally expected airglow lines, and be aware that they are always brightest for observations obtained during the daytime portion of the orbit. Thus, comparing day and night spectra can reveal airglow lines (see Fig. 7.1).

The second order solar spectrum does not behave in the same way. Nevertheless, like airglow, it fills the aperture. Therefore, on a spectral image constructed from the IDF file, it will extend beyond the region of the detector occupied by the point source spectrum. Finally, the scattered sunlight (see below) is observed only in the SiC channels during orbital day. Thus, comparing a SiC daytime spectrum with an overlapping LiF channel spectrum or a night time SiC spectrum should identify it.

7.2 Additional Contributions to the Background

7.2.1 Stray and Scattered Light

It is important to differentiate between stray light and grating scattered light. Stray light is defined as light falling on the detector from a source other than the optical system, whereas grating scattered light is defined as out-of-band light that the grating scatters into the *FUSE* bandpass. Stray light has been seen on segments 1A, 1B, and 2A. On these segments it is seen as a vertical band running the full height of the detectors (see Fig. 7.2). The brightness of these stray light bands varies during an orbit and analysis showed that the variation matches the variation of the airglow lines. Therefore, it is likely the bands are stray airglow emission (most likely Lyman α) entering the spectrograph cavity. On average, the stray light stripe on segment 1A produces about 1 count s^{-1} cm^{-2}.

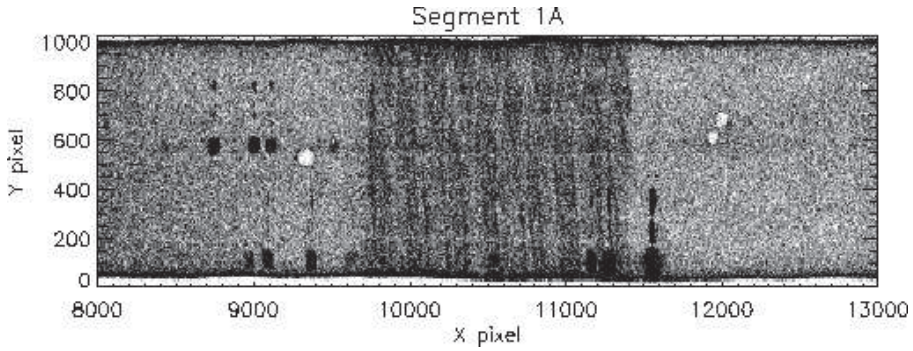

Figure 7.2: *A portion of Segment 1A showing the stray light band in an airglow spectrum. Note the pattern of alternating bright and dark arcs. LiF Lyman β is on the upper left and SiC Lyman β is on the lower right. The greyscale has been reversed so that darker shades of grey represent more counts.*

The preflight requirements for scattered light from the *FUSE* grating were very strict: the amount of light scattered into the *FUSE* bandpass from bright lines outside the band should be less than the detector background. The as-built *FUSE* holographic gratings exceeded this requirement, but the scattering is not completely negligible. This scattering is predominantly in the dispersion plane, so the normal background subtraction performed by CalFUSE will not remove it. The result is that the flux level will not quite be zero even in the bottoms of black *resolved* absorption lines. The scattering of light by the gratings effectively leads to very long tails on the LSF, that extend for hundreds of Angstroms. The amount of scattered light present in any given spectrum is the convolution of this extended LSF with the stellar spectrum, the reflectivities of the mirror and grating, and the detector quantum efficiency.

The KBr photocathodes on the *FUSE* detectors are sensitive far beyond the edge of the *FUSE* bandpass, so the scattering cannot be accurately estimated from *FUSE* data alone. However, reasonable estimates can be obtained. It is rare for the absorption lines of interstellar atomic gas to be broad enough for the profiles to be resolved and flat-bottomed. The HI Lyman lines are broad enough for some lines of sight, but geocoronal emission is often present, making it difficult to be sure that grating-scattered light is the primary contributor to flux at the

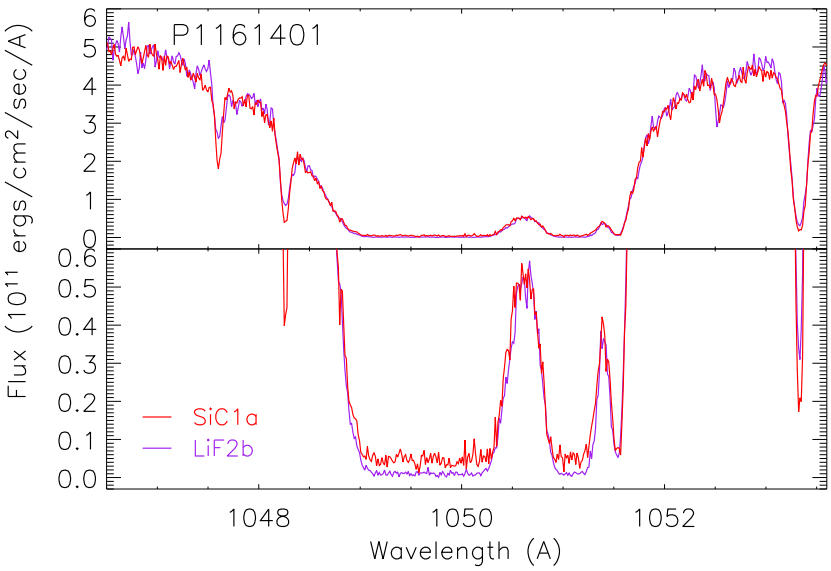

Figure 7.3: *A small region of the LiF2B and SiC1A spectra from P1161401 is plotted, showing saturated H_2 absorption. The lower panel gives a magnified view showing the difference in the scattered flux in the two channels.*

Table 7.2: Ratio of Grating-Scattered Light to Continuum Flux

Observation	LiF1A	LiF2B	SiC1A	SiC1B	SiC2A	SiC2B
P1018801	0.0037	0.0024	0.0073	0.0126	0.0150	0.0044
P1161401	0.0034	0.0019	0.0092	0.0295	0.0319	0.0035
P1162501	0.0023	0.0018	0.0087	0.0215	0.0226	0.0028
P1163101	0.0019	0.0015	0.0054	0.0304	0.0261	0.0023
P3020701	0.0034	0.0035	0.0205	0.0140	0.0124	0.0091

bottoms of the lines. Molecular H_2 absorption provides an ideal means of measuring grating scatter: for lines of sight with a large column density of H_2, there will be numerous absorption troughs many tenths of an Angstrom wide distributed over 912Å to 1110Å. Figure 7.3 shows an example of the residual flux in such lines.

Table 7.2 gives the ratio of residual flux at the bottom of the H_2 absorption troughs to an estimated mean continuum, for six detector segments in each of five observations. The spectra were obtained through the LWRS aperture, except for P3020701, which used MDRS. The P3020701 observation also differs from the others in that the continuum is essentially flat across the *FUSE* waveband, while the continuum flux declines by a factor of several towards shorter wavelengths in the other observations.

The general trend is that the LiF channels exhibit less residual background than the SiC channels, though SiC2B is close to LiF1A. For both SiC1 and SiC2 LWRS data, the short-wavelength segment shows markedly higher residual background flux than the longer-wavelength

Table 7.3: Ratio of Grating-Scattered Light to $F_\lambda(1150)$

Observation	LiF1A	LiF2B	SiC1A	SiC1B	SiC2A	SiC2B
P1018801	0.0025	0.0015	0.0054	0.0050	0.0067	0.0036
P1161401	0.0016	0.0008	0.0048	0.0033	0.0047	0.0021
P1162501	0.0011	0.0008	0.0048	0.0036	0.0027	0.0017
P1163101	0.0006	0.0004	0.0020	0.0024	0.0027	0.0010
P3020701	0.0033	0.0033	0.0200	0.0103	0.0101	0.0093

segment. This trend is not present in the P3020701 observation, however. To test whether this is the result of an artifact in the background subtraction, particularly for SiC1, for which the spectra are located close to the edge of the detector, or the result of the residual flux being dominated by scattering of much higher continuum flux at wavelengths beyond the individual detector segments, the flux ratio was also computed with respect to the flux at 1150Å instead of the local continuum. The results are in Table 7.3.

Scaling the fluxes relative to that at 1150Å does improve the consistency between detector segments for the SiC channels, though only for the LWRS data. The MDRS residuals remain considerably higher than for LWRS, suggesting that scattering from the edges of the aperture may be significant.

7.2.2 Event Bursts

Occasionally, the *FUSE* detectors register large count rates for short periods of time. The phenomenology of the bursts have been characterized but their cause has remained elusive. These event bursts can occur on one or more detectors at the same time and often have a complex distribution across the detector (see *Instrument Handbook (2009)*). Typical bursts last for about 1 min, though durations from 1 s to 10 min have been seen. Event bursts have been seen on all 4 segments, though they are most common on segments 1A and 1B. CalFUSE screens the data to identify and exclude bursts for TTAG data only (Dixon et al. [2007]). It does this by sampling the background count rates in selected regions of the detector and rejecting time intervals in which the background rate rises rapidly, as when an exposure extends into an SAA or the target nears the earth limb. The background rate computed by the burst-rejection algorithm is stored in the BKGD_CNT_RATE array of the timeline table and included on the count-rate plots (`*rat.gif`) generated for each exposure. Event bursts are usually inconsequential for HIST data because the target count rates are so high. The portion of the TTAG data screened out due to burst events can be seen in the file generated for each exposure (see Fig. 4.3). Observers should still examine their raw data to determine if event bursts occurred during the exposure and if they were properly removed, especially when working with data obtained for faint targets. Ancillary data, such as the count rate plots, may also be useful for this assessment.

7.3 Detector Effects

7.3.1 Moiré Pattern

Strong fixed-pattern noise has been reported especially in HIST spectra of bright sources. It is strongest in segment 2B but has been seen in segments 1A and 1B as well. This noise is due to beating among the arrays of micro-channel pores in the three layers of the Microchannel Plate (MCP) stack (Tremsin et al. [1999]). On the detector, the moiré pattern appears hexagonal (see *Instrument Handbook (2009)*), but in extracted HIST spectra it appears as high-frequency fringes as shown in Fig 7.4 (see also Dixon et al. [2007]). When present, users are advised to smooth or bin their spectra by ∼8-10 pixels to average out the effect.

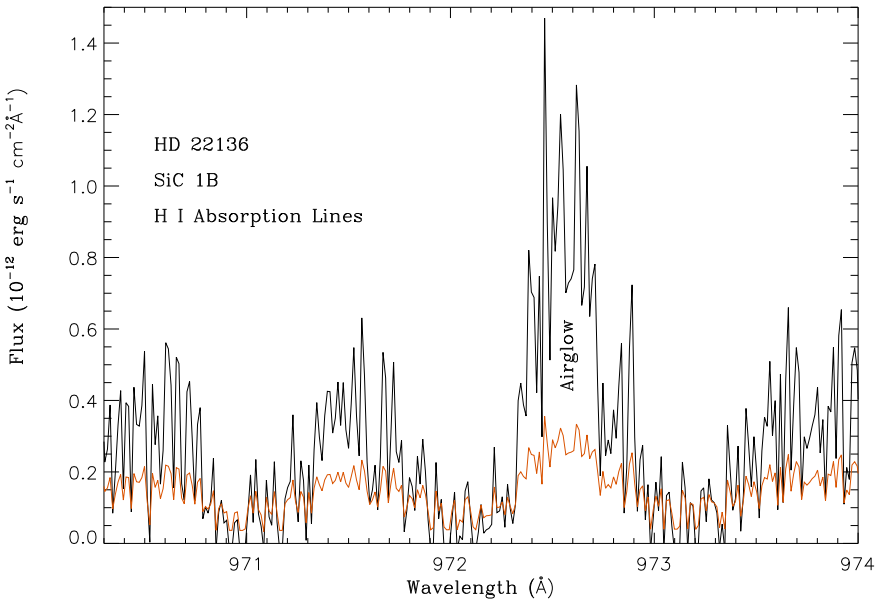

Figure 7.4: *Fixed pattern noise due to moiré structure in the SiC1B HIST data from target HD 22136 (program Z9011501). The moiré ripples are strongest in segment 2B, but are also seen in segments 1A and 1B as shown here (see also Dixon et al. [2007]). Associated errors are overplotted in red. The upward peak is due to H I airglow emission.*

7.3.2 Grid Wires and the Worm

Two grids of fine wires partially shadow the active area of the detectors (see *Instrument Handbook (2009)* for details). Their interaction with the horizontal focus of the spectrograph produces shadows on the detectors known as "the worm" (or more generally "worms" since they appear in multiple channels). These shadows can attenuate up to 50% of the incident flux and vary as a function of wavelength. Their location changes in the dispersion direction depending on the vertical position of the source in the aperture. Since the location of the focus point is wavelength-dependent, the strength of the worm is sensitive to the exact position of the spectrum on the detector. This position cannot be determined reliably enough to automatically compensate for the flux loss due to worms. Hence, worms are not corrected by CalFUSE.

Worms have been seen in all segments but they are most prevalent in the LWRS LiF1B segment. Figure 7.5 illustrates the effects of the worms on *FUSE* data. The redundant wavelength coverage of the *FUSE* channels can be used to diagnose and potentially mitigate the effects of the worms (see Figs. 7.10 to 7.12). Observers who require absolute spectrophotometry should carefully examine *FUSE* spectral plots for the presence of this effect.

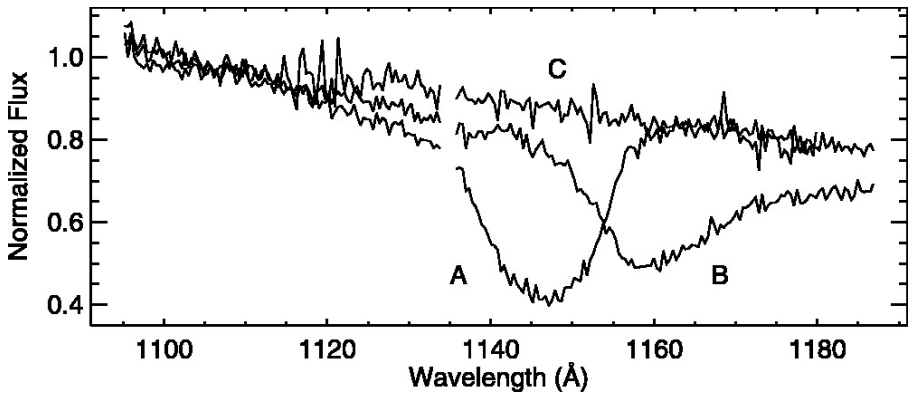

Figure 7.5: *LWRS point-source spectra obtained with the LiF1B (spectra A and B taken at different vertical positions) and LiF2A (spectrum C) segments. The large depressions occuring around 1145 Å in spectrum A and 1160 Å in spectrum B are due to worms. Note that spectrum C is unattenuated in this particular case (see Dixon et al. [2007]).*

7.3.3 Dead Zones

Dead zones appear as opaque spots on the detector image. They are small regions on the detector where the sensitivity is truly reduced. Type I dead zones are simply regions of decreased sensitivity. Type II dead zones, in addition to showing a loss of sentivity at the center of the spot, also exhibit bright rims around them. Discussion of the origins of this rim can be found in the *Instrument Handbook (2009)*. Unlike Type I dead zones, Type IIs have been seen to vary in size and shape with high-voltage cycling. Both types of dead zones are difficult to correct but are noted by their QUALITY flag in the extracted spectral file. In cases where the dead zone is smaller than a single resolution element (most cases), masking the region out of the spectral extraction is sufficient. However, the larger features will affect the quality of extracted spectra. Observers are advised to examine the IDF files (using the cf_edit.pro tool described in the *FUSE* Tools in C package, for instance) for the presence of dead zones to avoid confusing these artifacts with real absorption lines. A comparison between spectra from channels with overlapping wavelength ranges is also recommended, as is shown in the right panel of Fig. 7.6. The left panel displays the IDF file for that same exposure.

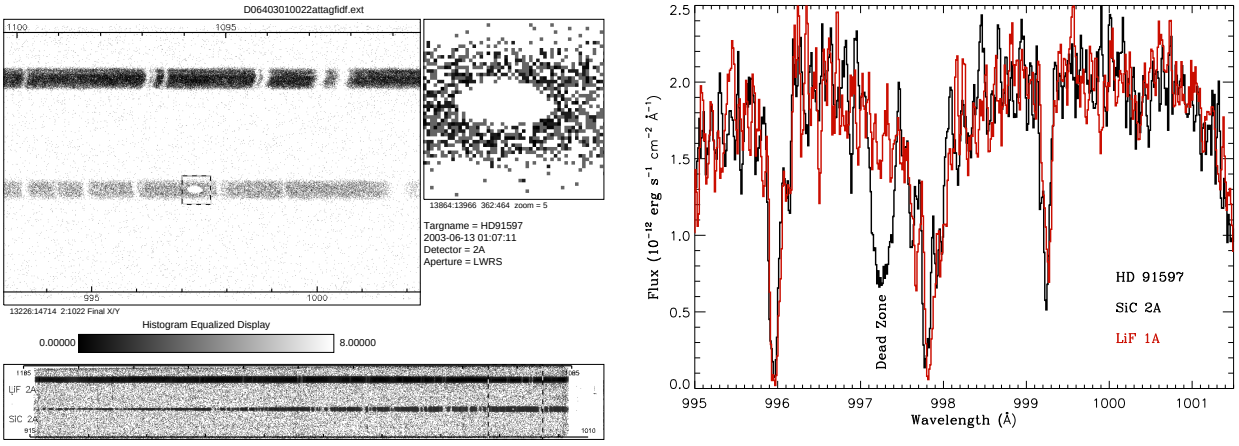

Figure 7.6: *Left: Data from the IDF file for segment 2A of exposure D0640301002 obtained by observing target HD 91597 in LWRS. The cf_edit.pro routine (see Chapter 8) was used to display this IDF file and shows the full spectra displayed in the bottom panel of the plot. The top panels show the presence of a Type I dead zone in the SiC2A segment around 997 Å. This plot displays reversed colors where absorption features appear as bright stripes against the dark continuum emission. Right: A comparison of the extracted spectra from segment SiC2A (black trace) and LiF1A (red trace) over their overlapping wavelength range for target HD 91597. In SiC2A, the strong absorption feature around 997 Å is spurious and due the presence of a dead zone at this particular detector location. Note its absence in the LiF1A spectrum.*

7.3.4 Gain Sag and Detector Walk

The *FUSE* detectors convert each ultraviolet photon into a cloud of electrons, for which the detector electronics calculates the X and Y positions and the intensity, or pulse height. Prolonged exposure to photons caused the detectors to become less efficient (a phenomenon called gain sag), and thus the mean pulse height slowly decreased with increased exposure. Unfortunately, the X location of lowest pulse-height photon events is systematically miscalculated by the detector electronics. As the number of low pulse-height events increases, spectral features appear to "walk" (or shift centroid) across the detector. The effects of the walk vary as a function of both pulse height and position on the dtetector. A common example is the shoulder apparent on the short-wavelength side of the Lyman β airglow line in the LiF1A channel.

To combat this problem, the detector high voltage was periodically raised. Table 7.4 lists the HV settings and the dates that they were in effect for each detector and segment. (Note: these digital HV settings are the values a user will see in the file headers, but are not actual voltages. See the *Instrument Handbook (2009)* for more information.) While the CalFUSE pipeline largely is able to correct for the walk in TTAG data, for which the pulse height of individual photon events is recorded, the correction applied to HIST data is only approximate. Line locations and equivalent width measurements are likely to be in error on segments affected by the walk, so results should be carefully compared to data from other segments when possible. Figure 7.7 shows the effect of the gain sag and subsequent walk on observations taken before (upper panel) and after (lower panel) raising the high-voltage in 2002. Users interested in specific HIST data are advised to compare the observation dates against those listed in Table 7.4. Note that segment 2A was below its ideal voltage after late 2002 due to problems in raising the voltage on this segment. More information can be found in the *Instrument Handbook (2009)*.

Table 7.4: Dates of High Voltage Setting Changes

UT Date	Nominal High Voltage Setting			
	1A	1B	2A	2B
1999-08-13	129	129	0	0
1999-08-26	129	129	129	102
2001-01-24	141	137	137	108
2001-07-31	147	143	149	113
2002-02-19	155	151	161	119
2002-04-14	155	151	149	119
2002-12-08	161	157	161[a]	124
2002-12-16	161	157	134[a]	124
2003-02-03	161	157	149	124
2003-08-16	164	160	149	126
2004-07-20	165	162	149	127

[a] Attempts to raise the high voltage on segment 2A in 2002 led to repeated detector shutdowns. Stable operations were possible only by keeping the high voltage at a lower than ideal level. Hence, walk effects will be most significant for segment 2A.

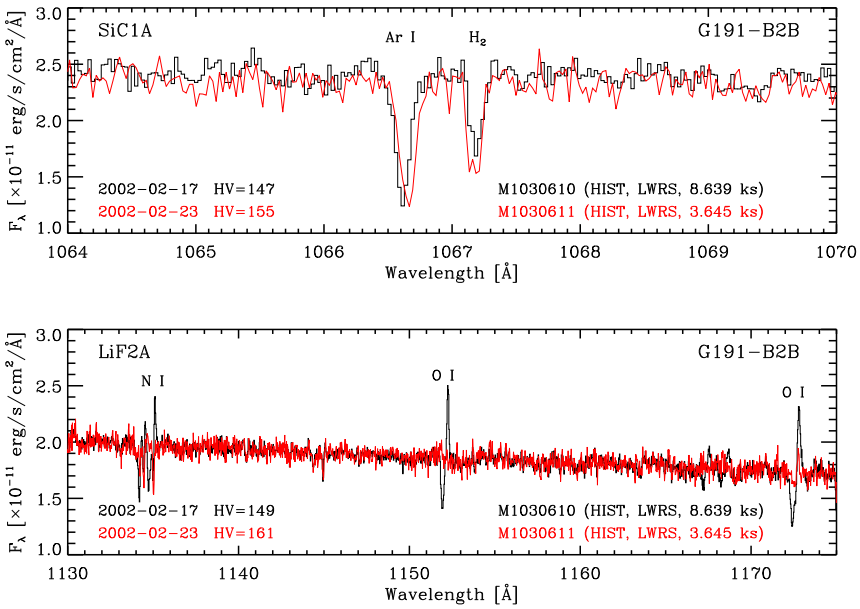

Figure 7.7: *The effect of gain sag and walk is illustrated in spectra of the photometric standard G191–B2B taken immediately before and immediately after the largest change in detector high voltage. Top: Although the S/N is different in the two spectra, notice how walk subtly shifts the position and shape of the prominent interstellar absorption lines. Bottom: The narrow "P Cygni" morphology of lines in black is a diagnostic of gain-sag in regions of the detector that have been heavily overexposed. In this case, the over-exposure is quite localized due to the presence of strong airglow lines of N I and O I. Gain sag in these regions causes the positions of photon events to be misregistered, which produces the tell-tale morphology. Raising the high-voltage compensates for the gain sag, and the strange morphology disappears. However, only a crude walk correction is available for HIST spectra. The correction for these effects is much better for data obtained in TTAG mode.*

7.3.5 Fixed-pattern Noise and FP splits

The *FUSE* detectors are affected by fixed-pattern noise – see *Instrument Handbook (2009)*. The astigmatism (large Y height) due to the instrument's optics as well as spectral thermal motions (in both X and Y) partially mitigate this effect, but signal-to-noise (S/N) ratios above 30 could not be obtained unless something specific was done to further smear out fixed-pattern noise. To do so, an observational technique called Focal Plane splits (FP splits) was used. This technique consisted in taking a series of exposures at several FPA X positions, hence, shifting each exposure's location in the dispersion direction on the detector. If the S/N ratio obtained at each FPA position was high enough, combining all data averaged out the noise and allowed the user to reach S/N higher than 30 in the combined spectrum. Note that CalFUSE does not automatically combined those data. It is left to the user to perform the appropriate coaddition to reach the highest S/N. Figure 7.8 displays a portion of the LiF1A (top panel) and LiF2A (bottom panel) spectra obtained for target HD220057 using the FP split technique. In both segments, S/N ratios of 40 or above were reached.

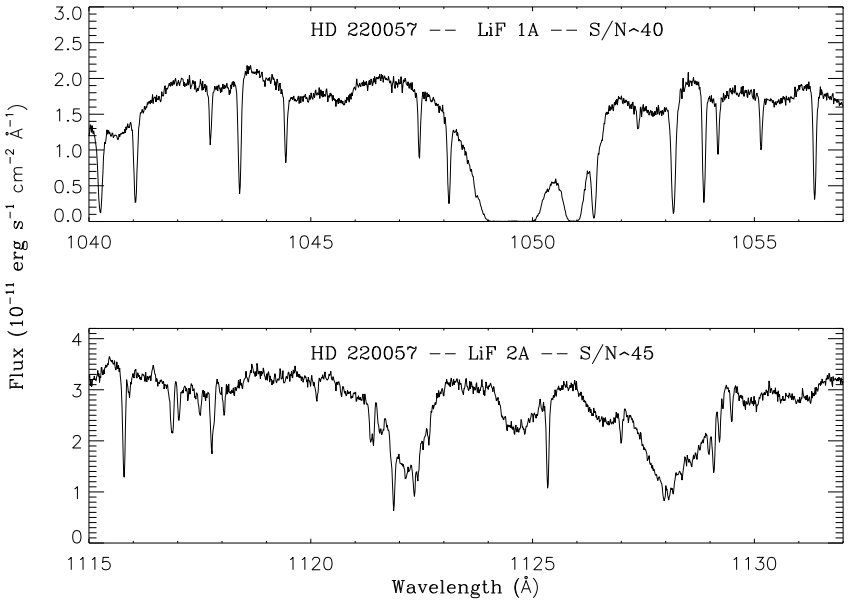

Figure 7.8: *Use of FP splits to achieve S/N ratios above 30. Top: Portion of the LiF1A spectrum for target HD220057. These observations used the FP split technique in order to achieve S/N ratios ∼40. Most sharp absorption lines are due to the presence of molecular hydrogen (H_2). Bottom: Portion of the LiF2A spectrum for target HD220057. Most sharp absorption lines are due to the presence of C I, corresponding fine-structure lines C I* and C I** and Fe II. The broader features have a stellar origin.*

7.4 Instrumental Effects

7.4.1 Spectral Motion

The position of a target image on the detectors can vary significantly due to the exact positioning of the target in the aperture and to movements of various optical components and the spacecraft itself. The exact position of the spectra must be determined to perform proper wavelength and flux calibrations. A brief description of these various motions is given below. More details can be found in Chapter 2 and the *Instrument Handbook (2009)* and Dixon et al. [2007].

Grating motions: are induced by small thermal variations of the gratings on orbital, diurnal and precessional timescales. These motions can shift the target by as much as 15 pixels (peak-to-peak) in both the X and Y directions in LiF. They affect the SiC channels the most since these channels alternately see direct sunlight (or not) around the orbit. For TTAG data CalFUSE applies a grating-motion correction to each photon in the event list. Because all photons in HIST data are given the same arrival time, all the photons in an exposure receive the same grating-motion correction.

Mirror motions: are induced by thermal variations of the mirrors. Consequently, the target image moves within the spectrograph's aperture and the spectrum position shifts in X and Y on the detector. When LiF1 was used for guiding, its motion was corrected by the spacecraft itself. Only the LiF2 and SiC spectral positions need to be corrected by CalFUSE. (After 12 July 2005, when LiF2 was the guide channel, this channel was corrected automatically and the remaining three were corrected in CalFUSE.)

Focal Plane Assembly (FPA) motion: FPA motions in the X direction are used to correct for mirror misalignments and to perform FP splits (see above). FPA motions in the Z direction are used to place the apertures in the focal plane of the spectrograph. Both motions change the spectrograph entrance angle, shifting the target spectrum on the detector.

7.4.2 Astigmatism

Spectral features show considerable curvature parallel to the dispersion direction and significant astigmatic height perpendicular to this direction (see Fig. 7.9). These distortions are a natural consequence of the *FUSE* optical design. Astigmatism corrections were derived from observations of the central star of the Dumbbell Nebula (M27). Because astigmatism corrections have been derived only for point sources, no correction is performed on spectra of extended sources, airglow spectra, or observations taken with the target at the RFPT.

7.5 Flux Calibration

The major issues that affect the absolute flux calibration of *FUSE* data are target motions on the focal plane, which tend to affect the overall normalization of the entire spectrum from a channel, and "worms" which affect specific spectral regions (see Section 7.3.2).

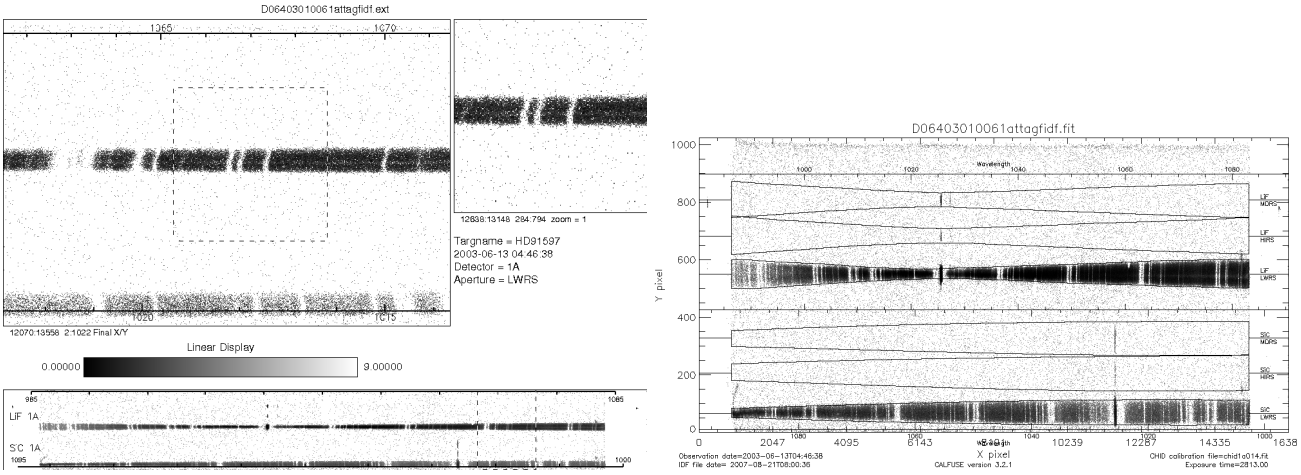

Figure 7.9: *Left: Data from the IDF file for segment 1A of exposure D0640301006 obtained by observing target HD 91597 in LWRS. The spectral line curvature and their variable heights induced by astigmatism are obvious in LiF1A and SiC1A spectra. Note that colors are inverted so that absorption features appear as bright stripes. Right: Image (*`*ext.gif`*) of detector segment 1A once the data for exposure D0640301006 have been fully corrected for astigmatism, detector effects and other effects described in this Chapter.*

7.5.1 Definition and Internal Consistency

The *FUSE* flux calibration is defined by synthetic spectra of six hot DA white dwarfs. The six stars include the four DAs used as primary standards for HST: GD 71, GD 153, HZ 43, and G 191-B2B, plus GD 659 and GD 246. The stars have a wide range of effective temperature, 32,800 K to 61,200 K, to minimize potential systematic errors in the calibration arising from uncertainties in the model parameters for individual stars and from uncertainties in the line broadening theory. The derivation of the effective area calibration is described by Dixon et al. [2007]. In this section the internal consistency of the final calibration is tested by comparing the spectra of each of the stars against their respective synthetic spectra. For this exercise, all data were re-reduced with CalFUSE 3.2.2 and new synthetic spectra were computed.

The atmospheric models were computed in NLTE with TLUSTY 200 [Hubeny & Lanz , 1995], using the model parameters from Dixon et al. [2007] shown in Table 7.5. The models were computed using 200 depth points, and the Lyman line profile calculations employed the tables computed by Lemke [1997]. Synthetic spectra were computed with Synspec 49 (Ivan Hubeny, private comm.). The spectra were normalized to the V magnitudes shown, and shifted to the appropriate absolute velocity. Absolute velocities were taken from the literature, or determined from fits to narrow photospheric lines in the *FUSE* spectra.

Table 7.5: *FUSE* Calibration Star Parameters.

Stellar Parameters for FUSE Calibration Stars				
Star	Teff (K)	Log g	V	Vrad (km/s)
GD 71	32,843	7.783	13.032	30.
GD 659	35,326	7.923	13.36	34.3
GD 153	39,158	7.770	13.346	20.
HZ 43	50,515	7.964	12.909	20.6
GD 246	53,000	7.865	13.094	-13
G 191-B2B	61,193	7.5	11.781	26.

All LWRS observations providing usable data were included. Spectra from individual exposures within an observation were normalized to the exposure with the peak flux in that observation; those with less than 40% of peak were discarded. Exposure times were scaled by the inverse of the normalization factor. No other re-normalization was performed. Spectra were co-aligned to place interstellar lines at known absolute velocities, and were combined by weighting by exposure time.

The results are shown in Figs. 7.10 through 7.12. The observed spectra from all channels are shown, over-plotted by the synthetic spectra. The ratios of the observed to synthetic spectra are plotted in the lower panel of each figure. The overall agreement is excellent: typical *rms* deviations are about 5%, with no apparent systematic bias in the overall slope of the effective area across the *FUSE* band. There are, however, a number of systematic effects of note:

- The worm feature in LiF1B is obvious in all the spectra, and shows significant effects throughout the LiF1B band. Because this feature is strong and variable, *neither the absolute flux level nor the continuum shape is reliable in LWRS LiF1B data.*

- The effective temperature of the GD 246 model is clearly too low. If the parameters from Finley et al. [1997] are used, Teff=58701K and log g=7.807, the agreement between the model and *FUSE* spectrum is similar to that of G 191-B2B. A plot comparing this model with the MDRS spectrum of GD 246 is shown in Fig. 7.24. The source of this disagreement is still under investigation.

- The Lyman line profiles in the models appear to be systematically deeper than the data for Lyman γ, δ, and ϵ, though not for Lyman β.

- There is a worm present, intermittently, in LWRS SiC1B spectra that affects wavelengths longward of about 975Å. It appears prominently in the GD 659 spectrum, but weakly or not at all in the other spectra. The strength of such features depends sensitively on the position of the star in the spectrograph aperture, so users should compare the SiC1 data at these wavelengths with SiC2, LiF1, and LiF2 data to assess its quality.

- The SiC1 calibration appears systematically low in the GD 153 data, and to a lesser extent in the GD 71 data. This illustrates the magnitude of the uncertainties that may be present in the corrections for time-dependent variations in the effective area; these are discussed in the next section.

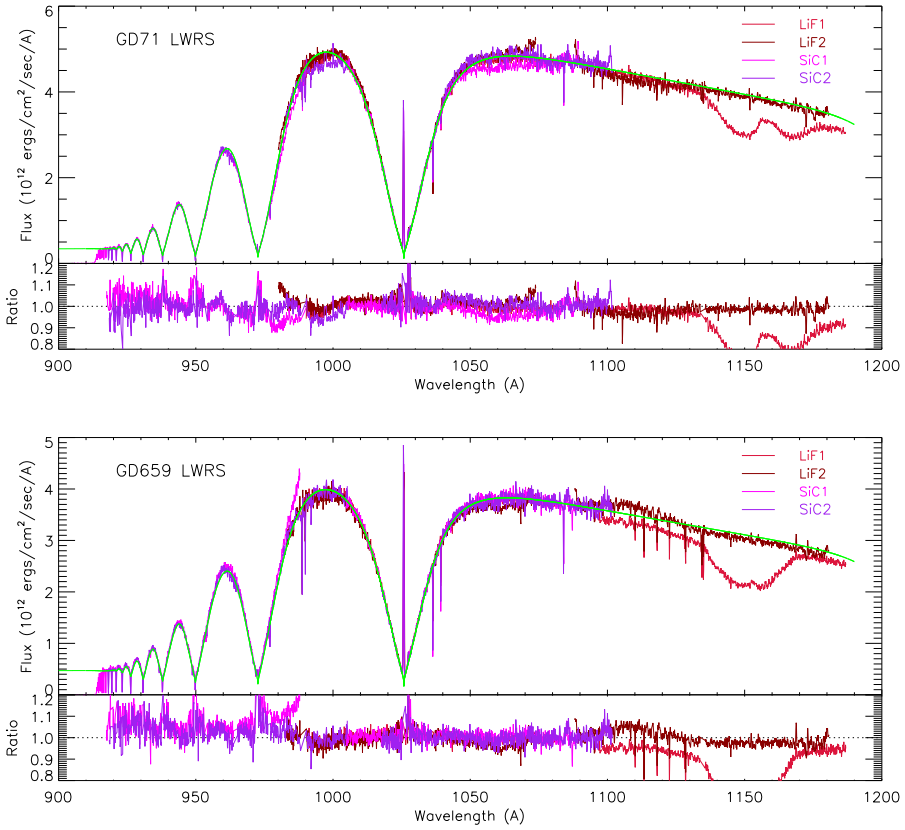

Figure 7.10: *The FUSE spectrum of GD 71 is plotted in the upper figure, along with the synthetic spectrum (see text). All LWRS observations have been combined; data from each channel are color-coded as described below. The bottom panel in each figure shows the ratio of the data to the model. The lower figure provides the same information for GD 659. In all panels, the red trace represents LiF1, the brown trace represents LiF2, the purple trace represents SiC1, and the majenta trace represents SiC2. The model spectrum is plotted in green.*

- There is a broad, systematic bump in the LiF2A effective area apparent in the GD 659 spectrum and in some of the individual observations of other stars. This is a manifestation of the shortcomings in the time-dependent corrections for the LiF2A LWRS effective area. This portion of the detectors accumulated the highest cumulative exposure, and the high voltage on segment 2A could not be raised much to compensate. The magnitude of this effect proved difficult to track over time, however, perhaps as a result of dependence on position of stars in the spectrograph aperture or perhaps as a result of weak worm features. The magnitude of the variation of this effect is discussed in the next section.

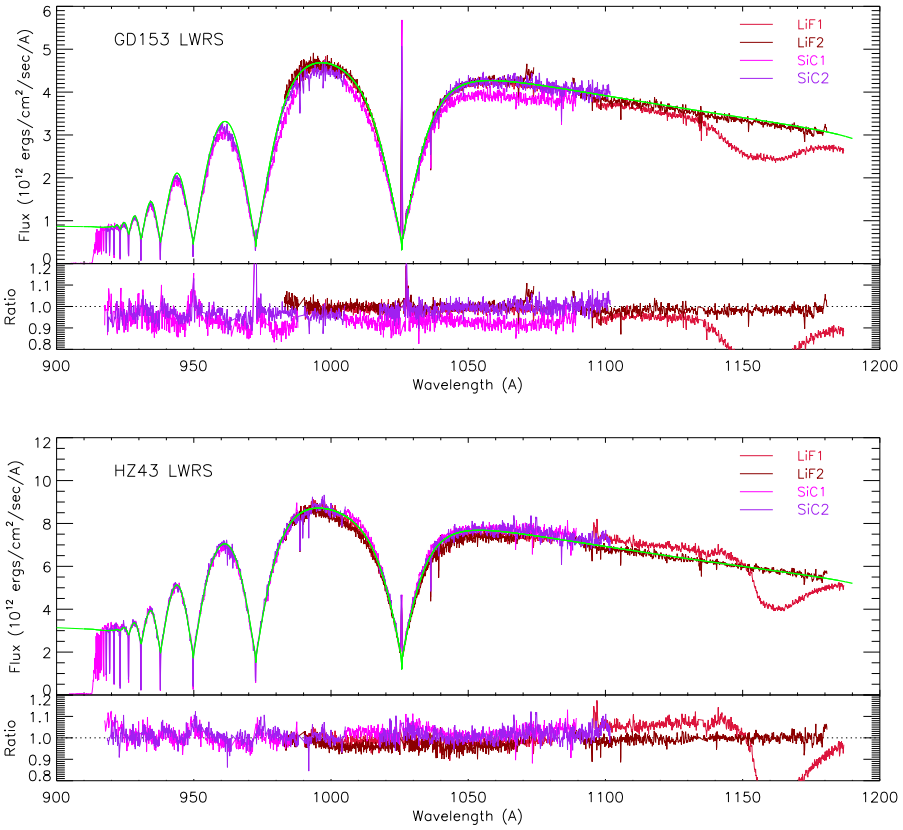

Figure 7.11: *Same as Figure 7.10 above, but for GD 153 (Top) and HZ 43 (Bottom).*

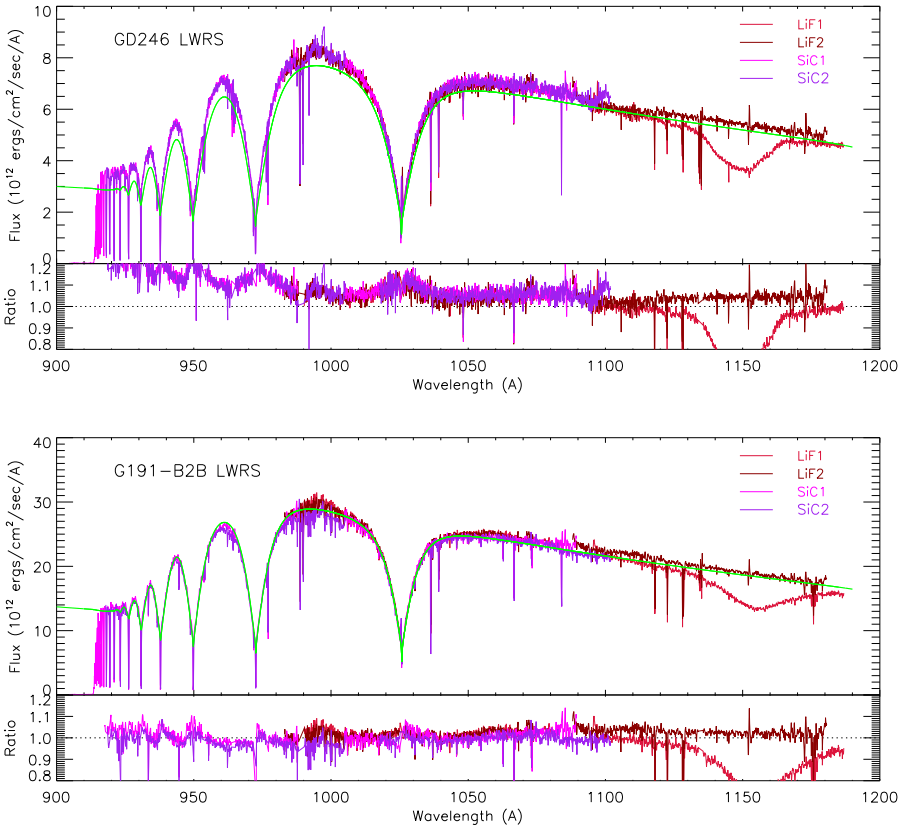

Figure 7.12: *Same as Figure 7.10 above, but for GD 246 (Top) and G 191-B2B (Bottom).*

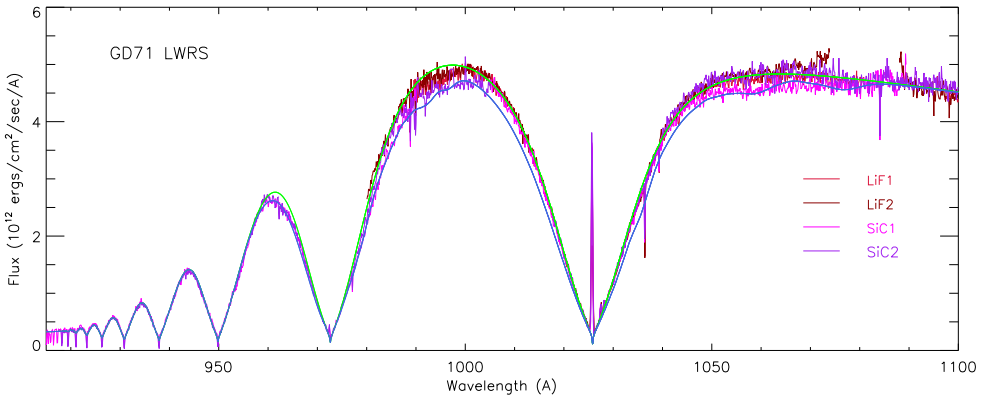

Figure 7.13: *A zoomed-view of the spectrum of GD 71 is shown, as in Figure 7.10 above. The synthetic spectrum computed using Allard's line profiles is over-plotted in blue. The Lyman β, γ profiles appear too broad (see text), but the discrete absorption features do appear in the spectrum.*

7.5.2 Quasi-molecular Satellite Features

Quasi-molecular satellite lines of the Lyman lines have long been known to be present in the spectra of cool DA white dwarfs (Allard et al. [2004a]; Allard et al. [2004b], and references therein). It was not expected that such features would be present at the high effective temperatures of the stars used in the *FUSE* calibration, and such features were not included in the synthetic spectra used to define the *FUSE* calibration, nor in the models plotted above. However, a close examination of the GD 71 spectrum revealed some weak systematic discrepancies with the model that suggested that such features might be present. Lyman β profiles were calculated for effective temperatures of 30kK, 40kK, 50kK, and 60kK, and Lyman γ was calculated for 30kK (graciously provided by Nicole Allard). The models for all of the stars were re-computed using these profiles; results for a subset of the stars are shown in Figs 7.13 through 7.15.

Inclusion of the quasi-molecular features has two effects on the model spectra: isolated absorption features appear at a number of wavelengths, but the overall Lyman line absorption is increased as well. An examination of the GD 71 spectrum shows that this overall broadening improves the match to the data at 960Å, and the isolated absorption features between 990Å and 1000Å appear as a significant flattening of observed spectrum. The features at 1055Å and 1075Å are broader and not clearly present in the data. For the somewhat hotter star GD 659 the isolated features are weaker-still, and are difficult to discern in the data.

The plot of the HZ 43 spectrum and model shows that the broadening of the Lyman line profiles by the quasi-molecular satellites is present even at high effective temperature. Because such effects were not expected at high effective temperature, no systematic testing or tuning of the models has been done under these conditions. The broader Lyman lines predicted by these models appear to conflict with the data, but this conflict may be a consequence of the fact that the calibration was defined by models that did not include such features. Ideally, the calibration would be derived with both sets of models, and the best one selected by testing

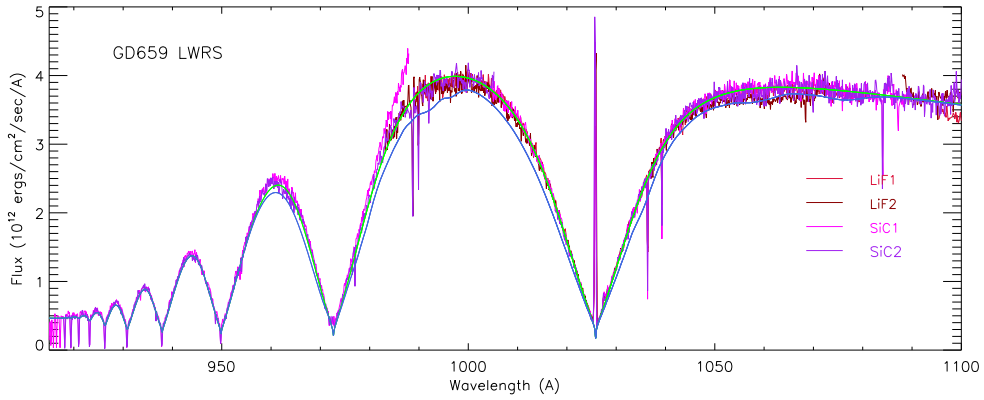

Figure 7.14: *A zoomed-view of the spectrum of GD 659 is shown, as in Figure 7.13 above. The quasi-molecular satellites are too weak to be apparent at this higher effective temperature.*

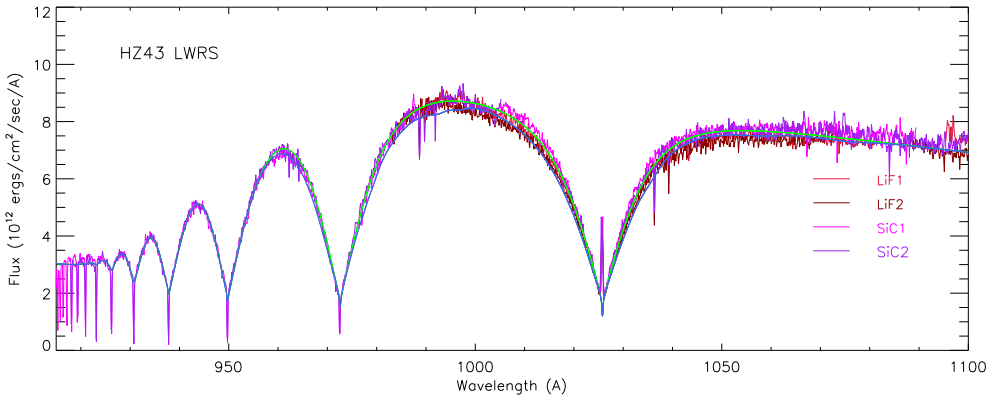

Figure 7.15: *A zoomed-view of the spectrum of HZ 43 is shown, as in Figure 7.13 above. The discrete quasi-molecular features have essentially disappeared at this temperature, but the Lyman β and Lyman γ profiles are still measurably broader than in the nominal model (see text).*

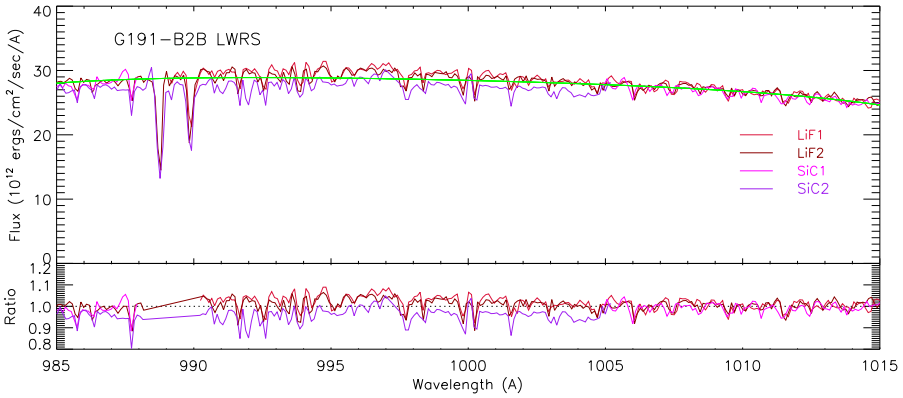

Figure 7.16: *A zoomed view of a small region of the spectrum of G 191-B2B is shown, illustrating the presence of numerous weak metal lines. Over half of the pixels shown are affected by absorption amounting to several percent of the continuum.*

against a wide range of DA spectra. Such an analysis has not been performed. As a result, there are minor additional systematic uncertainties of several percent in the *FUSE* flux calibration in the vicinity of Lyman β, which gradually decrease for the higher Lyman series lines.

7.5.3 G 191-B2B

The star G 191-B2B has long been known to contain a significant quantity of heavy elements in its photosphere. These trace elements have a dramatic effect on the emergent spectrum at EUV wavelengths (Dupuis et al. [1995]), but weak absorption features are numerous at FUV wavelengths as well. Despite this, pure hydrogen models have been used successfully for calibration purposes (e.g. Bohlin [2000]). The neglect of these lines will result in an underestimate of the effective area at FUV wavelengths. This can be seen in Fig. 7.16, which shows a region of the *FUSE* spectrum in which nearly half of the pixels are affected by weak absorption lines.

7.5.4 Time Dependence

The sensitivity of *FUSE* varied significantly throughout the mission. Plots of the effective area in each channel are shown in Figs. 7.17 and 7.18. The curves shown in these plots are the effective areas taken from the CalFUSE calibration files. These were derived at roughly 3-month intervals from Launch through late 2004. After that time, while *FUSE* was operating with only a single reaction wheel, it was difficult to schedule observations of the stars used for monitoring the calibration. The last three curves were obtained in 2006 and early 2007.

A number of features of these plots are worthy of note. The LiF channel sensitivity drops abruptly shortward of 1000Å, but does not go to zero. Significant throughput is present to the point where the edge of the detector cuts off the spectra. The throughput of the SiC channels degraded steadily throughout the mission, while the throughput of the LiF channels stabilized after an initial decline.

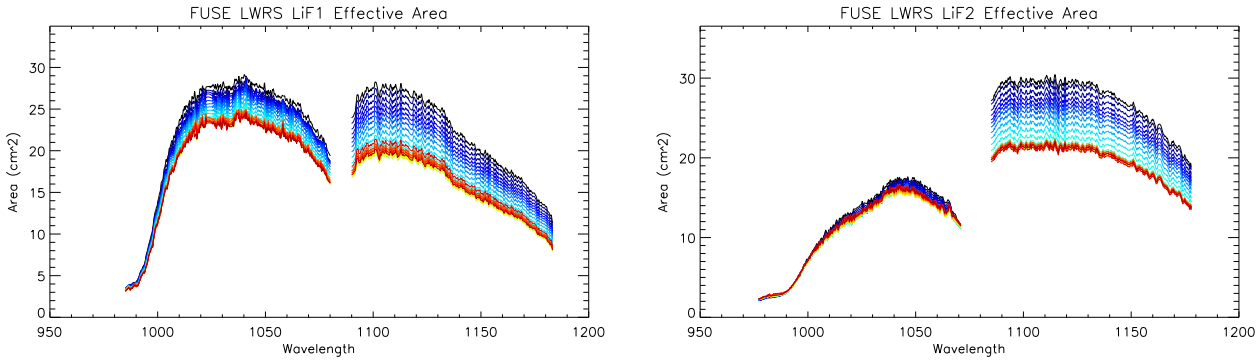

Figure 7.17: *The effective area of the LiF1 channel through the LWRS aperture is shown in the left panel; each curve represents a different time during the mission. The dramatic drop shortward of 1000Å is caused by the decrease in transmission of the LiF layer applied to protect the Aluminum coating. The right panel shows the evolution of the LiF2 channel sensitivity. The sensitivity of LiF2B is substantially less than LiF2A, due to the low QE of the MCPs in detector 2B.*

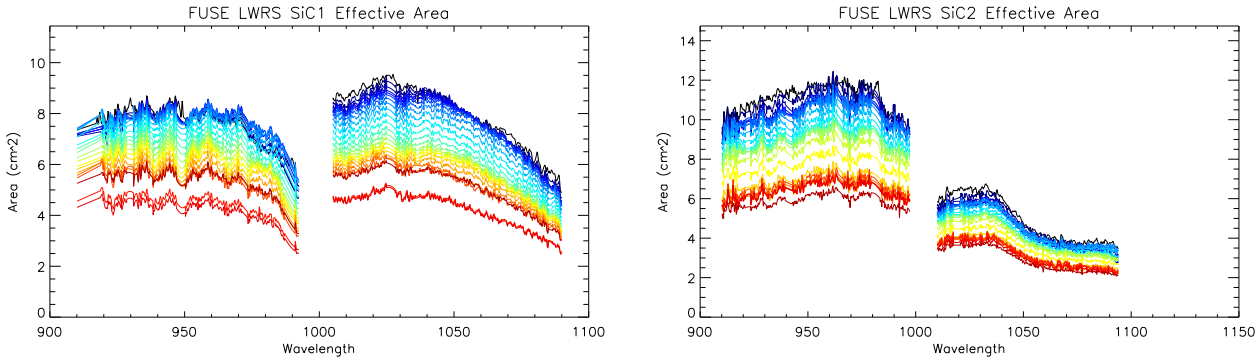

Figure 7.18: *The effective area of the SiC1 and SiC2 channels through the LWRS aperture are shown in the left and right panels, respectively; each curve represents a different time during the mission. The sensitivity of SiC2B is much less than that of SiC2A due to the low QE of detector 2B.*

Because the worm in LiF1B LWRS is both strong and highly variable, no wavelength-dependence to the evolution in sensitivity could be derived for this channel-segment combination. Instead, a simple scale factor was applied to adjust the effective area over time. Similarly, it was difficult to determine a consistent solution for the wavelength-dependence of the LiF2A sensitivity evolution. It too was approximated by a time-dependent scale factor. The reason for this difficulty was not clear, but perhaps the worm features in this portion of the detector were also variable, though not nearly as badly as LiF1B LWRS. Further information and images of the worm features in each detector segment can be found in Section 4.3.4 of the *Instrument Handbook (2009)*.

Three stars were used for tracking the instrument sensitivity during the first several years of the mission: G 191-B2B, WD 2211-495, and WD 1634-573. These stars were chosen because they were stable, at convenient locations on the sky, and bright enough that sufficient signal-to-noise could be obtained in brief observations. After the loss of reaction wheels limited access to much of the sky, K1-16 was added to the sensitivity monitoring program. Other white dwarfs provided occasional additional datasets for this program, but these four stars were the primary targets.

An assessment of the accuracy of the time-dependent flux calibration was performed in the following manner. All the LWRS data for these four stars were reduced in the same manner as described above in Section 7.5.1. For each observation, the mean flux was calculated for wavelength bins of 15–20Å, giving five bins per channel and detector segment. The ratio of each such average flux to that of the first observation of each star was computed; the results are plotted in Figs. 7.19 through 7.22. Splitting each spectrum into these broad bands helps check for potential systematic errors in the overall slope and to detect the influence of worm features.

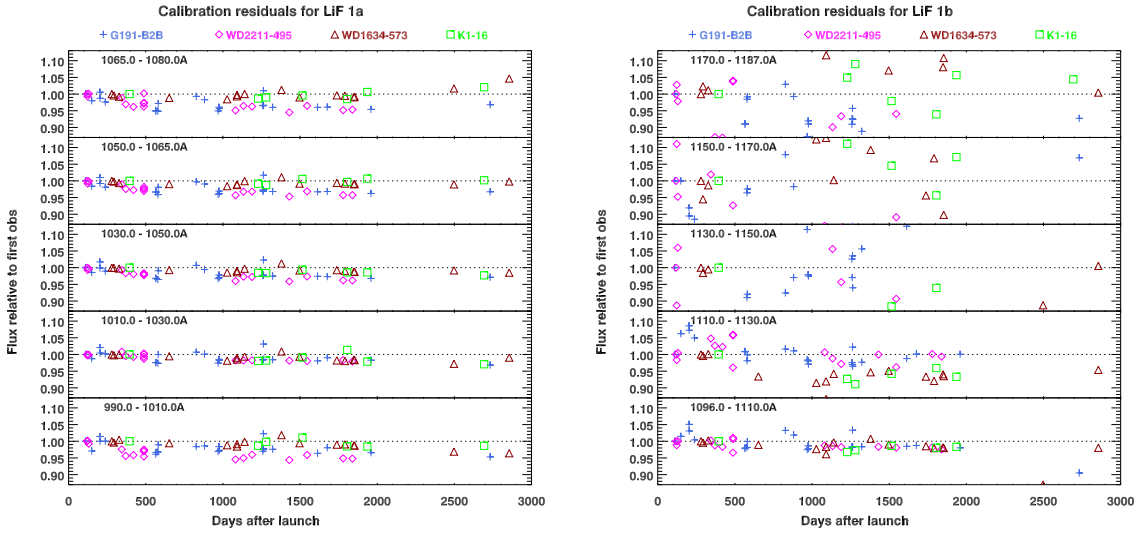

Figure 7.19: *This Figure shows the variations in LWRS LiF1 response over the course of the FUSE mission, as determined from relative changes in measured fluxes for the four primary monitoring stars. Each panel shows the variations for a 15–20Å portion of the spectrum. LiF1A is shown in the Left panel: the tight clustering of ratios about unity shows that the variations in sensitivity were well-corrected for LiF1A. LiF1B is shown in the Right panel: the wide scatter of points for four of the five spectral bins is due to the strong worm in LWRS LiF1B.*

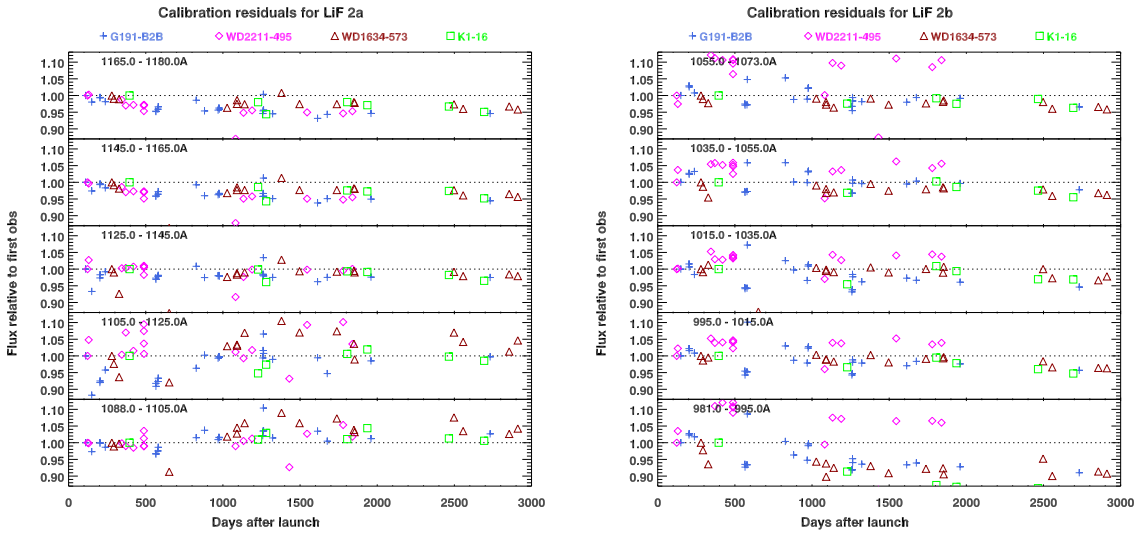

Figure 7.20: *Same as Fig. 7.19 above, but for LiF2A and LiF2B.*

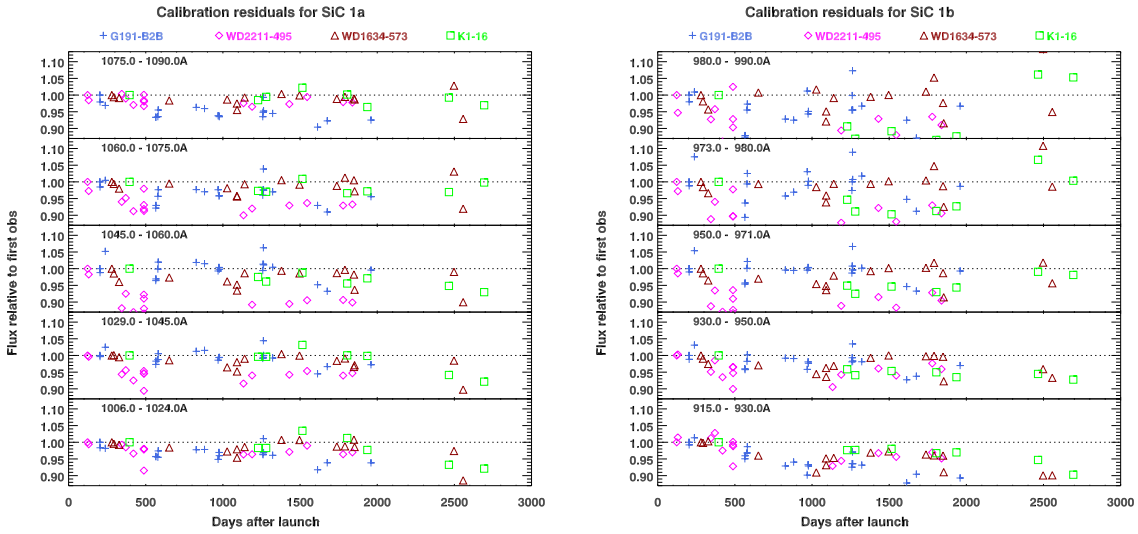

Figure 7.21: *Same as Fig. 7.19 above, but for SiC1A and SiC1B.*

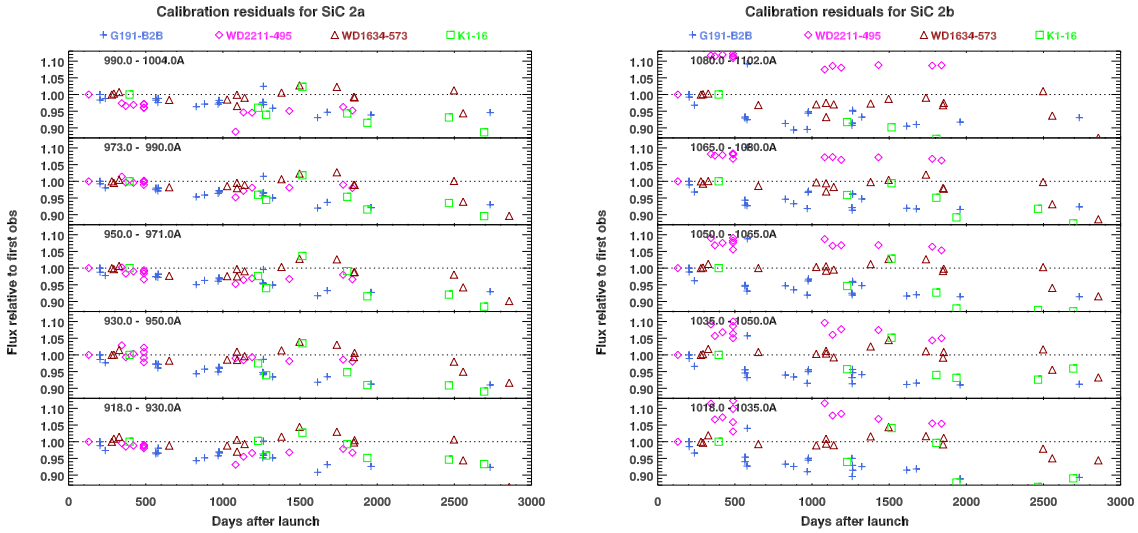

Figure 7.22: *Same as Fig. 7.19 above, but for SiC2A and SiC2B.*

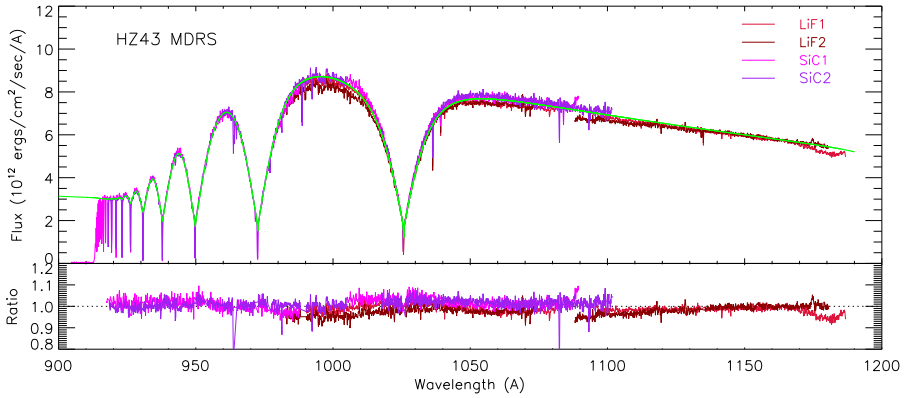

Figure 7.23: *Same as Figure 7.10 above, but for the MDRS spectrum of HZ 43.*

7.5.5 MDRS and HIRS Calibration

The calibrations of the MDRS and HIRS apertures were performed in the same manner as for LWRS. These apertures were never intended to produce accurate absolute fluxes, but in practice the MDRS aperture did often produce spectra of good photometric quality. Variations of the channel alignment on orbital time scales often resulted in lost flux, especially for the SiC channels. However, an examination of the count rates during an observation would often permit determination of the true absolute flux.

Because the HIRS and MDRS apertures were used much less often than LWRS, the regions of the detectors illuminated by these apertures suffered less degradation over the mission. Apart from localized areas "burned-in" by geocoronal emission lines, the predominant cause of change in sensitivity was degradation of the optics. As a result, the corrections for time-dependence of the instrument sensitivity derived for LWRS should provide reasonable results for MDRS and HIRS.

Figures 7.23 through 7.25 show the MDRS spectra of HZ 43, GD 246, and G 191-B2B. The data were reduced in the same manner as described for the LWRS data in Section 7.5.1. There were enough individual exposures of these stars so that there was at least one that was close to photometric in each channel, with the result that the overall normalization turned out to be close to correct. The exception was LiF1B for GD 246 and G 191-B2B, which was off by about 10% in both cases. The shortcomings in the corrections for time-dependence of the LiF2A calibration are evident in the the G 191-B2B spectrum: this spectrum is dominated by data obtained early in the mission, so the initial high throughput at 1095Å – 1135Å manifests itself in a measured flux that is too high by 5–10% at these wavelengths.

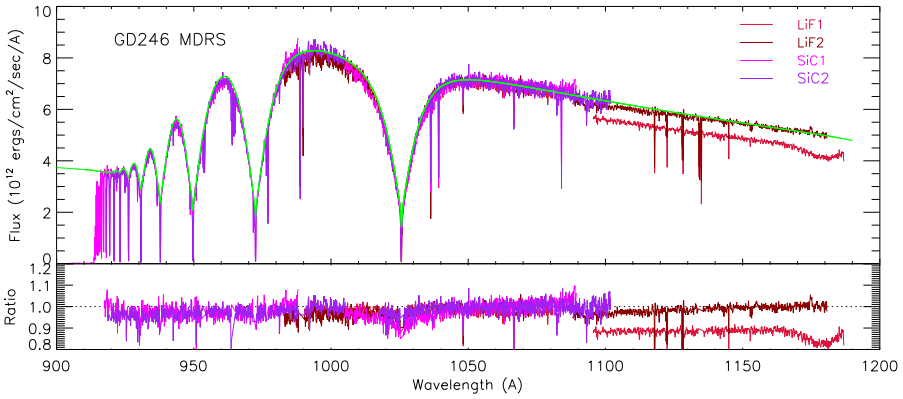

Figure 7.24: *Same as Figure 7.10 above, but for the MDRS GD 246 spectrum. The synthetic spectrum shown here was calculated with* $T_{\rm eff}$*=58,700 K and* $\log g$*=7.807 rather than the parameters shown in Table 7.5. The overall agreement in the shape of the spectrum is much better than that shown in Figure 7.12 for the nominal parameters.*

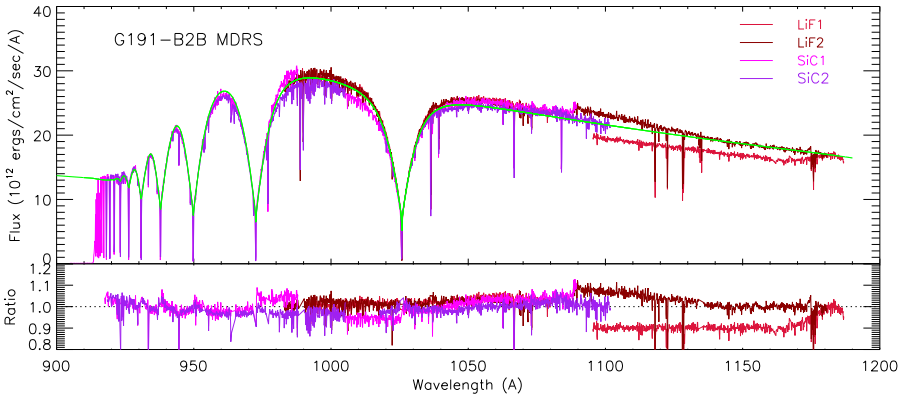

Figure 7.25: *Same as Figure 7.10 above, but for the MDRS spectrum of G 191-B2B.*

7.5.6 High-Order Sensitivity

The holographic diffraction gratings should have significant efficiency in second and higher orders, and the detectors should have good QE at EUV wavelengths, so the *FUSE* instrument may have substantial sensitivity in second and higher order. Such sensitivity is limited by the low reflectivity of the coatings in the EUV, but it cannot be assumed to be negligible. Indeed, geocoronal emission of He I 584Å is often seen in second order at 1168Å for observations of faint sources during orbital day. The high-order throughput of *FUSE* has not been calibrated, but some estimates can be made.

The second-order bandpass for the SiC channels spans 450Å–550Å. The reflectivity of SiC is typically just over 30% in the *FUSE* first-order bandpass, declining gradually with decreasing wavelength. At shorter wavelengths the reflectivity drops more steeply, reaching about 10% at 584Å, 5% at 522Å, and ∼2% at 460Å. These values were obtained from pre-flight measurements of witness mirrors coated along with the *FUSE* optics, and are consistent with other SiC mirrors (see Kruk et al. [1999] Fig. 14 for the HUT primary mirror reflectivity). Thus, in the SiC channels the *FUSE* second order sensitivity will be a factor of 20 – 100 lower than in first order. For solar system objects, this might still yield useful throughput. Beyond the solar system, the most likely candidate to be affected might be HZ 43, where the combination of high $T_{\rm eff}$ and low H I column density gives a fairly high ratio of 550Å to 1100Å flux. However, even here the number of detected second-order photons is likely to be no more than a few percent of the first-order photons. This is likely to drop quickly with decreasing wavelength.

The second-order bandpass for the LiF channels spans 490Å–590Å. Pre-flight measurements of the LiF witness mirrors gave reflectivity similar to the SiC mirrors at 584Å, but which dropped off more slowly, to a somewhat higher value of ∼ 5% at 460Å. Because geocoronal He I 584Å emission is seen in the LiF channels, this opens up the possibility that there might be useful second-order throughput at shorter wavelengths. One of the likely applications for second-order sensitivity would be to use the He I ionization edge at 504Å for studies of the local ISM. However, a preliminary examination of the cumulative HZ 43 and G 191–B2B spectra described above revealed no apparent evidence for this feature. A careful analysis might be able to extract a weak signature from these observations, but it is clear that the second-order sensitivity is too low for this to be generally useful in *FUSE* archival data.

7.6 Residual Wavelength Errors

Errors in the wavelength calibration were measured by comparing the positions of interstellar absorption features in the spectra of white dwarf stars with those of synthetic spectra. For spectra rich in H_2 features (program M107), the wavelength solution could be sampled on sub-Å scales across the *FUSE* bandpass. In general, the wavelength errors were found to be quite small. Figure 7.26 shows the residual wavelength errors in the LiF1A spectrum of the white dwarf KPD 0005+5106 observed through the LWRS aperture. This star was observed a number of times throughout the mission. The data from each observation were reduced independently. For each channel (LiF and SiC), detector segment (1A, 1B, 2A, and 2B), and aperture (LWRS, MDRS, and HIRS), all available spectra were shifted to a common wavelength zero point and combined into a single spectrum. The spectral-fitting routine Owens (Lemoine et al. [2002])

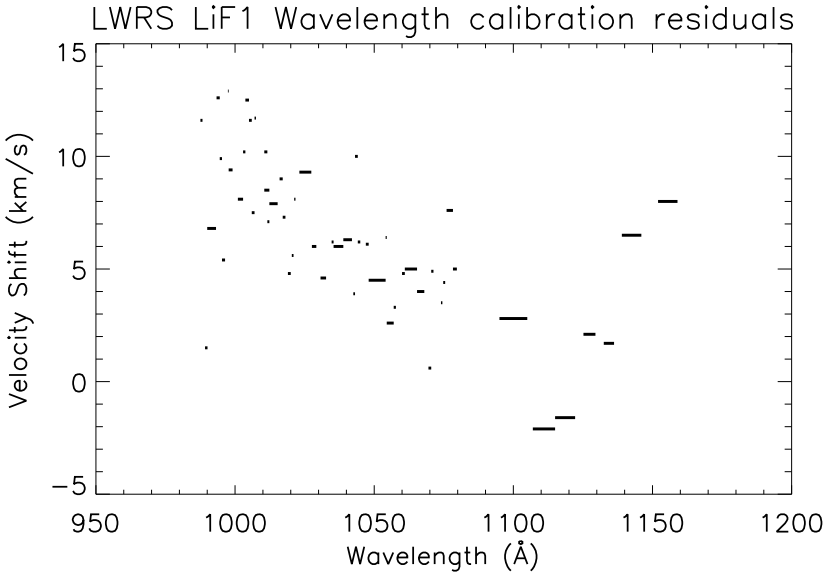

Figure 7.26: *Residual wavelength errors in the LiF1 spectrum of the white dwarf KPD 0005+5106 observed through the FUSE LWRS aperture. Horizontal lines represent the width of a window over which wavelength errors differ by less than half a pixel.*

was used to fit an interstellar absorption-line model to each of the resulting spectra. The fitting windows were repeatedly divided into smaller wavelength intervals until the offset between the model and the data for each line in a window was less than half a pixel. Some windows were several Å wide; others encompassed a single line.

The wavelength shifts necessary to align the LWRS LiF1 spectrum with the model are plotted in Figure 7.26. Several features seen in this plot are repeated in those for other channels and apertures. Similar residual plots for the LWRS LiF2, SiC1 and SiC2 channel, as well as for the HIRS and MDRS apertures can be found in Appendix F. We typically see a linear stretch in the wavelength scale of approximately 10 km s^{-1} over an entire detector segment, particularly near the ends of the detector. On smaller scales, local distortions of 4 to 5 km s^{-1} (about one 0.013 Å pixel) over scales of a few Å are common. Such small-scale variations are impossible for the pipeline to correct. When fitting features occurring throughout the *FUSE* bandpass, it is therefore recommended that the users divide the spectra in small windows of 1–3 Å allowing for the line centers to vary in order to correct for those small-scale deviations to the wavelength solution.

7.7 *FUSE* Resolving Power

The *FUSE* resolving power ranges from ∼15000 to ∼20000. Because of the combined effects of target motion, gain sag and astigmatism, the point source resolving power of *FUSE* data can in principle vary between observations and from exposure to exposure within a given observation

and is wavelength-dependent. Since CalFUSE applies a correction for these effects to each photon in the event list for TTAG data (unlike HIST data), TTAG data will always exhibit a slightly higher resolving power than HIST data obtained with the same aperture. These same effects render the *FUSE* point-spread function (PSF) and the *FUSE* line-spread function (LSF) variable as well.

Under most circumstances, a Gaussian LSF corresponding to R = 20,000 provides a reasonable representation of the FUSE LSF. At high signal-to-noise, the LSF in the SiC channels is better represented by two gaussians, with a narrow component corresponding to R = 20,000 and a broader component with extended tails; see Kruk et al. [2002] and Wood et al. [2002] for details.

The LSF in the MDRS and LWRS apertures is expected to be slightly asymmetric even after astigmatism corrections are applied; however this asymmetry is only apparent and significant at signal-to-noise of 30 and above.

Additional information on the FUSE LSF can be found in Section 4.3.1 of the *Instrument Handbook (2009)*.

7.8 Background Subtraction

The background sensed by the *FUSE* detectors is thought to be composed of three distinct components: Detector background, stray light that enters the spectrograph from outside the nominal optical path, and scattered light from the far wings of the grating PSF (see Section 7.6).

For TTAG data, CalFUSE ignores the light scattered by the grating and assumes that the observed background consists of three independent components: 1) a spatially uniform dark count; 2) a spatially variable day component, and; 3) a spatially variable night component. Thus, for TTAG data, it fits unilluminated portions of the detector to a model for these three components. However, when the observed background is poorly defined, CalFUSE assumes that the uniform component equals the dark-count rate scaled by the exposure time and fits the day and night components.

No model fit is performed for HIST data or TTAG data with very bright backgrounds, e.g., from nebular emission. Instead, the day and night model components are scaled by the day and night exposure times, and the dark-count rate is scaled by the total exposure time to produce the model background image. This scheme is adequate for HIST observations because they are typically short exposures of bright targets, making the background relatively faint. More details can be found in the *Instrument Handbook (2009)* and Dixon et al. [2007].

NOTE: A few items must be noted about the CalFUSE background correction. First, grating scattering along the dispersion direction is not taken into account. This can be significant, being as much as 1–1.5% of the continuum flux in the SiC channels but 10 times less in the LiF channels. Second, CalFUSE treats uncertainties in the background as systematic errors and does not include them in the (purely statistical) error bars of the extracted spectra. Third, as discussed by Dixon et al. [2007], there are shortcomings in the *FUSE* background model. Specifically, some portion of the uniform component may actually be due to scattered light, and temporally variable. As a consequence, the model fit can over estimate the background

(for possible solutions see Dixon et al. [2007].

Typical diagnostics that suggest improper background corrections are flux levels systematically below zero, and, contrarily, fluxes systematically above zero in regions expected to be at zero (e.g. saturated absorption lines). One way to increase the fidelity of the background correction is to increase the signal-to-noise of the background sources by adding several IDF files before applying the background correction. Tools to accomplish this are discused in Chapter 8. It is also instructive to examine the discussion of background corrections given by Grimes et al. [2007], in their search for Lyman continuum emission from star-forming galaxies at low redshift.

7.9 Detector Grid Voltage Tests

During in-orbit checkout, a small number of observations were performed with no voltage applied to the detector QE grid. The data obtained in this manner will be normal except that the sensitivity will be reduced and the reported fluxes will be low by about 30 percent. The observations and exposures affected are listed in Table 7.6.

Table 7.6: Observations affected by the QE grid voltage tests.[a]

Observation ID	Exposure
I9040601	001 - 004
I2051601	001 - 005
M1030505	001
M1030502	001
M1030401	001
M1030603	001 - 004
I2051702	001 - 004

[a] QE grid voltage off during observation

Chapter 8

Retrieving and Analyzing *FUSE* Data

This chapter highlights the locations where *FUSE* data can be obtained and also provides brief descriptions of available tools that can be useful for analyzing and interpreting *FUSE* spectra. More information can be found on the CalFUSE Page. Lists of computer software, spectral atlases, and papers dealing with particularly difficult *FUSE* analysis problems are also given.

The contents of this chapter are relevant to all future *FUSE* users regardless of their expertise level ("Casual", "Intermediate" or "Advanced").

8.1 Retrieving *FUSE* Data

FUSE data are available through three different on-line interfaces. These are:

- The Multimission Archive at STScI (MAST) archive.stsci.edu/
- The Canadian Astronomy Data Centre www2.cadc-ccda.hia-iha.nrc-cnrc.gc.ca/cadc/
- The Institut d'Astrophysique de Paris (IAP) fuse.iap.fr/

Each of these sites has its own strengths and is worth examining. In each case, their pages, forms and search procedures are well documented, although MAST maintains far more supporting material than the others. A detailed description of the files and file extensions archived at MAST is given in Chapter 4 of this document. The users are encouraged to refer to Table 4.1 prior to downloading data from the MAST interface.

8.2 Analyzing *FUSE* data

Because *FUSE* data are standard FITS files, they can be read and displayed with all standard astronomical software packages. There are also several customized *FUSE* analysis packages written in IDL and in C that will assist the user in displaying and analyzing *FUSE* data. These tools, and their accompanying documentation, are available from the MAST or IAP web sites and are only briefly described here.

8.2.1 IDL Analysis Packages

Considerable effort has been put into developing IDL software for analyzing *FUSE* data. In this section, we describe a few of the well-developed and documented packages and procedures.

First, Don Lindler has written a comprehensive suite of IDL routines customized to handle *FUSE* data. These are called ltools. The complete package and some documentation are available from the MAST *FUSE* web pages. The following is an outline of the capabilities of ltools, and some of its major elements.

cf_edit.pro allows the user to examine, manipulate, and combine the intermediate data files (IDFs) generated by CalFUSE. Users without access to IDL can use the "Virtual Machine" version of the program. The best introduction to the IDF files is probably the User's Guide to cf_edit

fuse_scan.pro allows interactive manipulation of FUSE images and time-tag files. The data are displayed as an image and can be overlayed with an approximate wavelength scale. Statistics can be computed for the whole image or a selected region, and the program has a variety of tools to manipulate time-tag data. (You can even make a movie!) The program has tools to fit Gaussian emission or absorption features or to produce surface or contour plots of small regions of the image. Documentation is available in fuse_scan_reference.pdf

fuse_analysis.pro is an interactive viewer for calibrated *FUSE* data. The program can simultaneously display spectra from all four detector segments for a single exposure. In addition to plotting the calibrated results, it will display regions of the raw image from each detector.

fuse_register.pro is an interactive tool for registering, scaling, and coadding calibrated *FUSE* spectra. The routine allows you to register and coadd multiple exposures for the same channel, or to register, scale, and merge data from multiple channels.

lineplot.pro is a general-purpose plotting tool used by the *FUSE* IDL data-analysis widgets. It allows the user to overplot up to 10 plots. It can be used as a stand-alone widget or called from another widget.

line_edit.pro is a general purpose tool used by the *FUSE* IDL data analysis widgets for creating data masks of 1-dimensional data. It can be used as a standalone widget or called from another widget.

xgaussfit.pro is an interactive least-squares multiple Gaussian fitting routine.

line_norm.pro is an interactive tool for continuum normalization of a spectrum. The tool can be used as a stand-alone routine or called from another widget.

line_eqwidth.pro is a spectral-feature analysis tool using the algorithms of the International Ultraviolet Explorer Feature routine. It can be used as a stand-alone routine or called from another widget.

NOTE: Don Lindler's routines have been updated to work with IDL 6.3. If you are unable to display spectra when running fuse_register or cf_edit on a Mac or PC, try installing the latest versions of the `astron` and `ltools` libraries. Another trick is to add the following lines to your idl_startup.pro file.

```
;  Let's deal with the 24-bit display issues.
device, true_color=24
window, /free, /pixmap, colors=-10
wdelete, !d.window
device, decomposed=0, retain=2, set_character_size=[8,10]
device, get_visual_depth=depth

;  Print helpful information at login.
print, ' '
print, 'Display depth: ' + strtrim( depth, 2 )
print, 'Color table size: ' + strtrim( !d.table_size, 2 )
print, ' '
$pwd
$hostname
print, ' '
```

Some additional utility routines are:

readit.pro is a utility program which will read *FUSE* format raw FITS files for the purpose of turning them into 2D images for display. It automatically determines the file type from the file header. It is used by some of the other programs provided here.

plotrate.pro reads in a raw ttag FITS file and plots the count rate as a function of time.

showdetector.pro reads in a FUSE raw FITS file and makes a gray-scale image plot of the detector segment for printing.

allsegments3.pro plots extracted spectra from all 4 detector segments onto a single sheet of paper.

wfusehist.pro, and **wfusettag.pro** write *FUSE* HIST or TTAG files.

Here are some additional contributions.

idf_shift.pro was written by John Grimes and used to modify the wavelength arrays of the LiF and SiC target spectra within an individual IDF. It is useful, for example, if you want to align the spectra from individual exposures to a common wavelength scale before combining their IDFs. The program, idf_shift.pro, can be called from the command line using the Perl script idf_shift.pl.

idf_jitter.pro is an IDL script that identifies times when a bright target was out of the aperture. It uses the count-rate array in the timeline table of the IDF to construct a count-rate histogram, then rejects times when the count rate was more than 3σ below the mean. For such times, the jitter bit is set in both the timeline table and the photon list.

[H2ools] is a package of IDL routines written by Steve McCandliss for modelling molecular hydrogen absorption. His page provides all sorts of tools and support materials, and the programs are documented in McCandliss [2003].

[XIPLOT] The spectral manipulation tool XIPLOT is an IDL program available at the French *FUSE* site.

A final IDL tip to those users wishing to read *FUSE* data on their own: when using the IDL Astronomy User's Library routine `mrdfits.pro`, the keyword `fscale` should be set to automatically scale numbers to floating point format when needed.

8.2.2 C Analysis Packages

FUSE `Tools in C` is a package of data analysis tools distributed along with the CalFUSE pipeline. They come with the document *FUSE Tools in C*, which reviews each routine. A subset of these programs is designed specifically for the manipulation of IDF files, and is described in the *IDF Cookbook*, which is available in both PDF and HTML versions on the *FUSE* Tools web page (http://archive.stsci.edu/fuse/analysis/toolbox.html).

These tools have the flexibility to perform many common tasks, including trimming, modifying and manipulating large sets of multiple data files. For example, when combining spectra of bright targets, the goal is usually to to maximize spectral resolution, so it is important to align the spectra from individual exposures precisely before combining them. The *FUSE* Tools in C package includes routines to accomplish this task. In contrast, when combining spectra of faint targets, the goal is typically to maximize the fidelity of the background correction by increasing the signal-to-noise ratio on unilluminated regions of the detector. To accomplish this, the IDF files must be combined before extracting the spectra. This is easily done with the Tools, and there are detailed instructions in the *IDF Cookbook* available on the CalFUSE Page. The tools also have routines that enable one to divide an IDF file into multiple time segments in order to examine time dependence.

In a few cases, it may be necessary to reprocess the data using the CalFUSE pipeline. The CalFUSE source code and documentation for installing and using it are available at http://archive.stsci.edu/fuse/analysis/calfuse.html.

8.3 *FUSE* Data Quality Check-List

Before performing detailed science investigations with *FUSE* data, it is recommended that the user (regardless of expertise level) go through the sanity checks given below to avoid erroneous results and interpretations.

- Compare SiC data with overlapping LiF data or night-only SiC data to identify scattered solar light.
- Compare SiC and LiF data with corresponding night-only data, when present, to understand and identify airglow contamination.

- Examine IDF files to search for dead zones, remaining scattered light, background contamination (due to the presence of an extended source).
- Compare spectra from multiple segments to identify exposures where flux was lost due to "worms" or target motions.
- Check count-rate plot (`*rat.gif`) to understand flux loss to due target motions.
- Examine HIST data for evidence of fixed-pattern noise.
- Check background subtraction accuracy: verify that the flux at the center of a damped line reaches zero.
- To ensure highest spectral resolution when combining extracted spectra, cross-correlate individual exposures with unblended, sharp and solitary lines in the wavelength range of interest. Don't combine spectra from different channels if highest spectra resolution is important.
- To mitigate the effects of the walk and the non-linearity of the wavelength solution, limit the range over which spectral line modeling is performed to 1–3 Å maximum. Produce as many such small windows as required to fit the lines of interest. Beware of detector segment 2A for data obtained after mid-2002, especially in the vicinity of the airglow lines noted in Section 9 of the *Instrument Handbook (2009)*. See Figure 7.7 for an example of the effects of localized gain sag induced by airglow exposure in segment 2A.

8.4 Additional Analysis Aids and Atlases

There are a number of additional resources that are useful for analyzing *FUSE* data. These include line lists, spectral atlases, and a few other resources.

8.4.1 Atomic and Molecular Line Data

Don Morton has published an atlas of atomic data, complete with finding lists. These are available in the publication by Morton [2003]. Because molecular hydrogen absorption is so prevalent in *FUSE* spectra, it is also important to be aware of the following references to the basic H_2 data: Abgrall et al. [1993a] and Abgrall et al. [1993b]. These are the data used by the McCandliss [2003] H2ools analysis package described above. The atomic data for interstellar Fe II lines (Howk et al. [2000]), interstellar Cl I lines (Sonnentrucker et al. [2006]), and stellar Fe II lines (Harper et al. [2001]) were also revised and should be considered for use in future studies.

8.4.2 *FUSE* Interstellar Absorption Spectra

Because a continuum source observed by *FUSE* with a color excess of only a few tenths will be littered with strong interstellar absorption lines, it is useful to have a rough idea of their expected strengths. Sembach [1999] provides lists of important interstellar features and detailed plots

of synthetic interstellar spectra. The latter are especially useful for line identification purposes. The publications by McCandliss [2003] and Rachford et al. [2001] are also useful for their presentation of H_2 spectra.

8.4.3 Atlases of *FUSE* Stellar Spectra

Table 8.1 lists the atlases of FUV spectra that were produced during the operational lifetime of the *FUSE* satellite. These atlases provide a useful introduction to the FUV spectra of a wide variety of Galactic and extragalactic objects. In many cases, the processed spectra can be downloaded for immediate inspection. Consequently, these atlases are valuable resources for many purposes, especially for researchers who are new to the FUV region of the spectrum.

Table 8.1: Published Atlases of *FUSE* Spectra

Spectra	Reference	Online Availability
AG Dra (Symbiotic Star)	Young et al. [2005]	...
Cool Stars	Dupree et al. [2005]	...
Galactic OB Stars	Pellerin et al. [2002]	`http://archive.stsci.edu/prepds/atlasfuse/`
Magellanic OB Stars	Walborn et al. [2002]	`http://archive.stsci.edu/prepds/atlasfuse/`
Wolf-Rayet Stars	Willis et al. [2004]	`http://archive.stsci.edu/prepds/fuse_wratlas/`
Starburst Galaxies	Pellerin & Robert	`http://archive.stsci.edu/prepds/fuse_galaxies/`
Quasar Composite	Scott et al. [2004]	`http://archive.stsci.edu/prepds/composite_quasar/`

8.4.4 *FUSE* Airglow Spectra

Because *FUSE* spectra are always contaminated to some level by airglow, it is useful to be familiar with airglow spectra. Feldman et al. [2001] present an extensive set of airglow spectra observed with *FUSE*.

8.4.5 *IUE* Object Classes and Class #99 Observations

With the availability of a large body of *IUE* data already in the MAST archive, the *FUSE* project adopted an only slightly modified version of the *IUE* Object classes for use by *FUSE*. Table 8.2 lists the *FUSE* Object Classes.

Under class 99, Nulls & Flat Fields, the *FUSE* project has entered the following data types:

STIMLAMP: These are pseudo flat field exposures, taken with the internal lamps. They expose all of the flaws, grid wires and shadows on the *FUSE* detectors (see the *Instrument Handbook 2009*).

STIMPULSE: These are exposures containing only the electronically injected pulses described in Chapter 2.

BKGND-DOORS-CLOSED: These are essentially dark exposures. They were obtained with the outer doors of the *FUSE* telescopes closed at the end of the mission. The only events detected in these exposures are true dark counts and any stray light that may find its way onto the detectors through an unintended route.

MT-TEST: This stands for moving target test. These observations were obtained as part of a program testing the ability of *FUSE* to follow a moving target.

Table 8.2: Object Classes

Class - Object	Class - Object	Class - Object
0-Sun	31-A4-A9 V-IV	60-Shell Star
1-Earth	32-A0-A3 III-I	61-ETA Carinae
2-Moon	33-A4-A9 III-I	62-Pulsar
3-Planet	34-AE	63-Nova-Like
4-Planetary Satellite	35-AM	64-Other
5-Minor Planet	36-AP	65-Misidentified Targets
6-Comet	37-WDA	66-Interacting Binaries
7-Interplanetary Medium	38-HB Stars	69-Herbig-Haro Objects
8-Giant Red Spot	39-Composite Sp Type	70-PN + Central Star
10-W C	40-F0-F2	71-PN - Central Star
11-WN	41-F3-F9	72-H II Region
12-Main Sequence O	42-FP	73-Reflection Nebula
13-Supergiant O	43-Late-Type Degen	74-Dk Cld (Abs Spectrum)
14-OE	44-G V-IV	75-Supernova Remnant
15-OF	45-G III-I	76 Ring Neb (Shk Ionized)
16-SD O	46-K V-IV	80-Spiral Galaxy
17-WD O	47-K III-I	81-Elliptical Galaxy
19-Other Strong Sources	48-M V-IV	82-Irregular Galaxy
20-B0-B2 V-IV	49-M III-I	83-Globular Cluster
21-B3-B5 V-IV	50-R, N, or S Types	84-Seyfert Galaxy
22-B6-B9.5 V-IV	51-Long Period Var Stars	85-Quasar
23-B0-B2 III-I	52-Irregular Variables	86-Radio Galaxy
24-B3-B5 III-I	53-Regular Variables	87-BL Lacertae Object
25-B6-B9.5 III-I	54-Dwarf Novae	88-Em Line Gal(Non-Seyf)
26-BE 27-BP	55-Classical Novae	90-Intergalactic Medium
28-SDB	56-Supernovae	98-Wavelength Cal Lamp
29-WDB	58-T Tauri	99-Nulls & Flat Fields
30-A0-A3 V-IV	59-X-Ray	

Chapter 9

Special Cases and Frequently Asked Questions

In this chapter, we provide a few references and examples of non-standard data types which highlight particular, but not frequently utilized, capabilities of *FUSE*. This information is primarily relevant to "Advanced" users even though "Intermediate" users might find it useful. This information might not be highly relevant to the "Casual" user.

9.1 Special Cases

9.1.1 Extended Sources

Table 9.1 gives the measured full widths of Lyβ airglow lines in the LiF1A segment. An extended source in the HIRS aperture has nearly the same resolution as a point source. It is a little less because of the astigmatic curvature orthogonal to the dispersion, which degrades the overall resolution. As with point sources, the exact resolution depends on wavelength and segment.

Table 9.1: Extended Source Resolution[a]

Aper.	Δv (km s^{-1})	$\Delta\lambda$ (Å)
LWRS	106	0.362
MDRS	30	0.102
HIRS	20	0.068

[a] For Lyβ on LiF1A

When interpreting observations of very large extended sources (such as the Cygnus Loop or large reflection nebulae), it is also important to keep two additional facts in mind. First, for TTAG data there may be useful information in apertures other than the one specified by the observer. Spectra from these other apertures will not be extracted by CalFUSE by default, and one must return to the IDF file to extract these spectra. Second, to interpret the data from the other apertures, one needs to know their physical relationships (see Table 2.1 and Fig. 2.2).

Together with the aperture position angles, these values can be used to determine the locations of the other apertures on the sky. Examples of the analysis of extended source observations can be found in the papers by Blair et al. [2002], Dixon et al. [2006], Sankrit et al. [2007a] or Ghavamian et al. [2007].

9.1.2 Time Variable Sources

Due to its ability to obtain time-tagged data and to the rapid and sequential accumulation of histogram spectra, *FUSE* could technically be used to study time-variable phenomena. The interested reader can find examples of time variability studies in the following references: Kuassivi & Ferlet [2005], Massa et al. [2000] and Prinja et al. [2005]. Note that these studies were all performed before the introduction of the IDF files; one would now use them as the natural starting point for time variability studies. **Remember that target motion in and out of one of more channels could mimic time-variability (see Section 2.3). It is therefore strongly recommended that users examine the count-rate plots (see 4.2.1.4) before claiming detection of intrinsic source time variability.**

9.1.3 Earth Limb Observations

In certain cases, *FUSE* was intentionally pointed toward the Earth's limb, in order to obtain airglow spectra. (This was avoided in normal *FUSE* science observations.) These observations are part of programs M106 and S100. These specialized airglow observations are accessible using a separate interface under the *FUSE*MAST main page. Users can download those data at the following link: http://archive.stsci.edu/fuse/airglow.html.

9.1.4 Background Limited Observations

Extremely faint extended and point sources often require additional analysis, in particular to perform the most careful background processing and subtraction. Fechner et al. [2006] provide an example of detailed analysis of a very faint point source, while Sankrit et al. [2007b] and Danforth et al. [2002] examine the problems encountered with faint extended sources.

9.1.5 Moving Targets

Moving targets were also observed by *FUSE* during its mission. Detailed descriptions of the data acquisition and data analysis specific to moving targets can be found in papers by Feldman et al. [2002] and Weaver et al. [2002].

9.2 Frequently Asked Questions

Q: What is the best way to combine spectra of bright targets?
A: For bright targets, the goal is to optimize spectral resolution, so you will want to cross-correlate individual exposures on narrow absorption lines before combining the spectra. For

TTAG exposures of moderately-bright objects, it is occasionally beneficial to split long exposures into shorter time segments and coalign the individual segments before re-combining.

Q: What is the best way to combine spectra of faint targets?
A: In this case, it is best to optimize the background model, so you will want to combine IDF files for the individual exposures prior to extracting the spectrum.

Discussions regarding both techniques (bright and faint targets) are provided in the document "FUSE Tools in C" at http://archive.stsci.edu/fuse/calfuse.html

Q: How do I improve the background subtraction at the short-wavelength end of the SiC1B channel?
A: The LWRS spectrum of the SiC1 channel falls very near the edge of the detector (see, for example, Fig. 4.1), where the background rises steeply. The scattered-light model used by CalFUSE, when scaled to match the counts in the center of the detector, does not accurately reproduce the background near the edge, and can cause an over-subtraction of the background, with the shortest wavelengths on SiC1B being most susceptible. In principle, one could use the dark exposure data taken near the end of *FUSE* operations to perform a custom background fit, but this would require specific expertise and would be a difficult task. In practice, one can compare the data from the SiC1B and SiC2A channels for consistency. Only very faint targets should have a concern with this issue.

Q: What if the stim pulses are missing for one or more of my exposures?
A: In most cases the STIM pulses were turned on briefly at the beginning and end of each exposure. However, some exposures don't include any STIMs at all. If that's the case, the cf_thermal_distort routine of CalFUSE will output a warning message to the trailer file (see Appendix C of this document). Since the thermal correction of the detector pixel scale is based on the STIM positions, CalFUSE has to make an approximate correction in these cases, based on typical STIM positions. This correction will only be approximate, and thus the wavelength scale may be slightly incorrect for such exposures. The errors will be largest at times when the temperatures were changing rapidly, such as after the detector high voltage state has changed. Unless you are really interested in the most accurate wavelengths possible, you should not have to worry about this. Alternatively, one could choose to drop such exposures from the total observation when the individual exposures are combined to assess any possible impacts.

Q: How do I find and retrieve the special case of bright-earth observations?
A: There are two types: (1) The S100 program, executed in the fall of 2007, obtained several weeks of downward-looking airglow spectra. (2) Throughout the mission (particularly early on), we obtained approximately 1300 bright-earth exposures during earth occultations of some 200 targets. All of these data have the program ID of the science program and target, but have exposure numbers of 901 and above (see Chapter 4). These data can be retrieved as special cases from the MAST archive.

Q: How do I extract spectra from non-target apertures?
A: This can only be done for TTAG mode data and the exact technique depends on whether the new target is an extended or a point source:

- *Extracting Spectra from Non-Target Apertures: Extended Sources*

  1. Run the CalFUSE pipeline normally. Delete extracted spectra and BPM files.
  2. Use cf_edit or modhead to modify background regions of the first IDF file. (Since idf_combine copies the header from the first input file into the output file, you need modify the background regions only once.)
  3. Use modhead (or some other tool) to change these keywords in all of the IDF files:
     SRC_TYPE Change point source to extended source if appropriate (PC to EC, PE to EE)
     If the original target is an extended source, then you need not modify SRC_TYPE.
     APERTURE Change to the desired aperture.
  4. Run cf_bad_pixels on all IDF files to generate bad-pixel map for the new aperture.
  5. Combine IDF and BPM files using idf_combine and bpm_combine.
  6. Run cf_extract_spectra on combined file.

- *Extracting Spectra from Non-Target Apertures: Point Sources*

  1. You must modify the raw data files before running the pipeline.
  2. Change the header keywords (step 3 above) in the raw data files.
  3. Run the pipeline on each exposure. Delete extracted spectra.
  4. Modify the background regions in the first IDF file.
  5. Combine IDF and BPM files.
  6. Run cf_extract_spectra.

Q: How to learn how to get the most out of the *FUSE* IDF files?
A: The best introduction to the IDF files is probably the User's Guide to cf_edit http://archive.stsci.edu/fuse/calfuse.html, along with the discussion of the file format provided in Chapters 4 & 5 and Dixon et al. [2007]. If heavy data processing is anticipated, "FUSE Tools in C" documentation should be consulted as well.

Bibliography

Abgrall, H., Roueff, E., Launay, F., Roncin, J.Y., & Subtil, J.L. 1993a, A&AS, 101, 273

Abgrall, H., Roueff, E., Launay, F., Roncin, J.Y., & Subtil, J.L. 1993b, A&AS, 101, 323

Allard, N.F., Hébrard, G., Dupuis, J., Chayer, P., Kruk, J.W., Kielkopf, J.F., & Hubeny, I., 2004, ApJ 601 L183

Allard, N.F., Kielkopf, J.F., Hébrard, G., & Peek, J.M., 2004, Eur. Phys. J. D 29 7

Blair, W.P., Sankrit, R. & Tulin, S. 2002, ApJS, 140, 367

Bohlin, R.C., 2000 ApJ 120 437

Danforth, C. W., Howk, J. C., Fullerton, A. W., Blair, W. P., & Sembach, K. R. 2002, ApJS, 139, 81

Dixon, W. V. D., Sankrit, R., & Otte, B. 2006, ApJ, 647, 328

Dixon, W.V., Sahnow, D.J., Barrett, P.E., Civeit, T., Dupuis, J., Fullerton, A.W., Godard, B., Hsu, J.-C., Kaiser, M.E., Kruk, J.W., Lacour, S., Lindler, D.J., Massa, D., Robinson, R.D., Romelfanger, M.L. & Sonnentrucker, P. 2007, PASP, 119, 527

Dupuis, J., Vennes, S., Bowyer, S., Pradhan, A.K., Thejll, P., 2000, ApJ 455 574

Dupree, A.K., Lobel, A., Young, P.R., Ake, T.B., Linsky, J.L. & Redfield, S. 2005, ApJ, 622, 629

Fechner, C., Reimers, D., Kriss, G.A., Baade, R., Blair, W.P., Giroux, M.L., Green, R.F., Moos, H.W., Morton, D.C., Scott, J.E., Shull, J.M., Simcoe, R., Songaila, A. & Zheng, W. 2006, A&A 455, 91

Feldman, P.D., Sahnow, D.J., Kruk, J.W., Murphy, E.M. & Moos, H. W. 2001, JGR, 106, 8119

Feldman, P. D., Weaver, H. A., & Burgh, E. B. 2002, ApJ, 576, L91

Finley, D. S., Koester, D., & Basri, G. 1997, ApJ, 488, 375

Ghavamian, P., Blair, W. P., Sankrit, R., Raymond, J. C., & Hughes, J. P. 2007, ApJ, 664, 304

Grimes, J.P., Heckman, T., Strickland, D., Dixon, W.V., Sembach, K., Overzier, R., Hoopes, C., Aloisi, A. & Ptak, A. 2007, ApJ, 668, 891

Harper, G. M., Wilkinson, E., Brown, A., Jordan, C., & Linsky, J. L. 2001, ApJ, 551, 486

Howk, J. C., Sembach, K. R., Roth, K. C., & Kruk, J. W. 2000, ApJ, 544, 867

Hubeny, I., & Lanz, T. 1995, ApJ, 439, 875

Kruk, J.W., Brown, T.M., Davidsen, A.F., Espey, B.R., FInley, D.S., & Kriss, G.A., 1999, ApJS 122 299

Kruk, J. W., et al. 2002, ApJS, 140, 19

Kuassivi, B.A. & Ferlet, R. 2005, A&A, 442, 1015

Lemke, M. 1997, A&AS, 122, 285

Lemoine, M., et al. 2002, ApJS, 140, 67

Massa, D., Fullerton, A.W., Hutchings, J.B., Morton, D.C., Sonneborn, G., Willis, A.J., Bianchi, L., Brownsberger, K.R., Crowther, P.A., Snow, T.P., & York, D.G. 2000, ApJ, 538L, 47

McCandliss, S.R. 2003, PASP, 115, 651

Morton, D.C. 2003 ApJS, 149, 205

Moos, H. W., et al. 2000, ApJ, 538, L1

Pellerin, A., Fullerton, A.W., Robert, C., Howk, J. C., Hutchings, J.B., Walborn, N.R., Bianchi, L., Crowther, P.A. & Sonneborn, G. 2002, ApJS, 143, 159

Prinja, R.K., Hodges, S.E., Massa, D.L., Fullerton, A.W. & Burnley, A.W. 2007, MNRAS, 382, 299

Rachford, B. L., et al. 2001, ApJ, 555, 839

Rose, J.F., Heller-Boyer, C., Rose, M.A., Swam, M., Miller, W., Kriss, G.A. & Oegerle, W.R. 1998, in Proc. SPIE 3349, Observatory Operations to Optimize Scientific Return, p. 410

Sahnow, D. J., et al. 2000, ApJ, 538, L7

Sankrit, R. Blair, W.P., Cheng, J.Y., Raymond, J.C., Gaetz, T.J. & Szentgyorgyi, A. 2007, AJ, 133, 1383

Sankrit, R, & Dixon, W. V. 2007, PASP, 119, 284

Scott, J. E., Kriss, G. A., Brotherton, M., Green, R. F., Hutchings, J., Shull, J. M., & Zheng, W. 2004, ApJ, 615, 135

Sembach, K.R. 1999, in The Stromlo Workshop on High Velocity Clouds, ASP Conf. Series 166, eds. B.K. Gibson & M.E. Putman (San Francisco: ASP), 243

Shchigolev, B.M. 1965, *Mathematical Analysis of Observations*, (Ilife Books, Ltd: New York), Chapter 15

Sonnentrucker, P., Friedman, S. D., & York, D. G. 2006, ApJ, 650, L115

Tremsin, A. S., & Siegmund, O. H. 1999, SPIE Proceedings, 3765, 441

Walborn, N.R., Fullerton, A.W., Crowther, P.A., Bianchi, L., Hutchings, J.B., Pellerin, A., Sonneborn, G. & Willis, A.J. 2002, ApJS, 141, 443

Weaver, H. A., Feldman, P. D., Combi, M. R., Krasnopolsky, V., Lisse, C. M., & Shemansky, D. E. 2002, ApJ, 576, L95

Willis, A.J., Crowther, P.A., Fullerton, A.W., Hutchings, J.B., Sonneborn, G., Brownsberger, K., Massa, D.L. & Walborn, N.R. 2004, ApJS, 154, 651

Wood, B. E., Linsky, J. L., Hébrard, G., Vidal-Madjar, A., Lemoine, M., Moos, H. W., Sembach, K. R., & Jenkins, E. B. 2002, ApJS, 140, 91

Young, P.R., Dupree, A.K., Espey, B.R., Kenyon, S.J. & Ake, T.B. 2005, ApJ, 618, 891

Appendix A

Glossary

Name	Definition
ACS	Attitude Control System
AIC	Active Image Counter
BPM	Bad pixel map
CalFUSE	The Science data pipeline
Channel	One of 4 (LiF1, SiC1, LiF2, SiC2) telescope – spectrograph combinations.
FARF	Flight Alignment Reference Frame
FEC	Fast Event Counter
FES	Fine Error Sensor (A or B)
FPA	Focal Plane Assembly
FPD	Fine pointing data
HDU	Header Data Unit
HIRS	High Resolution Aperture
HIST	Histogram mode for data collection
IDF	Intermediate Data File
IDS	Instrument Data System, the processor that controlled the *FUSE* instrument.
LiF1A	The A segment of the detector on the LiF channel of Side 1.
LiF1B	The B segment of the detector on the LiF channel of Side 1.
LiF2A	The A segment of the detector on the LiF channel of Side 2.
LiF2B	The B segment of the detector on the LiF channel of Side 2.
LWRS	Low Resolution Aperture
MCP	Micro Channel Plate
MDRS	Medium Resolution Aperture
MPS	Mission Planning Schedule
PHA	Pulse Height Amplitude
PSF	Point Spread Function
RFPT	Reference point on the FPA
SAA	South Atlantic Anomaly
SDAF	Science Data Assesment Forms
Segment	One of 2 (A and B) for each side. Four in all, 1A, 2A, 1B, 2B.
SIA	Spectral Image Allocation table
Side	A set of LiF and SiC channels that use the same set of detector.

Name	Definition
SiC1A	The A segment of the detector on the SiC channel of Side 1.
SiC1B	The B segment of the detector on the SiC channel of Side 1.
SiC2A	The A segment of the detector on the SiC channel of Side 2.
SiC2B	The B segment of the detector on the SiC channel of Side 2.
TTAG	Time tagged mode for data collection

Appendix B

Intermediate Data File Header Descriptions

CalFUSE keeps the data in the form of a time-tagged photon event list until spectral extraction. For histogram data, a photon event list is also created but all events are tagged with the same time value. This event list is stored in the Intermediate Data File (IDF; see also Section 4.2.1.3). IDFs are FITS files with four Header Data Units (HDU). Below is a description of the contents of each HDU.

HDU1 only contains a full header for TTAG data. However, for HIST data, HDU1 will also contain the SIA table used for the observation.

HDU2 contains several arrays. Their dimensions are determined by either the total number of events detected (TTAG data), or the number of pixels containing an event (HIST data). The specific arrays are:

`TIME`**:** For TTAG data, these are the arrival times copied directly from the raw data file. For HIST data, the arrival times are all equal and set to the mid-point of the exposure.

`XRAW` **and** `YRAW`**:** For TTAG data, these are copied directly from the raw data file. For HIST data, each non-zero pixel of a HIST image is converted into a single entry in the IDF, with XRAW and YRAW equal to the mean pixel coordinates of the binned image. This results in a "de-binned" image that exhibits a striped pattern since most rows in the de-binned raw image are empty.

`PHA`**:** This is the Pulse Height Amplitude. For TTAG data, the pulse height of each photon event is copied from the raw file to the IDF. Values range from 0 to 31. A typical pulse-height distribution has a peak at low values due to the intrinsic detector background, a Gaussian-like peak near the middle of the range due to real photons, and a tail of high pulse-height events. One can improve the signal-to-noise ratio of faint targets by rejecting photon events with extreme pulse-height values. Pulse-height limits are defined for each detector segment and saved in the main IDF FITS header as PHALOW and PHAHIGH.

The photon events with pulse heights outside of the nominal range are flagged by setting the appropriate bit in the LOC_FLGS array (below). None of this information is available for HIST data. Thus, for HIST data each entry of the PHA is arbitrarily set to 20.

`WEIGHT:` The photon weight array for TTAG data is initialized to unity. Photons whose X and Y coordinates place them outside of the active region of the detector are flagged and their weights are set to 0. For HIST data, the WEIGHT array for a pixel is initialized to the number of photon events in the pixel. The weights are later scaled to correct for detector dead time [Dixon et al., 2007].

`XFARF and YFARF:` These are the coordinate arrays corrected to the FARF (the Flight Alignment Reference Frame), which represent the output of an ideal detector, corrected for geometric distortions.

`X and Y:` These are the FARF coordinates corrected for mirror, grating, and spacecraft motions. These give the coordinates of an ideal detector, at rest with respect to the object.

`CHANNEL:` This array lists the numerical code for the channel assigned to the photon (see Table 4.10). The assignment is done on the basis of the location of the event on the detector and of the boundaries of the detectors defined by the active image masks.

`TIMEFLGS:` The screening routines use information from the timeline table (HDU4 below) to identify photons that violate pulse-height limits, limb-angle constraints, etc., Bad photons are not deleted from the IDF, but merely flagged. Flags are stored as single bits in an 8-bit byte (see Table 4.11). This set of flags indicates time-dependent (orbital) effects. For each bit, a value of 0 indicates that the photon is good, except for the day/night flag, for which 0 = night and 1 = day. It is possible to modify these flags in the IDF file without re-running the pipeline. For example, one could exclude day-time photons or include data taken close to the earth limb.

`LOC_FLGS:` This set of flags indicates detector-location dependent effects (see Table 4.12). They are similar to the TIMEFLGS.

`LAMBDA:` The LAMBDA array contains the heliocentric wavelength given to each photon assigned by CalFUSE.

`ERGCM2:` The ERGCM2 array records energy density in units of erg cm^{-2}.

$$\text{ERGCM2} = \text{WEIGHT} \times hc \,/\, \text{LAMBDA} \,/\, A_{\rm eff}(\lambda), \tag{B.1}$$

To convert an extracted spectrum to units of flux, one must divide by the exposure time and the width of an output spectral bin.

X and Y coordinates are written to the IDF as arrays of 8-bit integers using the FITS TZERO and TSCALE keywords. This process effectively rounds each element of XFARF and X to the nearest 0.25 of a detector pixel and each element of YFARF and Y to the nearest 0.1 of a detector pixel.

HDU3 gives the good-time intervals (GTIs), stored as two arrays, `START` and `STOP`. For TTAG data, the initial values are copied from the raw data file, but they are modified by CalFUSE by various screening routines. By convention, the `START` value of each GTI corresponds to the arrival time of the first photon in that interval. The `STOP` value is the arrival time of the last photon in that interval plus one second. The length of the GTI is thus `STOP`−`START`. For HIST data, a single GTI is generated with `START` = 0 and `STOP` = the exposure time.

HDU4 is called the timeline table. It contains several arrays composed of status flags and spacecraft and detector parameters used by the pipeline. The size of the arrays are set by the length of the exposure, with an entry created by CalFUSE for each second of the exposure.

`TIME`: For TTAG data, the first entry of this array corresponds to the time of the first photon event, and the final entry to the time of the final photon event plus one second. (Should an exposure's photon-arrival times exceed 55 ks, timeline entries are only created for each second in the good-time intervals.) For histogram data, the first element of this array is set to zero and the final element to the exposure duration computed by OPUS +1. Because exposure time is required to be equal to both Σ (STOP−START) summed over all entries in the GTI table, and the number of good times in the timeline table, the final second of each GTI is flagged as bad. No photons are associated with the STOP time of a GTI.

`STATUS_FLAGS`: Only the day/night and OPUS flags of this array are populated when the IDF is created; the other flags are set by the various CalFUSE screening routines.

`TIME_SUNRISE, TIME_SUNSET, LIMB_ANGLE, LONGITUDE, LATITUDE, ORBITAL_VEL`: These arrays are computed by CalFUSE from the orbital elements of the spacecraft.

`HIGH_VOLTAGE`: This array is populated with values from the time-engineering (housekeeping) file (§ 5.2).

`LIF_CNT_RATE, SIC_CNT_RATE`: For TTAG data, these arrays give the count rates within the target aperture, excluding regions contaminated by airglow. For HIST data, they are the dead time corrected values of the LiF and SiC counter arrays derived from the fields I_DET[1]C[SIC][A] in the housekeeping files. The bracketed quantities can be 1 or 2, SIC or LIF, and A or B, respectively, corresponding to the appropriate detector.

`FEC_CNT_RATE`: gives the Fast Event Counter (FEC) Rates. These are derived from the fields I_DET[1]CFE[A], given in the housekeeping file. The bracketed quantities can be 1 or 2, A or B, respectively.

`AIC_CNT_RATE`: gives the Active Image Counter (AIC) count rates. These are the dead time corrected values of the fields I_DET[1]CAI[A] in the housekeeping file. The bracketed quantities can be 1 or 2, A or B, respectively.

`BKGD_CNT_RATE`: For TTAG data, this array is the count rate in pre-defined background regions of the detector, excluding airglow features. The array is not populated for HIST data.

`YCENT_LIF, YCENT_SIC`: For TTAG data, these arrays trace the centroid of the target spectra with time *before* motion corrections are applied. These two arrays are not used by the pipeline, and they are not populated for HIST data.

Appendix C

Trailer File Warning Messages

If a user chooses to rerun the CalFUSE pipeline, occasional warning messages might appear in the trailer files if a pipeline module fails to run successfully. Below is a list of selected warning messages from CalFUSE and how to address them.

cf_bad_pixels: Array overflow. Truncating pseudo-photon list.
To make the array larger, replace nmax *= 1.5 with nmax *= 2 on line 508 of src/fuv/cf_bad_pixels

cf_hist_init: More than 10 hot pixels found.
"Hot pixels" in histogram data result from flips of high-order bits in the raw image array. A large number of bit flips suggest that the data may be corrupted.

cf_hist_init: [Input file] contains no extensions.
Raw data file contains no FITS extensions.

cf_apply_dead_time: DET_DEAD > 1.5. Setting dead-time correction to unity, or
IDS_DEAD > 1.5. Setting dead-time correction to unity.
Dead-time correction is unreliable. Observation is not photometric.

cf_apply_filters: Sum of day and night time differs from EXPTIME by > 10%.
The photon-screening routines have gotten confused. You may have found a bug in the code.

cf_astig_farf: Overflow of ASTG_CAL file in aperture [n].
Either there is a problem with the astigmatism-correction file, or you've found a bug in the routine that applies this correction.

various : Environment variable [variable name] undefined.
You must set the environment variables CF_CALDIR and CF_PARMDIR before running CalFUSE.

cf_check_digitizer: Digitizer keyword [keyword name] is out of bounds.
Keywords are read from the input file header. If their values are out of bounds, then the detector was not properly configured, and the data are suspect, if not useless.

cf_fpa_position: Keyword FPALXPOS is out of bounds. Setting FPADXLIF = 0. Keyword FPASXPOS is out of bounds. Setting FPADXSIC = 0.
Reported position of focal-plane assembly (FPA) is out of bounds. Expect a wavelength shift of the extracted spectrum.

cf_fuv_init: Keyword [keyword name] in master_calib_file.dat is unknown.
File parmfiles/master_calib_file.dat may be corrupted.

cf_fuv_init: Detector bias keywords are corrupted.
Minimum and maxximum detector voltage values are stored in the input file header. If high-voltage information is available in the housekeeping file, then the header values are ignored.

cf_geometric_distort: X and Y distortion images not the same size.
Geometric distortion calibration file (GEOM_CAL) is corrupted.

cf_init_support: Exposure appears to span [number] ks. Truncating.
If exposure time appears to be greater than 55 ks, photon arrival times are corrupted.

The following warnings are issued by cf_init_support only if there are no housekeeping data and the relevant file header keywords appear to be corrupted.

- Engineering snapshot time less than or equal to zero.
- Estimating LiF, SiC, FEC and AIC count rates from EXPSTART and EXPEND.
- Estimating LiF, SiC, FEC and AIC count rates from EXPTIME.
- Bad SiC counter. SiC count rate will be set to zero.
- Bad LiF counter. LiF count rate will be set to zero.
- Bad FEC counter

  FEC count rate will be computed from NEVENTS and EXPTIME.
  Electronic deadtime correction will be underestimated.
  Y stretch will be underestimated.

- Bad AIC counter

  AIC count rate will be computed from NEVENTS and EXPTIME.
  IDS deadtime correction will be underestimated.

If cf_init_support cannot read the SiC count-rate array from the housekeeping file, it issues one of the following warnings and uses file-header information to populate all of the count-rate arrays in the IDF:

Data missing from housekeeping column. Will treat file as missing.
Data column missing from housekeeping file. Will treat file as missing.

If any of the count rates computed by cf_init_support is absurdly high, then the program will issue one of these warnings and set the offending array elements to zero:

LIF_CNT_RATE out of bounds. Setting bad values to zero.
SIC_CNT_RATE out of bounds. Setting bad values to zero.
FEC_CNT_RATE out of bounds. Setting bad values to zero.
AIC_CNT_RATE out of bounds. Setting bad values to zero.

cf_make_wave_array: Requested value of W0 is less than recommended value. Requested value of WMAX is greater than recommended value. Requested value of WPC is less than recommended value.
The user can set the wavelength scale of the extracted spectrum by modifying the parameter files in the parmfiles directory. Bad choices trigger these warnings.

cf_pha_x_distort: NAXIS1 of [PHAX_CAL] ! = 16384
Walk-correction calibration file is corrupted.

cf_proc_check: Exiting. [Program name] has already been run on this file.
If you try to run a calibration step twice, you'll get this warning.

cf_proc_update: No PROCESSING STEP keyword is defined for [program name].
CalFUSE modifies file-header keywords, changing PERFORM to COMPLETE, as pipeline steps are completed. This warning means that the program cannot determine which keyword is associated with the current program. This should never happen.

cf_screen_high_voltage: Detector voltage is $< 90\%$ of optimal value.
Detector voltage is low, but data may still be OK. Examine pulse-height distribution. Look for strong fixed-pattern noise in the extracted spectrum.

cf_set_photon_flags: Time [XXX] not included in timeline table.
Photon-arrival time lies outside the range of values tabulated in the IDF. It will get a status flag, but perhaps not the correct one.

cf_thermal_distort: Cannot determine left STIM position. Estimating. Cannot determine right STIM position. Estimating.
If cf_thermal_distort cannot determine a STIM position, it will attempt to estimate the position using data in the STIM_CAL file. Wavelength errors may result.

read_tle: Orbital elements are more than 5 days old.
You are using an old version of the FUSE.TLE file. Get the end-of-mission version from the *FUSE* FTP site.

Appendix D

Format of Housekeeping Files

The housekeeping files contain time-resolved engineering data used by CalFUSE to correct science data for instrument and pointing problems during exposures (Section 5.2). Each type of parameter is checked for telemetry gaps based on its nominal update period. Gaps are reported in trailer files (Section 4.2.1.5) for the exposure according to the source telemetry file. A brief description of the content of housekeeping files is given below. More details can be found in the *Instrument Handbook (2009)*.

Table D.1: Formats of Housekeeping Files[a]

Array Name	Format	Description
HDU 1: Empty (Header only)		
HDU 2: Time ordered data		
MJD	double	Engineering time (Modified Julian Date)
AATTMODE	long	Attitude estimation mode 5=Fine 4=Coarse
AATTQECI2BDY_1	double	ACS estimated body quaternion X component
AATTQECI2BDY_2	double	ACS estimated body quaternion Y component
AATTQECI2BDY_3	double	ACS estimated body quaternion Z component
I_FPD_Q_ECI2BDY_1	double	IDS FPD measured quaternion X comp
I_FPD_Q_ECI2BDY_2	double	IDS FPD measured quaternion Y comp
I_FPD_Q_ECI2BDY_3	double	IDS FPD measured quaternion Z comp
I_FPDQ_ECI2BDYCMD1	double	IDS commanded ECI to body quat X comp
I_FPDQ_ECI2BDYCMD2	double	IDS commanded ECI to body quat Y comp
I_FPDQ_ECI2BDYCMD3	double	IDS commanded ECI to body quat Z comp
I_FPD_EXP_DURATION	float	FPD exposure duration (seconds)
I_FPD_MEAS_Q_VALID	long	FPD measured quaternion valid flag: 0,1
I_FPD_NEW_CMD_Q	long	FPD new commanded quaternion flag:(NotNew,New)
I_FPD_ROLLINFPRSNT	long	FPD roll information present: 0,1 (No,Yes)
I_FPD_STARFLD_KNWN	long	Tracking on Unknown/Known stars:(Unkn,Known)
I_FPD_TRACKING_ON	long	Moving target tracking on: 0,1 (Off,On)
CENTROID1_STATUS	long	Guidestar 1 Unused,Unver,Ver&Used,VerNotUsed
CENTROID2_STATUS	long	Guidestar 2 Unused,Unver,Ver&Used,VerNotUsed
CENTROID3_STATUS	long	Guidestar 3 Unused,Unver,Ver&Used,VerNotUsed
CENTROID4_STATUS	long	Guidestar 4 Unused,Unver,Ver&Used,VerNotUsed

Table D.2: Formats of Housekeeping Files (continued)

Array Name	Format	Description
CENTROID5_STATUS	long	Guidestar 5 Unused,Unver,Ver&Used,VerNotUsed
CENTROID6_STATUS	long	Guidestar 6 Unused,Unver,Ver&Used,VerNotUsed
I_AT_CMD_ATT	long	IDS at commanded attitude: 0,1 (No,Yes)
I_GMODE	long	IDS guide mode Idle,Slew,Img,UnIDtrk,IDtrk,MvT
I_NEW_QCMD_FLAG	long	FPD contains new commanded quaternion: 0,1
I_NEW_QMEAS_FLAG	long	FPD contains new measured quaternion: 0,1
I_TM_OUTPUT_RATE	long	Telem subset 0=A 5=B 7=Inval others:memorydump
I_CNFGCENT_FAIL_ST	long	ConfigCents status 0=ok 1=configure 2,3,4=err
I_MT_FAIL_STAT	long	MovingTarget status 0=ok 2=config 1,3,4,5=err
I_PO_FAIL_STAT	long	Pointing offset status 0=ok 1,2=err
I_PU_FAIL_STAT	long	peakup status 0=ok 1,2,3,4=err
I_TC_FAIL_STAT	long	target correction 0=ok 1=config 2,3,4=err
I_UTRACK_FAIL_STAT	long	Unidentified track ok,config,star_sel,reject
I_IDS_IGNORED	long	ACS uses/ignores IDS FPDs: 0,1 (Use,Ignore)
AQECI2BDYCMD_1	double	ACS commanded quaternion X axis: range (-1,1)
AQECI2BDYCMD_2	double	ACS commanded quaternion Y axis: range (-1,1)
AQECI2BDYCMD_3	double	ACS commanded quaternion Z axis: range (-1,1)
I_DET1CFEA	long	DET1 Counter Fast Events A
I_DET1CFEB	long	DET1 Counter Fast Events B
I_DET2CFEA	long	DET2 Counter Fast Events A
I_DET2CFEB	long	DET2 Counter Fast Events B
I_DET1CAIA	long	DET1 Counter Active Image A
I_DET1CAIB	long	DET1 Counter Active Image B
I_DET2CAIA	long	DET2 Counter Active Image A
I_DET2CAIB	long	DET2 Counter Active Image B
I_DET1CSICA	long	DET1 Counter SiC A
I_DET1CSICB	long	DET1 Counter SiC B
I_DET2CSICA	long	DET2 Counter SiC A
I_DET2CSICB	long	DET2 Counter SiC B
I_DET1CLIFA	long	DET1 Counter LiF A
I_DET1CLIFB	long	DET1 Counter LiF B
I_DET2CLIFA	long	DET2 Counter LiF A
I_DET2CLIFB	long	DET2 Counter LiF B
I_DET1CASA	long	DET1 SAA Counter A
I_DET1CASB	long	DET1 SAA Counter B
I_DET2CASA	long	DET2 SAA Counter A
I_DET2CASB	long	DET2 SAA Counter B
I_DET1HVBIASAST	long	DET1 MCP-A High Voltage Bias setting
I_DET1HVBIASBST	long	DET1 MCP-B High Voltage Bias setting
I_DET2HVBIASAST	long	DET2 MCP-A High Voltage Bias setting
I_DET2HVBIASBST	long	DET2 MCP-B High Voltage Bias setting

[a] Sampled once per second, and dimension set length of the exposure.

Appendix E

Format of Engineering Snapshots

Certain engineering parameters from the instruments, such as detector temperatures and voltages, were identified before launch as being necessary to process and calibrate science data. Engineering snapshots were, therefore, obtained at the beginning of an exposure and every 5 minutes thereafter, with a final one taken at the end of the exposure (Section 5.3). A brief description of the content of snapshot files is given below. More details can be found in the *Instrument Handbook (2009)*.

Table E.1: Formats of snap/snpaf/snpbf Files[a]

Array Name	Format	Description
HDU 1: Empty (Header only)		
HDU 2: Time ordered data		
I_UT_TIME_MJD	double	Snapshot time in MJD (days)
I_DET1ELTEMP	double	DET1 electronics temperature
I_DET1PLTEMP	double	DET1 Baseplate temperature
I_DET2ELTEMP	double	DET2 electronics temperature
I_DET2PLTEMP	double	DET2 Baseplate temperature
I_DET1XSCALEAST	double	DET1 segment A Time (X) image scale factor.
I_DET1XOFFSETAST	double	DET1 segment A Time (X) image postion offset.
I_DET1XSCALEBST	double	DET1 segment B Time (X) image scale factor.
I_DET1XOFFSETBST	double	DET1 segment B Time (X) image postion offset.
I_DET2XSCALEAST	double	DET2 segment A Time (X) image scale factor.
I_DET2XOFFSETAST	double	DET2 segment A Time (X) image postion offset.
I_DET2XSCALEBST	double	DET2 segment B Time (X) image scale factor.
I_DET2XOFFSETBST	double	DET2 segment B Time (X) image postion offset.
I_DET1TEMP	double	DET1 Detector temperature.
I_DET1HVMODLTEMP	double	DET1 High Voltage Module temperature.
I_DET1HVFLTRTEMP	double	DET1 High Voltage Filter temperature.
I_DET1AMPBTEMP	double	DET1 segment B Amplifier temperature.
I_DET1AMPATEMP	double	DET1 segment A Amplifier temperature.

Table E.2: Table E.1 (continued)[a]

Array Name	Format	Description
I_DET1TDCBTEMP	double	DET1 TDC B temperature.
I_DET1TDCATEMP	double	DET1 TDC A temperature.
I_DET1MCPBBIASCUR	double	DET1 MCP B Bias Current
I_DET1MCPABIASCUR	double	DET1 MCP A Bias Current
I_DET1HVBIASBST	double	DET1 MCP-B High Voltage Bias setting
I_DET1HVBIASAST	double	DET1 MCP-A High Voltage Bias setting
I_DET1UPRQTHRBST	double	DET1 TDC-B Upper Charge Threshold setting.
I_DET1UPRQTHRAST	double	DET1 TDC-A Upper Charge Threshold setting.
I_DET1BEGWLKBST	double	DET1 TDC-B Begin CFD Walk setting.
I_DET1BEGWLKAST	double	DET1 TDC-A Begin CFD Walk setting.
I_DET1ENDWLKBST	double	DET1 TDC-B End CFD Walk setting.
I_DET1ENDWLKAST	double	DET1 TDC-A End CFD Walk setting.
I_DET1BSLTHRBST	double	DET1 TDC-B charge Baseline inspector window Thr
I_DET1BSLTHRAST	double	DET1 TDC-A charge Baseline inspector window Thr
I_DET1LWRQTHRBST	double	DET1 TDC-B Lower Charge Threshold setting.
I_DET1LWRQTHRAST	double	DET1 TDC-A Lower Charge Threshold setting.
I_DET1LWRTTHRBST	double	DET1 TDC-B Lower Time Threshold setting.
I_DET1LWRTTHRAST	double	DET1 TDC-A Lower Time Threshold setting.
I_DET1HVGRIDST	integer	DET1 Grid High Voltage Status (0=OFF; 1=ON)
I_DET1HVPWRST	integer	DET1 Bias High Voltage Status (0=OFF; 1=ON)
I_DET1STIMLMPST	integer	DET1 Stimulation Lamp Status (0=OFF; 1=ON)
I_DET2TEMP	double	DET2 Detector temperature.
I_DET2HVMODLTEMP	double	DET2 High Voltage Module temperature.
I_DET2HVFLTRTEMP	double	DET2 High Voltage Filter temperature.
I_DET2AMPBTEMP	double	DET2 segment B Amplifier temperature.
I_DET2AMPATEMP	double	DET2 segment A Amplifier temperature.
I_DET2TDCBTEMP	double	DET2 TDC B temperature.
I_DET2TDCATEMP	double	DET2 TDC A temperature.
I_DET2MCPBBIASCUR	double	DET2 MCP B Bias Current
I_DET2MCPABIASCUR	double	DET2 MCP A Bias Current
I_DET2HVBIASBST	double	DET2 MCP-B High Voltage Bias setting
I_DET2HVBIASAST	double	DET2 MCP-A High Voltage Bias setting
I_DET2UPRQTHRBST	double	DET2 TDC-B Upper Charge Threshold setting.
I_DET2UPRQTHRAST	double	DET2 TDC-A Upper Charge Threshold setting.
I_DET2BEGWLKBST	double	DET2 TDC-B Begin CFD Walk setting.
I_DET2BEGWLKAST	double	DET2 TDC-A Begin CFD Walk setting.
I_DET2ENDWLKBST	double	DET2 TDC-B End CFD Walk setting.
I_DET2ENDWLKAST	double	DET2 TDC-A End CFD Walk setting.
I_DET2BSLTHRBST	double	DET2 TDC-B charge Baseline inspector window Thr
I_DET2BSLTHRAST	double	DET2 TDC-A charge Baseline inspector window Thr

Table E.3: Table E.1 (continued)[a]

Array Name	Format	Description
I_DET2LWRQTHRBST	double	DET2 TDC-B Lower Charge Threshold setting.
I_DET2LWRQTHRAST	double	DET2 TDC-A Lower Charge Threshold setting.
I_DET2LWRTTHRBST	double	DET2 TDC-B Lower Time Threshold setting.
I_DET2LWRTTHRAST	double	DET2 TDC-A Lower Time Threshold setting.
I_DET2HVGRIDST	integer	DET2 Grid High Voltage Status (0=OFF; 1=ON)
I_DET2HVPWRST	integer	DET2 Bias High Voltage Status (0=OFF; 1=ON)
I_DET2STIMLMPST	integer	DET2 Stimulation Lamp Status (0=OFF; 1=ON)
I_FPD_Q_ECIBDY1	double	ECI to body quaternion 1
I_FPD_Q_ECIBDY2	double	ECI to body quaternion 2
I_FPD_Q_ECIBDY3	double	ECI to body quaternion 3
I_FPD_Q_ECIBDY4	double	ECI to body quaternion 4

[a] All Temperatures are in Degrees, currents in Amps.

Appendix F

FUSE Residual Wavelength Errors

A quality assessment of the *FUSE* data archive, including analyses of the systematic errors in the effective-area and wavelength calibrations have been conducted. The white dwarf KPD 0005+5106 was used as wavelength calibration target. Observed throughout the mission, the data from each observation were reduced independently. For each channel (LiF and SiC), detector segment (1A, 1B, 2A, and 2B), and aperture (LWRS, MDRS, and HIRS), all available spectra were shifted to a common wavelength zero point and combined into a single spectrum. These spectra were then fitted to an interstellar absorption model. The wavelength shifts necessary to align the spectra with the model are plotted in Figures F.1 through F.3 for LWRS; in Figures F.4 through F.7 for MDRS; and in Figures F.8 through F.11 for HIRS. The length of each horizontal line represents the wavelength span of one window. Several features seen in this plot are repeated in those for other channels and apertures. Most show a linear stretch in the wavelength scale of approximately 10 km s^{-1} over an entire detector segment. Local distortions of 4 to 5 km s^{-1} (about one CalFUSE pixel) over scales of a few Å are common. The apparent offset between the wavelength solutions of detector segments A and B (spanning 905–993 and 1003–1090 Å, respectively) may be spurious, as their spectra were shifted to common wavelength zero points independently.

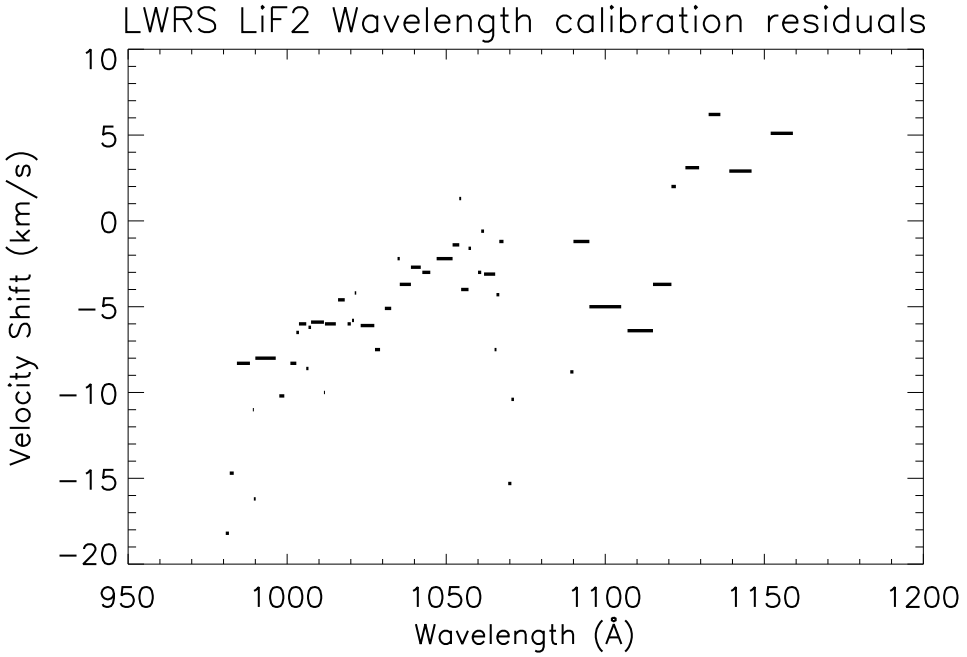

Figure F.1: Residual wavelength errors in the LiF2 spectrum of the white dwarf KPD 0005+5106 observed through the *FUSE* LWRS aperture. Horizontal lines represent the width of a window over which wavelength errors differ by less than half a pixel.

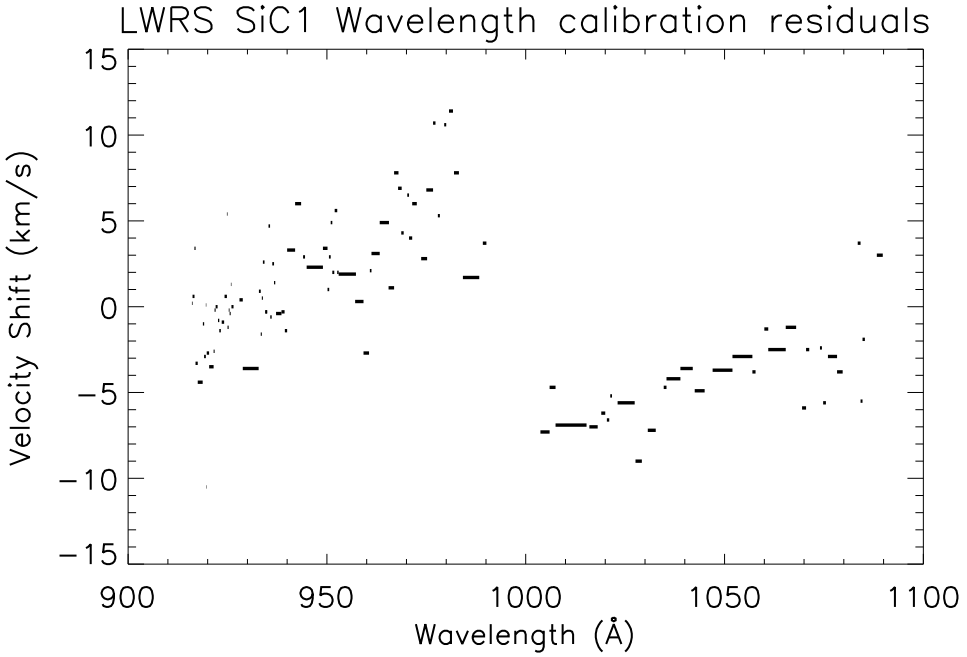

Figure F.2: Residual wavelength errors in the SiC1 spectrum of the white dwarf KPD 0005+5106 observed through the *FUSE* LWRS aperture. Horizontal lines represent the width of a window over which wavelength errors differ by less than half a pixel.

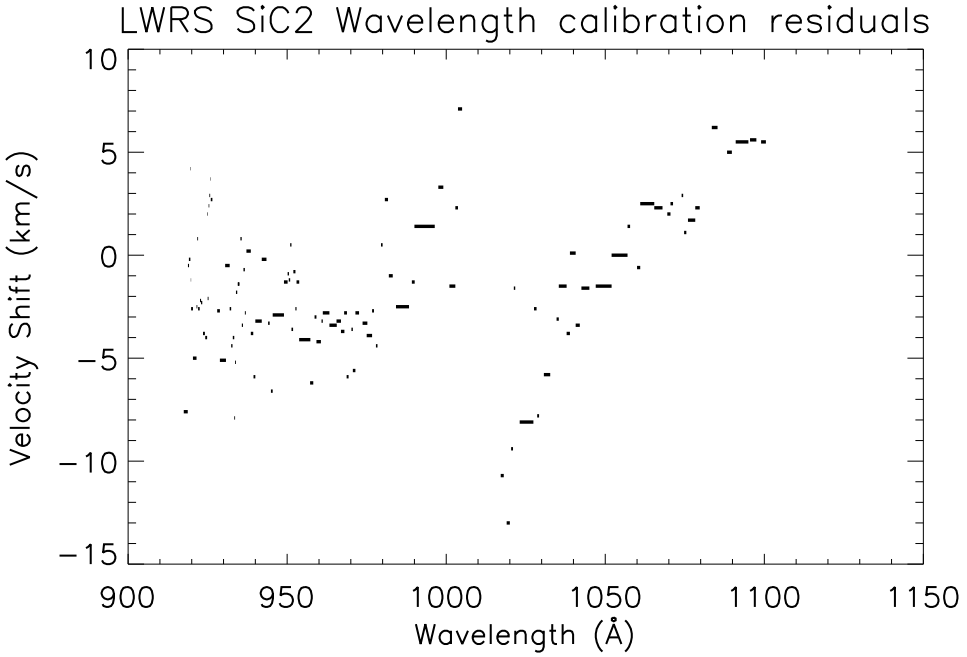

Figure F.3: Residual wavelength errors in the SiC2 spectrum of the white dwarf KPD 0005+5106 observed through the *FUSE* LWRS aperture. Horizontal lines represent the width of a window over which wavelength errors differ by less than half a pixel.

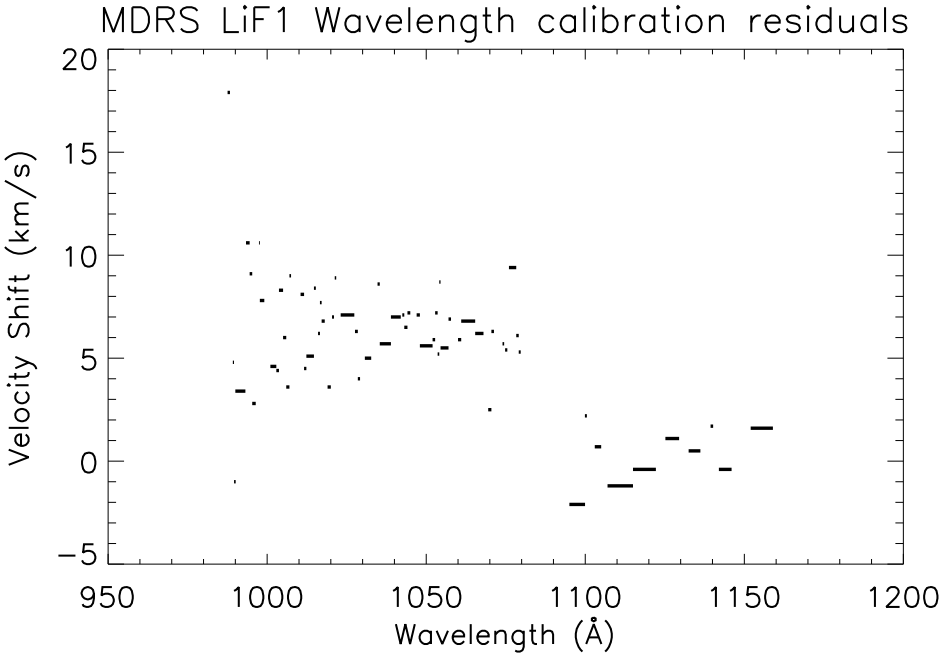

Figure F.4: Residual wavelength errors in the LiF1 spectrum of the white dwarf KPD 0005+5106 observed through the *FUSE* MDRS aperture. Horizontal lines represent the width of a window over which wavelength errors differ by less than half a pixel.

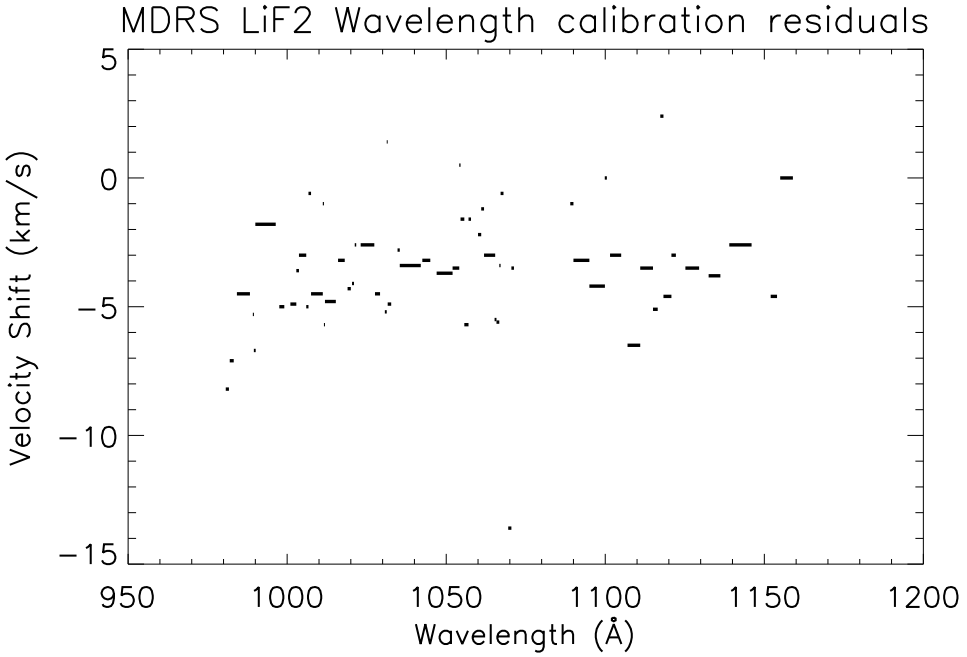

Figure F.5: Residual wavelength errors in the LiF2 spectrum of the white dwarf KPD 0005+5106 observed through the *FUSE* MDRS aperture. Horizontal lines represent the width of a window over which wavelength errors differ by less than half a pixel.

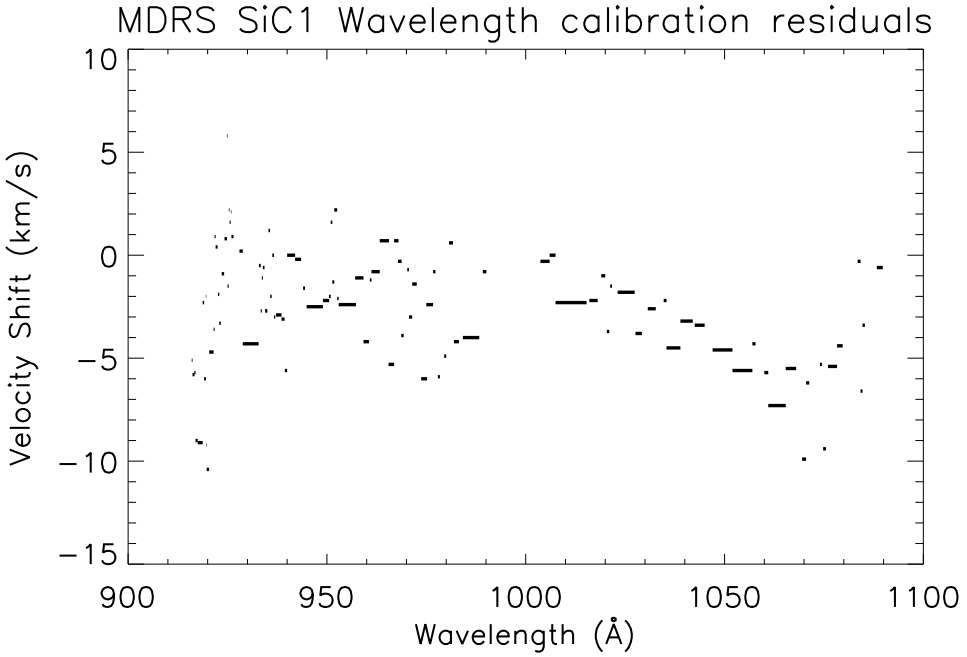

Figure F.6: Residual wavelength errors in the SiC1 spectrum of the white dwarf KPD 0005+5106 observed through the *FUSE* MDRS aperture. Horizontal lines represent the width of a window over which wavelength errors differ by less than half a pixel.

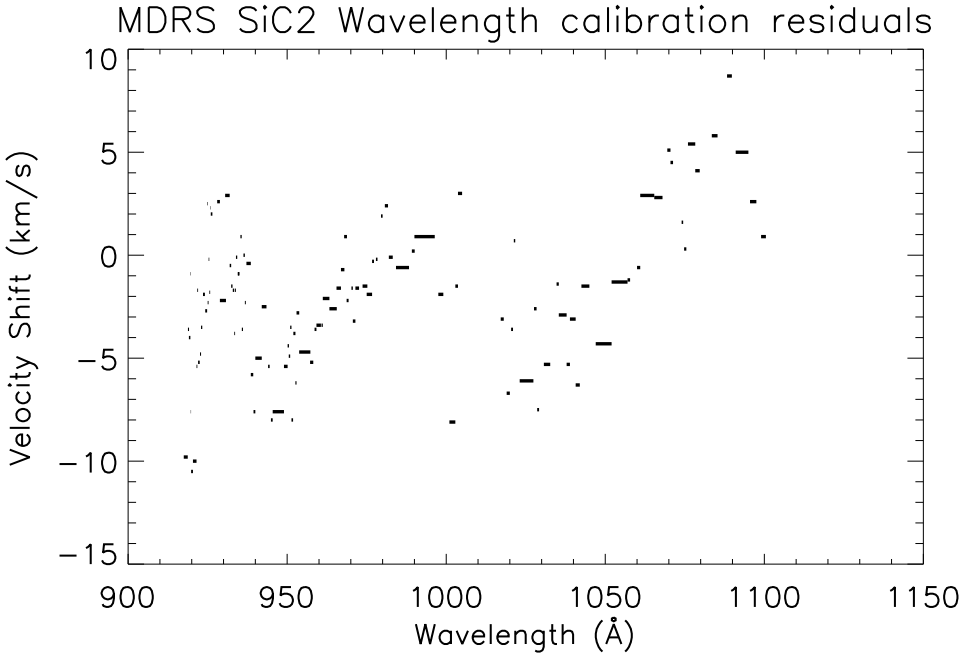

Figure F.7: Residual wavelength errors in the SiC2 spectrum of the white dwarf KPD 0005+5106 observed through the *FUSE* MDRS aperture. Horizontal lines represent the width of a window over which wavelength errors differ by less than half a pixel.

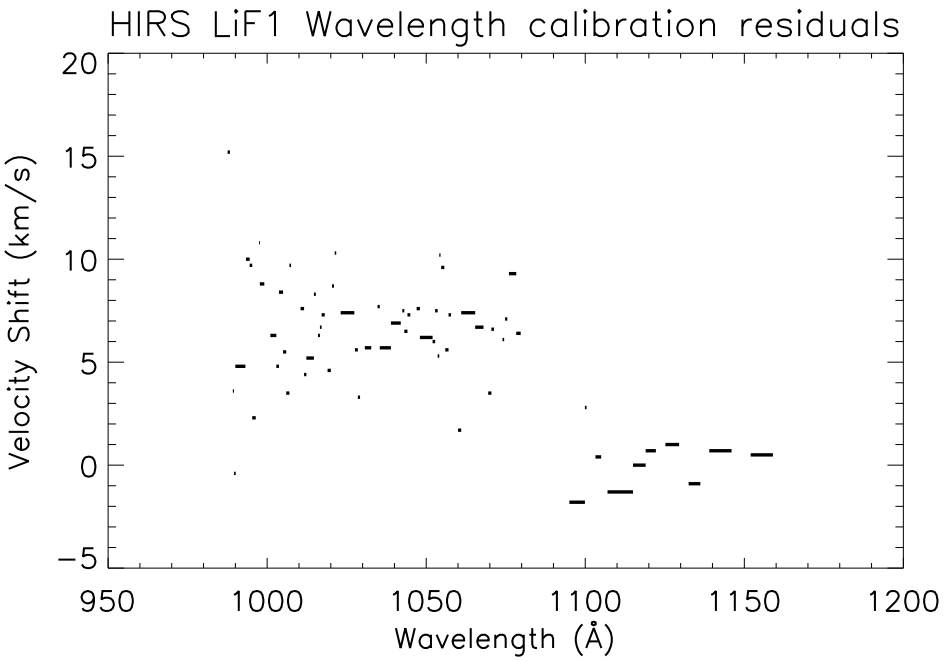

Figure F.8: Residual wavelength errors in the LiF1 spectrum of the white dwarf KPD 0005+5106 observed through the *FUSE* HIRS aperture. Horizontal lines represent the width of a window over which wavelength errors differ by less than half a pixel.

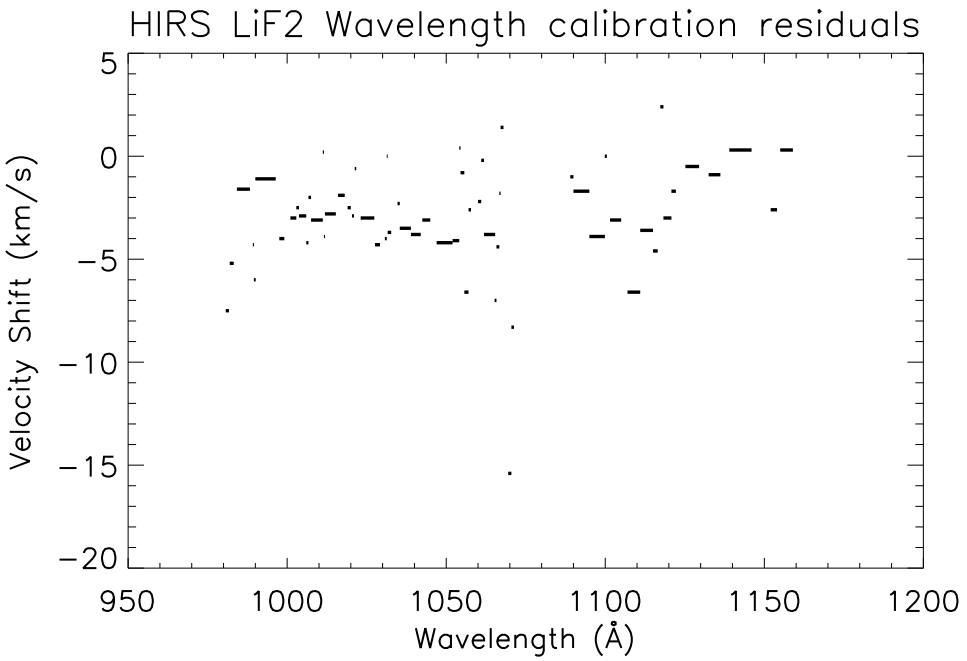

Figure F.9: Residual wavelength errors in the LiF2 spectrum of the white dwarf KPD 0005+5106 observed through the *FUSE* HIRS aperture. Horizontal lines represent the width of a window over which wavelength errors differ by less than half a pixel.

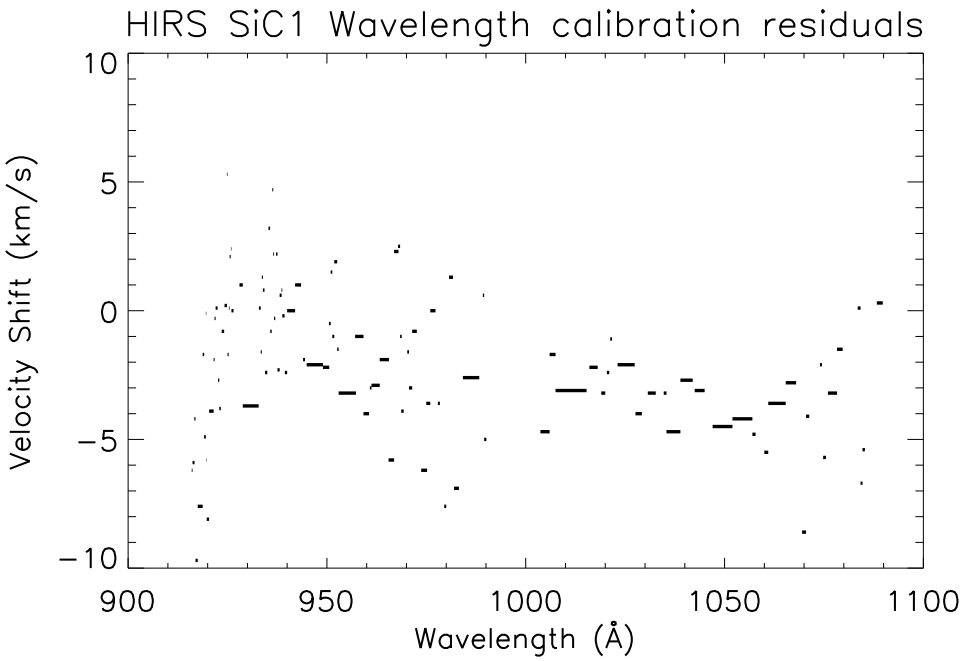

Figure F.10: Residual wavelength errors in the SiC1 spectrum of the white dwarf KPD 0005+5106 observed through the *FUSE* HIRS aperture. Horizontal lines represent the width of a window over which wavelength errors differ by less than half a pixel.

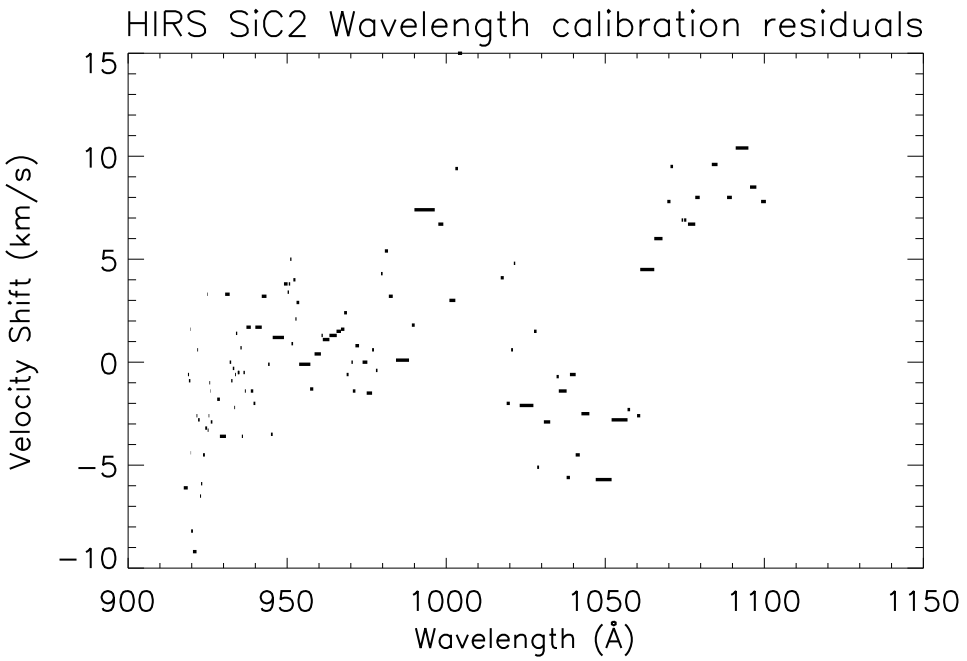

Figure F.11: Residual wavelength errors in the SiC2 spectrum of the white dwarf KPD 0005+5106 observed through the *FUSE* HIRS aperture. Horizontal lines represent the width of a window over which wavelength errors differ by less than half a pixel.